INTERNATIONAL LINEAR COLLIDER PHYSICS AND DETECTORS

2011 STATUS REPORT

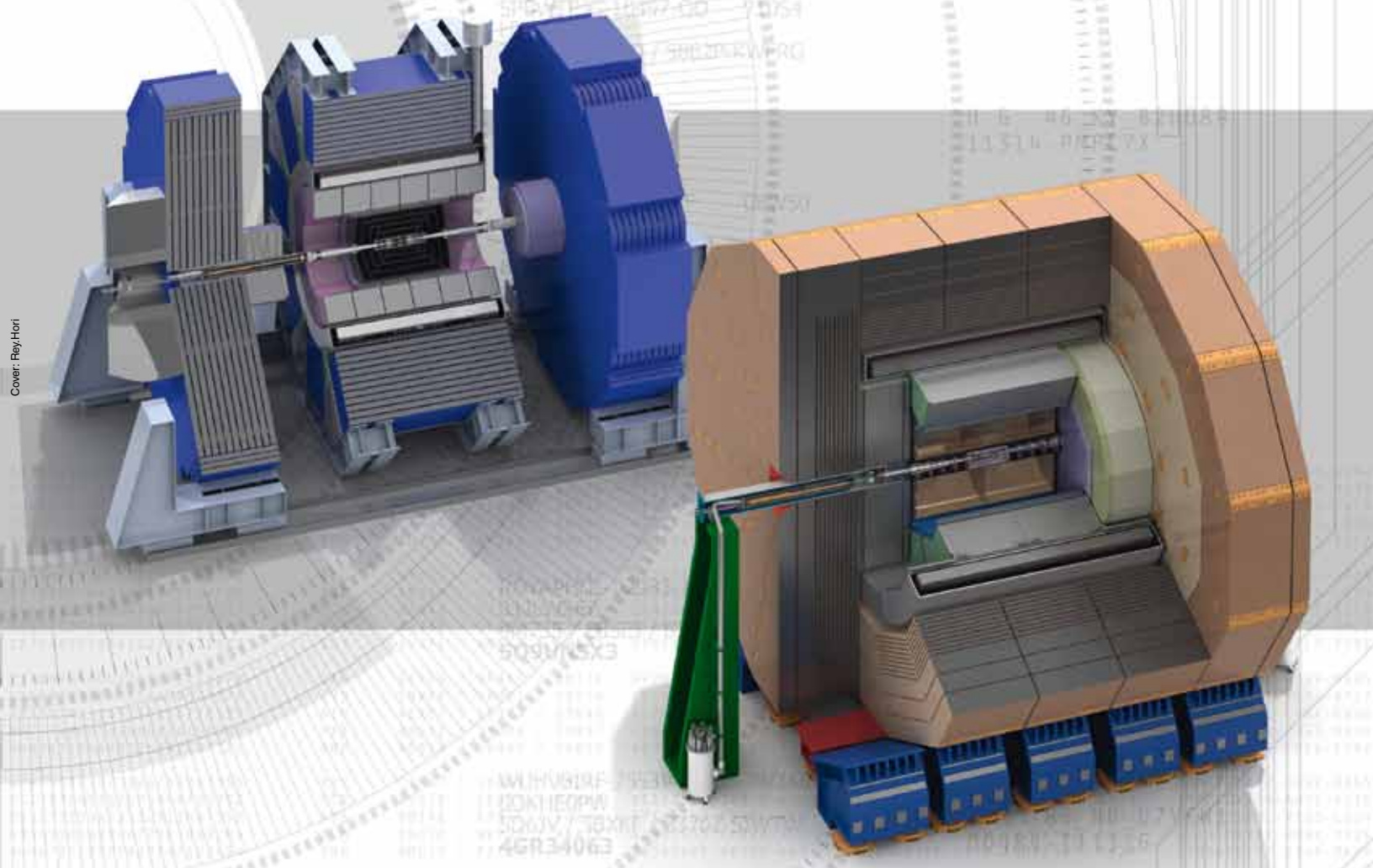

Cover: Rey Hori

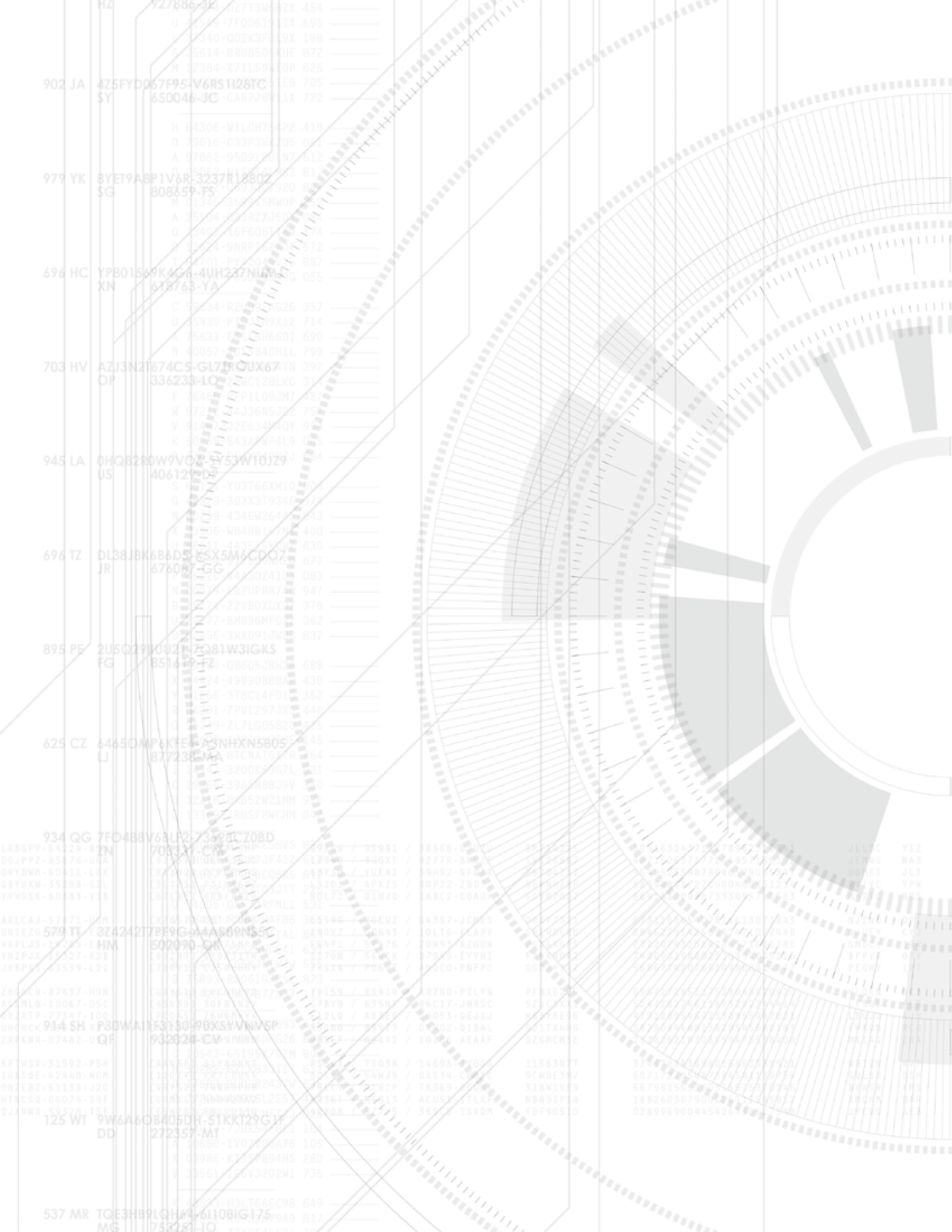

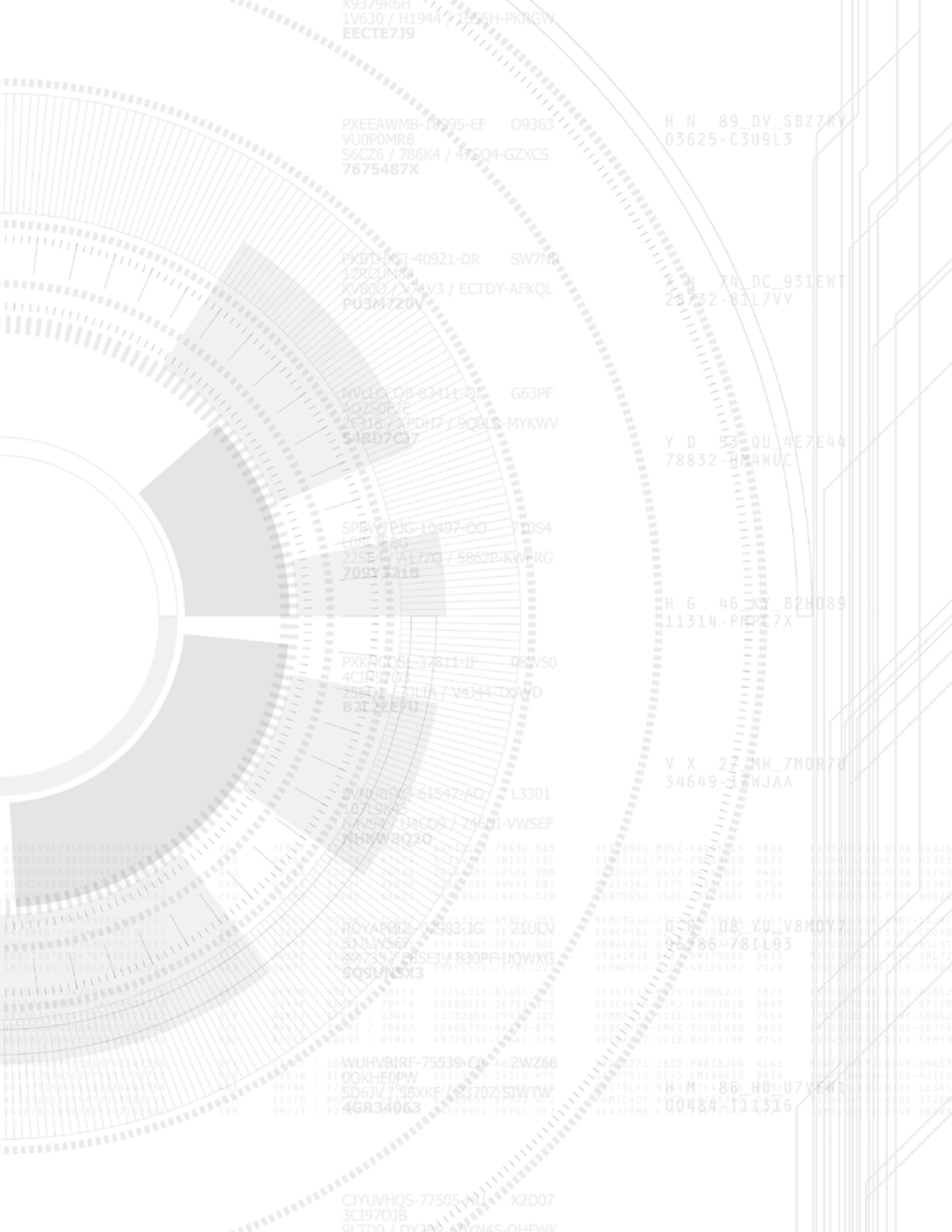

FOREWORD

The studies of physics and detectors for the International Linear Collider are an important parallel element to the effort for the ILC *Technical Design Report*. The studies comprise the physics opportunities, detector requirements, and detector development to achieve the challenging high performance demanded by the physics, as well as integration of detectors into the accelerator. The current phase of this effort began with a call for Letters of Intent (LOIs) in 2007 and will lead to the submission of *Detailed Baseline Design* (DBD) report together with the ILC *Technical Design Report* at the end of 2012. Here we summarise the current status of this process, review what it has accomplished and identify the work that still needs to be completed. This report, titled *International Linear Collider Physics and Detectors: 2011 Status Report,* does just this.

This report begins with a discussion of the outstanding issues in physics that motivate the construction of the ILC. It describes the organisation of the LOI process, the validation of the LOIs by the International Detector Advisory Group, and the results of R&D carried out to support the detector designs. The details of the concept detectors have already been published in the LOIs, which were completed in 2009. This report will, in a complementary way, describe the status of the detector R&D for each individual detector component and the status of the physics simulation infrastructure that has been built for the detector design process. Much of this work is carried out in cooperation between the two detector concept groups. This report describes the five common task groups and two working groups that have organised these cooperative activities.

Many members of the detector concept groups and the common task groups have contributed to this report. Many more people have carried out the actual work that is reviewed. The complete list of members of each detector concept group can be found from the author lists of the published LOIs. The members of the ILC physics and detector organisation are listed at the end of this document.

As we are now nearing the completion of the DBD phase, we are also entering a new stage of our preparation process. The experiments at the Large Hadron Collider at CERN, Switzerland, are accumulating data and are extending our knowledge of the physics of the teraelectronvolt energy scale. The LHC results may confirm the standard model of electroweak symmetry breaking or they may deliver something completely new. In either case, we believe, the ILC will be critical to resolve the questions that the LHC programme will bring forward. In any scenario, we will need very high-quality detectors and excellent technical and simulation capabilities. This report describes the status of our work in pursuit of that goal.

Sakue Yamada, ILC Research Director

EDITOR LIST

James E. Brau
University of Oregon, USA

Juan Fuster
IFIC-Valencia, Spain

Leah Hesla
Fermilab, USA

Monika Illenseer
DESY, Germany

Perrine Royole-Degieux
CNRS/IN2P3, France

Rika Takahashi
KEK, Japan

Barbara Warmbein
DESY, Germany

Sakue Yamada
KEK and University of Tokyo, Japan

Hitoshi Yamamoto
Tohoku University, Japan

Min Zhang
IHEP, China

CONTENTS

01

ILC PHYSICS

The International Linear Collider is designed as the next step in elementary particle physics beyond the Large Hadron Collider at CERN, Switzerland. It will continue the exploration of the distance scale of 10^{-18} metres – 1 one-thousandth of the size of an atomic nucleus – and the energy scale of several hundred gigaelectronvolts, or GeV – a few hundred times the rest energy or mass of the proton. Our current understanding of particle physics points to this distance scale as the key to the origin of the masses of the known elementary particles. It suggests that here, also, we will discover the particles that make up the dark matter of the universe. The ILC will bring new high-precision tools that will help us to solve these mysteries.

1.1 The current state of particle physics

At present, we know of two types of particles that we call elementary. The first are the matter particles. These include the electron and two heavier particles with the same interactions, the muon and the tau. These three particles and the massless, neutral, and elusive neutrinos are collectively called leptons. Matter particles also include the quarks, the basic constituents of strongly interacting particles such as the proton and neutron. In all, there are six types of leptons and six types of quarks. Only the electron and the u (up) and d (down) type quarks are found in atoms. The muon, the tau, and the remaining four quarks – s (strange), c (charm), b (bottom), and t (top) – are produced in high-energy reactions and rapidly decay to the less massive species. We do not understand the need for these particles or the pattern of their masses. The bottom quark has a mass about four times the mass of the proton; the top quark has a mass about 180 times the mass of the proton.

The elementary particles of the second type are the bosons, the quanta carrying the basic forces of nature. We know of three forces that operate at very short distances: the strong interactions, which bind quarks together and are responsible, more indirectly, for the structure of atomic nuclei; the weak interactions, which produce radioactive decay processes; and the electromagnetic interactions. The quantum of electromagnetism is the photon; the quanta carrying the strong and weak interactions are the less familiar gluons and W and Z bosons. These particles are similar, and all obey field equations of the form of Maxwell's equations of electromagnetism. The gluons, like the photon, have zero mass, but the W and Z bosons have masses about 90 times the mass of the proton.

The masses of the W and Z bosons give a hint as to the origin of all of the masses of these elementary particles. The equations of electromagnetism and the weak interactions put the W, Z and photon into a perfectly symmetrical relationship. This symmetry is visible in the experimentally determined values of the couplings of the W, Z and photon to quarks and leptons. If the symmetry were exact in all of nature, all three bosons would be massless. The observed pattern of masses follows if the symmetry is broken by an external entity, a new field in nature not otherwise visible. This field is called the Higgs field.

1.2 The hunt for new particles

The Higgs field has associated Higgs particles. These are new particles, ones that do not fit into the above classification. They couple both to leptons and quarks and to the W and Z bosons. It is not understood what force causes the Higgs field to take its required asymmetrical orientation. Models for this force bring in additional particles and fields of unprecedented types. One class of models, theories of supersymmetry related to the proposed superstring unified theories, requires new matter particles with the couplings of the photon and gluon and new force-carrying particles with the couplings of leptons and quarks. These new particles can serve other purposes than completing the theory of mass. A matter particle with the electromagnetic couplings of the photon would be a perfect candidate for the particle that makes up the mysterious dark matter, a neutral and weakly interacting substance, completely outside our current theory of particle physics, which makes up 80 percent of the matter in the universe.

The LHC at CERN is now engaged in the search for these particles. The technique used is to collide protons at extremely high energies. Pairs of quarks or gluons in the protons can annihilate and reform as particles of a completely new type. The rates predicted for these reactions are of the order of one part in ten billion of the rates for typical inelastic proton-proton collisions. Thus, only the most unusual and characteristic final states can be recognised. The events are very complex since they contain, in addition to the new particles, the leftover remnants of the original protons and the particles produced by quarks and gluons radiated from the annihilating pair. We expect that many of the predicted particles, including the Higgs boson, can be discovered in this environment. But, necessarily, most details of their properties will remain obscure.

The ILC will bring new tools to the study of these particles. The ILC will collide electrons and positrons at energies comparable to those of quark and gluon collisions at the LHC. Because electrons and positrons are elementary and couple through simple, point-like interactions, the rates for processes that create new particles are comparable to the total annihilation rate. And since they interact through forces much weaker than the strong interactions at work at the LHC, the annihilations produce events that are relatively free of background debris. That allows these events to be analysed as a whole, making use of all of their details to constrain the new particle properties. It also means that the experimental conditions will be much more benign, allowing the construction of detectors with unprecedented precision in energy and momentum measurement. Realising such unprecedented measurements requires the design and development of new detector technologies. For example, as compared to the detectors designed for LHC events, the ILC detectors will have only one tenth of the amount of obscuring material in front of the calorimeters that measure photon energies.

1.3 Experiment programme at the ILC

1.3.1 Experiments at the ILC: quarks and leptons

The first goal of the ILC programme will be to measure the simplest reactions of electron-positron annihilation into pairs of quarks and leptons. Currently, the measurements of these processes from CERN's former electron-positron collider, LEP, place the strongest constraints on possible substructure of quarks and leptons and are among the strongest constraints on new forces of nature beyond the weak interactions. Experiments at the ILC, at the energy of 500 GeV and full luminosity, will extend these searches by an order of magnitude in the mass of the particles that mediate the new forces. It is possible that new heavy bosons, partners of the W and Z, might be discovered at LHC as resonances in the production of electron or muon pairs. In that case, the ILC at 500 GeV can deliver the complete profile of the new bosons. The precision measurement of the pair production of leptons, of c-type quarks, and of b-type quarks using polarised electron and positron beams allows all couplings of this particle to be determined independently. *Figure 1.1* illustrates the ability of the ILC to discriminate from among a wide variety of possible models.

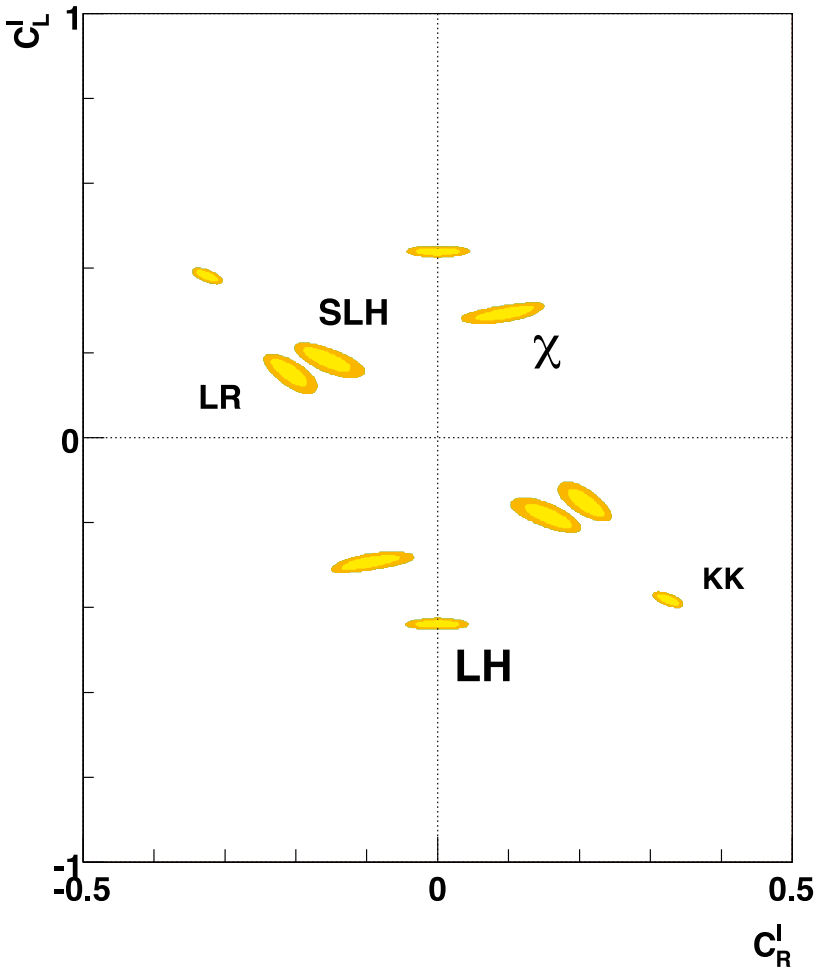

Figure 1.1 The expected ILC measurement of the couplings CL and CR of a Z' boson to left- and right-handed polarised leptons, expressed as an allowed region in the two-dimensional plane of these couplings. The mass of the boson is assumed to be 2 TeV. The various regions represent the expectations for different Z' models that have been discussed in the literature. The ILC experiments will select one of these regions unambiguously. *[1-1]*

1.3.2 Experiments at the ILC: top quark

The heaviest quark, the t or top quark, is the known particle most strongly coupled to the Higgs field and to other possible particles responsible for its symmetry breaking. The ILC will produce hundreds of thousands of top quark pairs. Both the production and decay of the top quark make use of parity-violating interactions sensitive to the particle spin. The use of polarised electron and positron beams will accentuate these effects. In the environment of the ILC, complete events with production and decay of a pair of top quarks can be reconstructed with high precision. The analysis of these events will probe the elementary couplings of this quark to electromagnetic and weak interactions and will, perhaps, reveal this particle's novel couplings or substructure.

1.3.3 Experiments at the ILC: Higgs boson

Although we expect that the LHC experiments will discover the Higgs boson, those experiments will not be able to definitively measure any of the Higgs boson couplings. The simplest model of the Higgs field predicts its couplings to each known particle as a precise value proportional to the mass of that particle. More complex models, for example supersymmetry, predict deviations from this law. At the ILC, large samples of Higgs bosons can be produced in a setting in which the decay of this boson to each possible final state can be recognised in an unbiased way. From these experiments, the presence or absence of a regularity in the set of Higgs boson couplings can be tested at the percent level of accuracy; see *Figure 1.2*. This will provide a definitive test of the simplest model of symmetry breaking in the weak interactions, or crucial clues if the true picture is more complex.

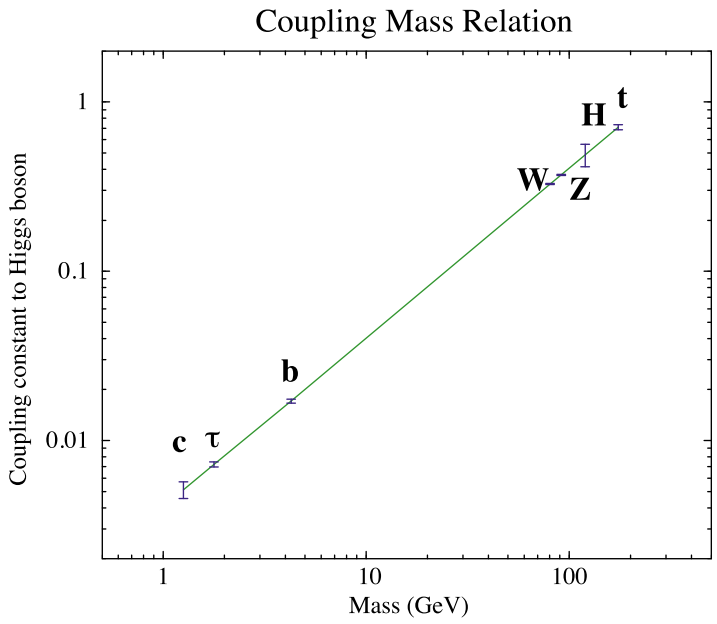

Figure 1.2 ILC expectations for the measurement of the Higgs boson coupling to quarks, leptons, and bosons, in the simplest model. *[1-2]*

1.3.4 Experiments at the ILC: new particles

We may soon know whether the LHC will discover new particles of the type that are predicted in models of weak interaction symmetry breaking and dark matter. In any case, the ILC will be able to make a definitive search for new particles with masses of up to 250 GeV. The ILC will produce these particles as pairs through weak and electromagnetic interactions. In this setting, the magnitude of the production rate, the angular distribution, and the asymmetry with respect to electron beam polarisation will definitively identify each particle's quantum numbers. As with the Higgs particles, the ILC experiments will be able to make unbiased measurements of the decay probabilities to possible final states.

Figure 1.3 shows an expected result from the ILC measurement of the decay of a supersymmetry partner of the W boson. This particle should decay to a quark-antiquark pair plus the supersymmetric partner of the photon, an invisible dark matter particle. The figure shows the distribution of the reconstructed energy of the quark-antiquark system. The detailed shape of this distribution is used to determine the couplings of the new particle. Further constraints on these couplings will be obtained from the angular distributions of the quark and antiquark relative to the electron beam direction, which can be obtained to an accuracy of the order of one degree. As with the top quark, angular asymmetries are enhanced by the use of electron and positron beam polarisation.

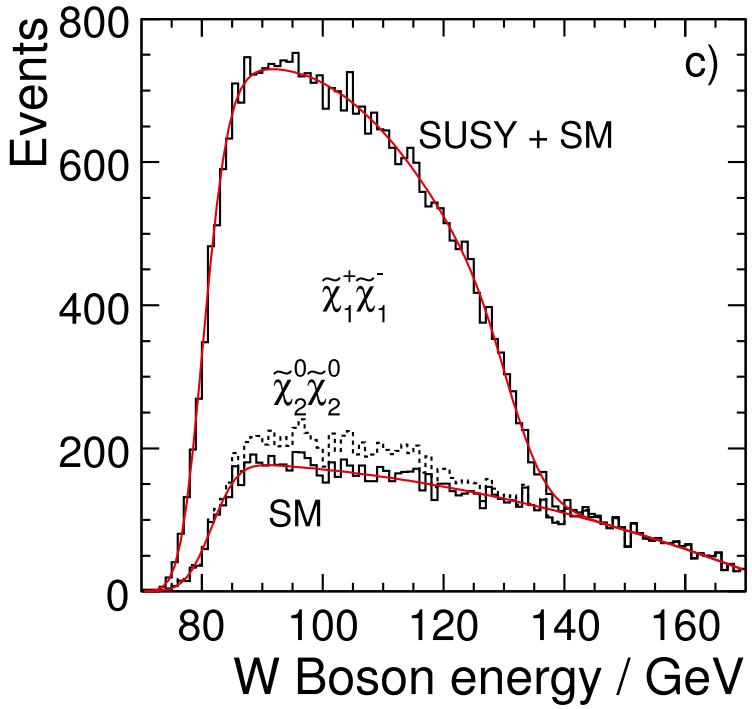

Figure 1.3 Distribution of the energy of the quark-antiquark system produced in the decay of the supersymmetry partner of the W boson, as it would be measured by the ILD detector. *[1-3]*

1.3.5 Experiments at the ILC: dark matter

The complete picture that the ILC will give of new elementary particles will address the question of whether the lightest of these particles makes up the dark matter of the universe. Measurements at the ILC will allow the cosmic density of that particle produced in the early universe and the interactions of that particle with ordinary matter to be predicted from elementary particle data alone. These predictions can then be matched against astrophysical measurements. One specific comparison of an ILC measurement to astrophysics is shown in *Figure 1.4*. This programme could provide a definitive test that we are making dark matter in the laboratory.

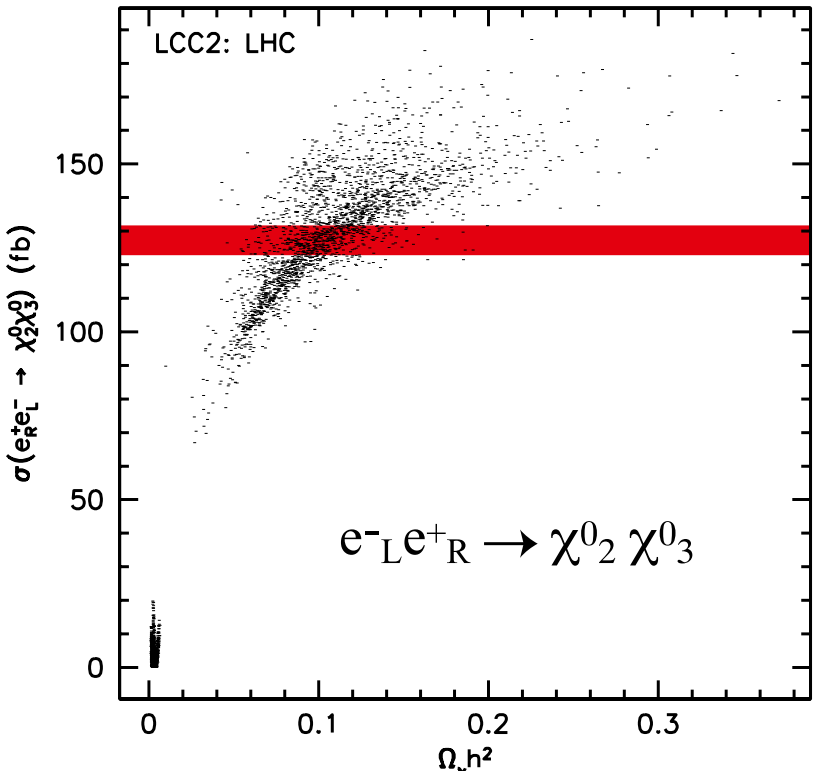

Figure 1.4 Scatter plot of the predictions of models of supersymmetric dark matter consistent with expected LHC data. On the vertical axis is one specific reaction rate that will be measured at the ILC with polarised beams. The horizontal axis is a quantity proportional to the density of dark matter in the universe; the current best value from astrophysics is close to 0.1. The ILC will provide many constraints of this type on the ability of observed new particles to explain dark matter. *[1-4]*

Summary

Elementary particle physicists expect that the CERN LHC will discover new types of elementary particles and will open a new chapter in the physics of the universe. But writing that chapter will require new tools that go qualitatively beyond the capabilities of the LHC. The ILC will provide them.

References

[1-1] Fig. 4a of "Distinguishing between models with extra gauge bosons at the ILC," Stephen Godfrey, Pat Kalyniak, Alexander Tomkins, hep-ph/0511335, presented at the Snowmass 2005 workshop on the ILC.

[1-2] Fig. 2.4 of the GLC report, K. Abe, et al,"GLC project: Linear collider for TeV physics," KEK-REPORT-2003-7, Sep 2003.

[1-3] Fig. 3-3.19(c) of ILD LOI, "The International Large Detector: Letter of Intent," Toshinori Abe (Tokyo U) et al, ILD Concept Group - Linear Collider Collaboration, FERMILAB-LOI-2010-03, FERMILAB-PUB-09-682-E, DESY-2009-87, KEK-REPORT-2009-6. Feb 2010. 189 pp. e-Print: arXiv:1006.3396 *[hep-ex]*

[1-4] Fig. 26(b) of "Determination of dark matter properties at high-energy colliders," Edward A. Baltz (KIPAC, Menlo Park), Marco Battaglia (UC, Berkeley & LBL, Berkeley), Michael E. Peskin, Tommer Wizansky (SLAC). Published in Phys.Rev. D74 (2006) 103521, e-Print: hep-ph/0602187. Expected ILC measurement of the quantity on the vertical axis is superposed on it.

02

DEVELOPMENT AND COORDINATION OF PHYSICS AND DETECTOR STUDIES

The physics and detector studies for the ILC have been organised since 2007 through a process of Expressions of Interest, Letters of Intent, and Detailed Baseline Design (DBD) report. As the plan to develop a technical design for the ILC in 2012 unfolded, the ILC Steering Committee (ILCSC) recognised the importance of defining detailed detector concepts that should be considered in the design of the ILC, particularly in addressing issues of the ILC interaction region. Coordinating with the ILC 2012 plan, the ILCSC initiated a parallel process for technical development of detector design. A Letter of Intent (LOI) process was initiated in 2007 in order to validate detector concepts to be developed by 2012. This LOI process and the framework for conducting it have guided organisational steps towards the detailed detector designs over the past few years. These steps are described briefly in this introduction.

2.1 Call for LOIs

In October 2007, the ILCSC announced a call for letters of intent to produce reference designs for two detectors for the ILC *[2-1]*. The proposed roadmap had been prepared by the World Wide Study Organising Committee (WWS-OC) and approved by the community through the discussion at the Linear Collider Workshop at DESY, Germany in 2007, in which the chairs of the International Committee for Future Accelerators, the ILCSC and the Global Design Effort (GDE) participated.

When the GDE published the ILC *Reference Design Report* in summer 2007, there were four detector concepts described in its detector volume. The call for LOIs was intended to lead the community to form two capable groups that would develop their concepts to a technically advanced stage and produce detailed baseline designs at the same time as the planned completion of the GDE accelerator *Technical Design Report* in 2012[1]. The submitted LOIs were planned to be reviewed by an advisory body called the International Detector Advisory Group (IDAG). In order to conduct the LOI procedure, ILCSC created simultaneously with the call of LOIs the position of research director, who was to set up a management structure and to compose IDAG with the approval of the ILCSC.

A detailed guideline for the preparation of the LOIs was published together with the call. It defined the contents of the LOIs and their lengths. As for the content, it says, “The LOI should contain information on the proposed detector, its overall philosophy, its sub-detectors and alternatives, and how these will work in concert to address the ILC physics questions. The evaluation of the detector performance should be based on physics benchmarks, some of which will be the same for all LOIs based on an agreed-upon list, and some of which may be chosen to emphasise the particular strengths of the proposed detector. It should contain a discussion of integration issues with the machine. It should be developed enough to allow a first preliminary assessment of civil engineering issues like the interaction hall, support halls, etc. It should enable the reader to judge the potential of the detector concept and to identify the state of technological developments for the different components.” Further, “the LOI should include a preliminary cost estimate for the detector. The overall length of the LOI should not exceed 100 pages.”

[1] The call for LOIs was originally planned for engineering designs of two detectors by 2010. The plan was soon modified at the ILCSC meeting in February 2008 due to the financial drawbacks for the activity. The completion of the detailed baseline designs was consequently pushed back to 2012. The due date for LOIs was accordingly extended to the end of March 2009.

The Software Panel of the World Wide Study prepared a list of key benchmarks to be studied for the LOIs. An agreement on the list was reached by end 2007 *[2-2]*.

2.2 The management of detector organisation

The first step for the Research Director was to form the central management, which would include a representative of the detector community of each region. With consultation and agreement of the steering body of each region, the three WWS co-chairs were requested to become the first regional contacts. This choice could be controversial since having representatives of so-called user representatives in the management might cause conflict. At a laboratory that runs an accelerator, such a choice does not happen. However, since the ILC is still in the R&D phase and our effort is to prepare for its realisation, good communication with the detector community would be only helpful. The choice was accepted as a temporary solution over the turn of the year. Jim Brau from North America, Francois Richard[2] from Europe and Hitoshi Yamamoto from Asia joined the management by January 2008.

[2] Juan Fuster took this role in February 2012.

The management started its work by listing possible candidates for IDAG members among the experimental physicists, phenomenology theorists and ILC accelerator experts, considering regional balance. Most candidates had been active in the field of electron-positron collision while some members shifted to other fields in the meantime.

We in the detector management requested Michel Davier to chair the group. With the approval of ILCSC on the possible members and the chair, each candidate was asked to serve. We were pleased that all of these competent candidates accepted and that IDAG could be set up by the end February. The present members are listed in *Table 2.1*. The TILC08 workshop of ILC in Sendai, Japan, in March 2008 was too early for the entire IDAG to meet, but some members were able to attend to collect information on the status of the detector activity and to conduct some preparatory discussions. In particular the chair and the Research Director discussed in some detail the aim of IDAG and how to carry out the LOI process.

Experiment & Detector	Michael Danilov	ITEP
	Michel Davier (Chair)	LAL/Université Paris Sud
	Paul Grannis	Stony Brook University
	Dan Green	FNAL
	Dean Karlen	Victoria
	Sun-Kee Kim	SNU
	Tomio Kobayashi	ICEPP Tokyo
	Weiguo Li	IHEP
	Richard Nickerson	Oxford
	Sandro Palestini	CERN
Phenomenology	Rohini Godbole	IIS
	Christophe Grojean	CEA-Irfu/CERN
	JoAnne Hewett	SLAC
Accelerator	Eckhard Elsen	DESY
	Tom Himel	SLAC
	Nobu Toge	KEK

Table 2.1 International Detector Advisory Group members

2.3 Organisation of detector activity

The management worked in the meantime on the framework to organise the detector activity. The scheme is illustrated in *Figure 2.1.* Much of the detector R&D and physics simulation was carried within the concept groups, which further collaborate with various R&D collaborations for certain components. Each group was expected to design a harmonised detector system along its concept to be outlined in its LOI. Required preparatory work was organised within each group. Nevertheless, it was thought that cooperation among the separate concept groups would be very important during the R&D phase. There were certain tasks like the push-pull studies that could be pursued only with close cooperation among the concept groups and with the accelerator team for the beam delivery system. Also sharing of commonly needed tasks was recommended to optimise the outcomes. In order to facilitate such cooperation and communication among the various concept groups, we planned to create five common task groups (CTG) consisting of members from all the concept groups. Detailed planning of the CTGs was made later together with the representatives of the concept groups.

The Physics and Experiment Board (PEB) was conceived as the decision-making body of the detector and physics community, which would comprise the representatives of the LOI groups, conveners of the CTGs and the management members.

In order to start practical work within this framework, the next step was to identify the concept groups that would submit LOIs in 2009. This was done by a call for Expression of Interest (EOI) to submit LOIs. The announcement was made in February 2008 with a short time window for the due date, the end of March 2008. Three groups responded with the required information, the names of two representatives and the participating institutions. They were ILD (International Large Detector), SiD (Silicon Detector) and Fourth. The ILD was a fusion of two large concept groups, GLD and LDC of the RDR plan, which had similar ideas and decided to make joint efforts for LOI. The representatives of the three groups joined in further discussions for details of the framework. For instance, the five common task groups that were agreed upon were the machine-detector interface (MDI) group, engineering tools group, detector R&D group, software group and physics group. The concept groups were requested to send their members for these common task groups so that they could be formed by end of May 2008. The MDI group was supposed to make a link to the beam delivery system group of the GDE and had to be set up as soon as possible. As for the physics common task group, we wished to invite theory members, too.

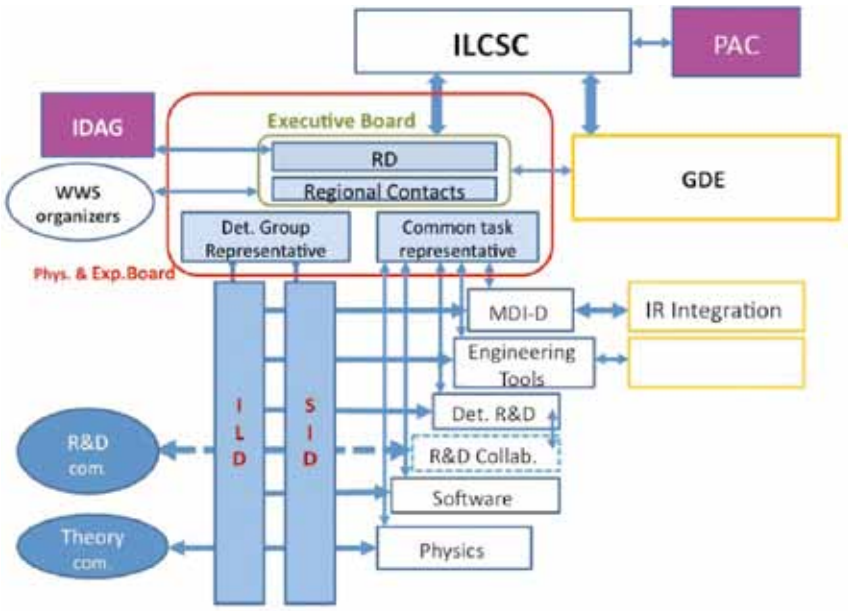

Figure 2.1 The organisation chart of the detector activity. Image: Sakue Yamada

During the European Committee for Future Accelerators (ECFA) workshop in Warsaw, Poland, in June 2008, the management met face to face for the first time with the concept representatives and with many of the common task members to clarify the detailed plan of the LOI process. Also the management could be informed of the situation of each concept group's possible issues in preparing LOIs. After the workshop, we nominated the conveners and deputies of all the common task groups, and the PEB could meet with full membership. The activity of each common task group is described later in this report.

Through the discussions with the detector groups, we became aware of the important roles played by the independent ("horizontal") R&D collaborations. Close cooperation with these groups was crucial to achieve the R&D goals of each concept group. So the detector management decided to invite representatives of major horizontal collaboration groups for calorimetry and tracking to join the R&D common task group for better communication.

2.4 IDAG beginnings

The first IDAG meeting was also held during the ECFA workshop in June 2008. Through face to face discussions, the detector management and IDAG discussed the role of IDAG for the validation process. A common understanding was reached about what features were required for validation of an LOI and its group. Specifically, IDAG would examine whether (1) the overall concept had an expected goal and performance suited to the physics programme of the ILC and (2) the proposing group had the scientific and technical ability to reach its goal.

Since this meeting, IDAG has met and interviewed the concept groups at each linear collider workshop. The second meeting was held in Chicago, US, during the American Linear Collider Physics Group (ALCPG) workshop in November 2008, where IDAG began to organise its validation of LOIs. The members divided tasks in two ways: each member would review the LOI of one of the groups, and each would review one particular topic for all of the LOIs, either key detector components or physics performance. This matrix of horizontal and vertical tasks ensured a thorough review engaging the IDAG membership in careful consideration of the concepts. At the Chicago meeting IDAG also issued a set of additional requirements, which were more concrete than those given in the LOI guideline, and they were to be answered in the submitted LOIs.

IDAG continued its preparation through telephone meetings until the LOI due date in order to update itself on the current status of the major detector components.

2.5 The LOIs

The three Letters of Intent were submitted as expected from the ILD, SiD and Fourth groups by the due date. As the allowed length of the LOIs was limited and could not include all detailed information, all groups submitted additional material and more information in separate documents to cover the details of their preparatory studies. IDAG began their examination for validation immediately and sent specific questions to each of group regarding its LOI contents.

During the TILC09 workshop in Tsukuba, Japan in April 2009 each concept group made two presentations on its LOI, one for the detector concept, design philosophy or optimisation principle, components and structure, and the other for its expected performance on the benchmark reactions. These presentations were attended by many people of the community and

IDAG members. Each concept group was interviewed separately by IDAG, where they answered IDAG's questions on the LOIs. Based on this interview IDAG issued further questions to the groups, which were to be answered at a special IDAG meeting in June 2009, held in Orsay, France; the final interviews with the concept groups led to the start of the final IDAG discussions and recommendations. IDAG began its written summary of their validation conclusions and recommendations.

It should be stressed that from the submission of the EOIs in March 2008 until the last interview with IDAG in June 2009, the members of the three concept groups devoted very large efforts in the preparation of the LOIs and presenting the concepts to IDAG, along with written answers to formal IDAG questions. IDAG also made very concentrated effort to examine carefully the huge amount of material in a short period.

2.6 IDAG recommendation and validation

IDAG sent the Research Director a recommendation for validation in August 2009. The conclusion that ILD and SiD be validated was presented by the Research Director during the ILCSC meeting a few days later and was approved. During the ALCPG workshop in Albuquerque, US, in September 2009, the IDAG examination process and the validation were reported by the chair *[2-3]*.

The validation made a clear milestone for the next step. In Albuquerque, there was a preliminary meeting between the management and available IDAG members, including the chair, about how to monitor the progress of the validated groups towards the detailed baseline design. In order to check the progress in detail we agreed that IDAG would examine the activity of each common task group, too. The idea was that common effort of the two groups would become more important and the expertise of IDAG would be helpful to strengthen it.

Following validation the organisation of the detector activity was modified: the PEB membership was reorganised to include members of the validated groups and the common task members. The CTGs were also reorganised with increased membership from ILD and SiD.

2.7 Planning for the detailed baseline designs

For the validated groups, the next step was to prepare a detailed plan to reach the final goal. In order to guide the planning, we agreed in the PEB meeting to prepare a list of the expectations for the DBD. The nine items on the list included subjects such as

- completion of R&D for critical detector components for their feasibility proof,
- defining a detailed baseline design of the detector system,
- setting up a realistic model of the detector for physics simulation,
- completion of studies of a push-pull scheme and integration into the interaction region,
- making physics simulations for a new set of benchmark reactions including some at 1 TeV.

New physics benchmark reactions were investigated by the physics CTG, which would best illustrate the ability of ILC for the expected new physics. The CTG proposed a list by the end of 2009, which also included a few reactions at 1 TeV. The high-energy case was included in view of the optional upgrade of ILC[3].

Each group submitted a time schedule by October with a caveat that it was made under the assumption that necessary resources would become available in due course. While certain anticipation for resources was included in the submitted LOIs, it was recognised that resources were not secured for the entire period or for all the tasks, and efforts had to be made by participating institutions. The first detailed planning assumed that such efforts would be successful.

The tentative planning towards the completion of the DBD and the expected role of IDAG were reported to ILCSC in February 2010 at Brookhaven National Laboratory, US. ILCSC extended the mandate of IDAG until the end of the ILC's technical design phase to monitor the progress of the detector groups. ILCSC also recognised the limited resources of the detector groups, in particular, the need of engineering support.

The first monitoring of the progress of the validated groups by IDAG was made during LCWS10 in Beijing, China in March 2010. By this time, both groups had tried to refine the first work plan in view of the updated scope for resources. The detector groups expressed uneasiness about the sign of declining resources all over the world and the lack of engineering support required for the integration studies. We revisited the planning in view of the projected resources and decided that all nine items to be referenced in planning would be retained while the level of accomplishment for each item would be adjusted according to the available resources. However, the minimum requirement should be satisfied. The difficulty and the corresponding strategy were understood by IDAG.

[3] The list was reconsidered later by a subgroup including representatives of the two groups and software common task groups for priority and work sharing. An updated list, which classifies the new benchmarks, was completed after careful study in January 2011.

2.8 Other working groups

In addition to the original five standing common task groups, we subsequently created some new working groups to solve specific tasks as they appeared and needed to be handled intensively in a relatively short period. These were organised in cooperation with the two detector groups and relevant common task groups as well. A good example is the SB2009 working group, which was organised soon after the ALCPG workshop in Albuquerque in order to evaluate the effects on experiments and the resulting physics consequences of the proposed SB2009 accelerator parameters. This working group communicated with the accelerator team systematically and organised necessary works among the participating bodies. The details of the activity are described later. There was a working group to study and arrange the work plan for the new benchmarks. It was led by the physics common task group and worked with the representatives of the two groups and the software common task group. It completed its work with a report on the list of priority- and work-sharing for each possible physics channel. Currently we have a new short-term working group to study a common costing method between the two groups.

The CLIC (Compact Linear Collider study)-ILC joint working group was initiated in early 2010 following discussions during the ILCSC meeting in Hamburg, Germany. It surveys ongoing cooperation and looks for further synergies between the two linear collider detectors. Before this working group was formed, there had already been much grassroots cooperation since 2008. This has become more intensive since CLIC deployed the two ILC concepts for its detectors. Now we observe an overlap of the members who prepare both CLIC *Conceptual Design Report* and the ILC DBD. The current situation is reported later in a separate chapter.

2.9 A way to go

Having passed through the midway point to publishing the DBD, the detector groups are continuing their efforts and making progress towards the detailed baseline design. We intend to be ready by the end of 2012 for the next step with the completed DBD, hoping that some new signal will be obtained at LHC by that time. We are also keen on how the completed DBD will become useful for the realisation of the project and for more advanced design studies.

The R&D for detector components, some of which are conducted in cooperation with R&D collaborations, are advancing, and crucial integration work like the push-pull study is approaching the pursued milestone. Also, more realistic simulation studies are being prepared. Many efforts are organised, led or carried out by the common task groups. IDAG monitors all these advancements regularly and gives us helpful advice. In the following sections, more details of these ongoing activities are described.

References

[2-1] Shin-ichi Kurokawa, http://ilcdoc.linearcollider.org/record/15684/files/CallForLOI.pdf, 4 October 2007

[2-2] http://ilcdoc.linearcollider.org/record/14681/files/Benchmark_Reactions_for_the_ILC_LOI.pdf

[2-3] http://ilcdoc.linearcollider.org/record/23970/files/IDAG_report_090816.pdf

03

DETECTOR R&D AND INTEGRATION

3.1 Detector concepts at the ILC

The International Linear Collider will be built to investigate properties of nature at very high energy with very high precision. This puts the highest demands not only on the accelerator, but also on the detectors. Currently the interaction region at the collider is designed to house two detectors, operated in a push-pull scheme to share the available luminosity. In an internationally coordinated effort two concept groups, which have formed over the last few years, propose detectors for experiments at this machine. Together with focused R&D groups they advance the state-of-the-art in detector technology to make them usable for these sophisticated experiments.

Both the ILD (International Large Detector) and the SiD (Silicon Detector) concepts are based on the paradigm of particle flow, an algorithm by which the reconstruction of both charged and neutral particles is accomplished by an optimised combination of tracking and calorimetry. Since, on average, a large fraction (roughly 60%) of the energy of a jet is in the form of charged hadrons, one can achieve a better measure of the energy deposited in the calorimeter by these particles using their tracking information. This requires that individual tracks be able to be followed from the tracking system into the calorimeter and their clusters of energy deposition be associated with the followed track. Once the association between charged tracks and their energy clusters has been made, those clusters can be removed from further consideration. It then remains to measure the energies of the other clusters deriving from neutral hadrons and photons, with allowance made for (minimum ionising) muons in the calorimeter. The photons have their energy measured in the first electromagnetic section of the calorimeter system and the neutral hadrons in the second hadronic section. The detailed use of individual tracks and energy clusters in the calorimeter demands a small cell size or high granularity. The net result is then improved charged particle and jet energy resolutions.

3.1.1 The SiD detector concept at the ILC

The SiD detector *(Figure 3.1)* is a compact detector designed to make precision measurements of physics variables and to be sensitive to a wide range of possible new phenomena. The design represents an optimised balance between cost and physics performance. The choice of silicon for the entire tracking system ensures that SiD is robust to beam backgrounds or beam loss. It provides superior charged particle momentum measurement and eliminates hits from tracks not in time with the main beam collisions. The SiD calorimetry is optimised for excellent jet energy measurement using the particle flow technique. The complete tracking and calorimeter systems are contained within a superconducting solenoid, which has a 5-tesla (T) field magnitude appropriate to the overall compact design. The coil, in turn, is located within a layered iron structure that returns the magnetic flux and is instrumented to allow the identification of muons. All aspects of the SiD detector are the result of intensive and leading edge research conducted to raise its performance to unprecedented levels. Members of SiD have been developing the detector design for several years, and will continue to work towards a baseline definition of the detector in 2012.

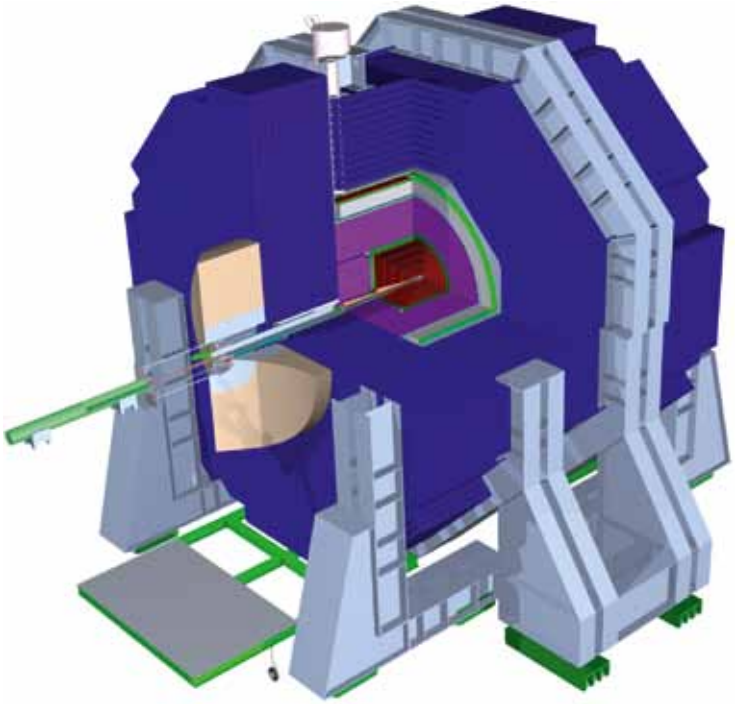

Figure 3.1 Three-dimensional view of the SiD detector.
Image: SiD

3.1.2 The ILD detector concept at the ILC

ILD detector *(Figure 3.2)* has been optimised for excellent jet energy resolution over a wide solid angle and for high-precision reconstruction of exclusive final states. A major goal in the design has been the event reconstruction within the particle flow paradigm. The detector is relatively large to improve the separation between neutral particles, has a sizeable magnetic field to separate charged from neutral particles and to sweep away low-momentum backgrounds and is optimised for highly efficient, precise particle reconstruction, in particular very robust, redundant pattern recognition of particles in the tracker and in the calorimeter.

The calorimeter plays a central role in the reconstruction of the complete event properties. A system of unprecedented granularity is proposed for ILD, both for the electromagnetic and the hadronic sections. The complete calorimeter is located inside the magnet. The flux from the coil is returned through an iron yoke, which is instrumented to serve as a muon filter in addition. It is complemented by a system of small, precise and radiation hard calorimeters in the very forward direction, used to complete the solid angle coverage, and to measure precisely the luminosity of the collider.

The tracker inside the calorimeter is a combination of a powerful large-volume time projection chamber (TPC) and an extensive silicon tracking system. The TPC provides up to 200 space points per particle, allowing efficient and highly redundant pattern recognition. It is combined with silicon tracking stations, both inside and outside of the TPC and covering the end plate, to provide addition high precision points. Located close to the beam pipe is a high-precision vertex detector.

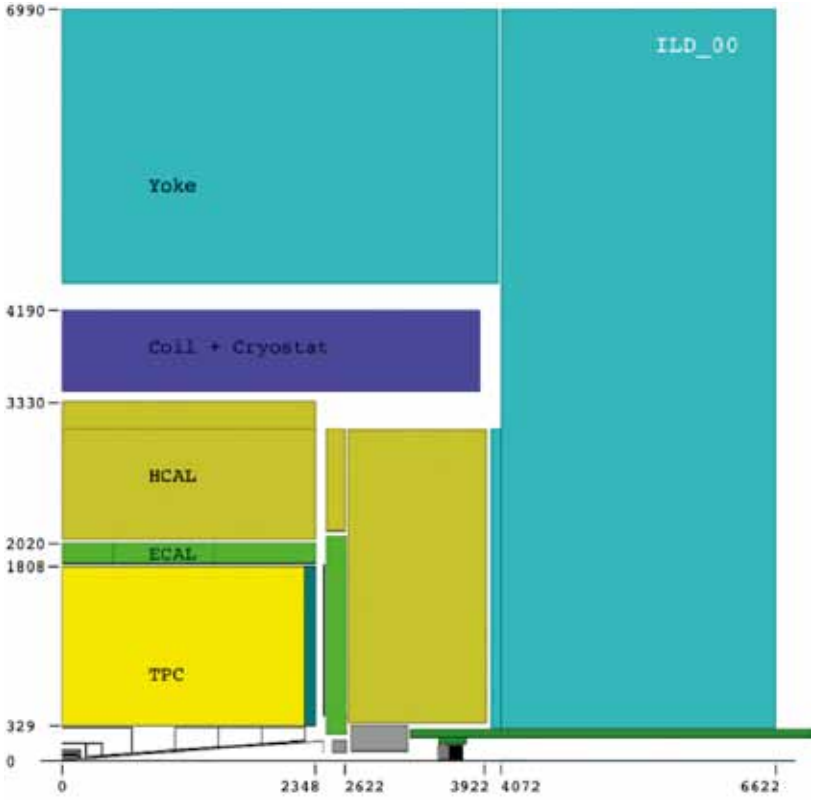

Figure 3.2 Quadrant view of the ILD detector model. The interaction point is in the lower left corner. Image: ILD

The ILD study group formed in 2007. It is a loose organisation with some 700 people from all three regions who signed the latest document, the Letter of Intent for ILD. The goal of the group is to prepare a coherent and integrated design of a detector for the ILC that meets the physics requirements in a way that is well balanced between cost and performance. The group closely cooperates with a number of detector R&D groups that develop technologies and sub-detector concepts for a detector at the ILC.

3.2 The vertex detector

To unravel the underlying physics mechanisms of new observed processes, the identification of heavy flavours will play a critical role. One of the main tools for heavy flavour identification is the vertex detector. The physics goals dictate an unprecedented spatial three-dimensional point resolution and a very low material budget. The running conditions at the ILC impose the readout speed and radiation tolerance. These requirements are normally in contradiction. High granularity and fast readout compete with each other and tend to increase the power dissipation. Increased power dissipation in turn leads to an increased material budget. The challenges on the vertex detector are considerable and significant R&D is being carried out on both the development of the sensors and the mechanical support.

The difficulty and novelty of the sensors drive the investigation of many different sensor designs worldwide and a wide array of sensor technologies is being considered. One architecture, which has been successfully employed before at an electron-positron collider, is based on a pixel-based charged-coupled device (CCD) technology. The new technologies are based on buried-channel CCDs with the charge collected from the thin epitaxial silicon layer. Typically only part of this epitaxial layer is depleted, and electrons created in this layer diffuse and are eventually collected in potential wells – the buried channel. The electrons generated during the passage of a charged track can spread over several pixels by diffusion and can serve to improve the position resolution. As the epitaxial layer is relatively thin, CCD-based pixel detectors have yielded the highest-performance vertex detector yet constructed. The new technologies are based on very small pixels, down to 5 × 5 micrometres square (μm^2) in size.

The depleted field effect transistor (DEPFET) detector is another major branch of sensor R&D. It combines the sensor and readout amplifier into the pixel FET structure such that the signal charge is collected on the internal gates of the transistors. Readout is performed by cyclically enabling transistor rows by a combination of steering and readout application-specific integrated circuits (ASICs) mounted at the ends and along the edges of the sensors. DEPFETs have the potential to be one of the technologies with the lowest power consumption. This technology, the development of which originated within the ILC community, is currently being developed for the vertex detector for the BELLE-II detector at KEK in Japan.

Another technology is the monolithic active pixel sensor (MAPS) architecture, which integrates, on the same substrate, the detector element with the processing electronics. This ability could prove very powerful for the demanding performance of vertex detectors. These devices can now be fabricated using standard CMOS processes available through many commercial microelectronics companies. The ability of the monolithic CMOS sensors to provide charged particle tracking has been demonstrated on a series of prototypes that have been successfully employed as tracking stations for the test beams at CERN in Switzerland and DESY in Germany.

There are two technologies for integrated detector and readout where the different functionalities are implemented in separate silicon tiers. The silicon-on-insulator (SOI) technology separates the detector element from the electronics tier through a thin buried oxide layer. Prototype devices

have been fabricated for imaging applications. A second technology is the 3-D vertical integrated silicon technology. This technology utilises vertical integration of several layers of electronics, where each layer can be as thin as 7 microns. The layers are electrically connected using micron-sized vertical metal connections called vias. The detecting element can be one of the layers or can be a separate layer optimised for the specific application, interconnected using the same bonding techniques.

An integral part of the development of a high-performance vertex detector is R&D in the support materials. Different groups are studying an array of low-mass materials such as various reticulated foams and silicon-carbide materials. An alternative approach that is being pursued very actively is the embedding of thinned, active sensors in ultra low-mass media. This line of R&D explores thinning active silicon devices to such a thickness that the silicon becomes flexible. The devices can then be embedded in, for example, Kapton structures, providing extreme versatility in designing and constructing a vertex detector.

Closely related to the material budget is the issue of power delivery. Higher power consumption in general increases the material budget because of the higher cooling requirements. The vertex detector designs assume that the power can be pulsed during bunch trains. Careful studies need to be carried out to evaluate the sensitive trade-off between ease of cooling and functionality, which requires more power and material budget.

The vertex detector for SiD uses a barrel-disk layout. The barrel section consists of five silicon pixel layers with a pixel size of 20 x 20 μm^2. The forward and backward regions each have four silicon pixel disks. In addition, there are three silicon pixel disks at a larger distance from the interaction point to provide uniform coverage for the transition region between the vertex detector and the outer tracker. This configuration provides for excellent hermeticity with uniform coverage and guarantees good pattern recognition capability for charged tracking and excellent impact parameter resolution over the whole solid angle. The layout of the vertex detector provides for stand-alone tracking capability, which in turn allows for a very compact tracking volume enabling an economic choice for a high-granularity calorimeter.

To provide for a very robust track-finding performance, the SiD detector has as its baseline choice for the vertex detector a sensor technology that provides putting a time stamp on each hit with sufficient precision to assign each hit to a particular bunch crossing. This significantly reduces the effective backgrounds. Two technologies are being researched. The first is a CMOS-based monolithic pixel sensor called chronopixel. The main goal for the design is a pixel size of about 10 x 10 μm^2 with 99% charged-particle registration efficiency. The second, more challenging technology, is the 3-D vertical integrated silicon technology.

The vertex detector for ILD is not required to have the time resolution to separate different beam bunches (approximately 700 nanoseconds apart) thanks to the very powerful track reconstruction capability of other tracking detectors, such as strip inner tracking detectors and TPC, surrounding the vertex detector. Therefore, it has a wider variety of options for the sensor

technology than the SiD detector concept. The technologies presently considered promising and the R&D under way are CMOS sensors, DEPFETs, fine-pixel CCDs (FPCCD), and in-situ-storage image sensors (ISIS). Recently, CMOS sensors exploiting vertical integration technology have also been developed.

There are two ideas of the sensor configuration of the ILD vertex detector as shown in *Figure 3.3*: the five-single-layer option and the three-double-layer (for a total of six layers) option. In both cases, pixel sensor layers surround the beam pipe coaxially and no forward disk, as is seen in SiD, exists. The angular coverage is $|\cos\theta| < 0.97$ for the innermost layer and $|\cos\theta| < 0.9$ for the outermost layer. R&D efforts for realising light material detectors with these sensor configurations as well as R&D for various sensor technologies are ongoing.

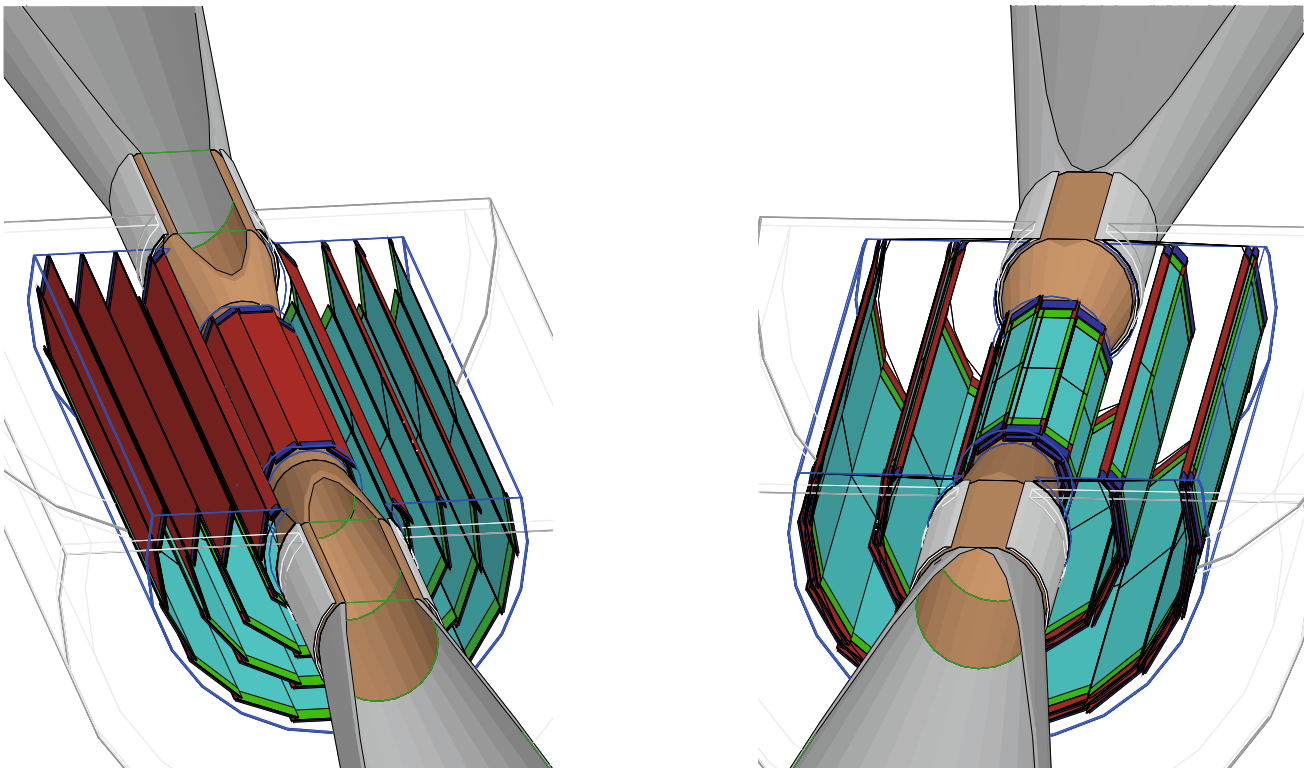

Figure 3.3 Vertex detector geometries for ILD. Left: five-single-layer option. Right: three-double-layer option. Image: ILD

3.3 Tracking for the linear collider detectors

The tracking system is a central part of the detector concepts at the ILC. The particle flow algorithm requires excellent tracking with superb efficiency and two-particle separation. The requirements from precision measurements, in particular in the Higgs sector, place high demands on the momentum resolution. The main performance goals of the tracker imposed by the physics are summarised in *Table 3.1*. The two ILC detector concepts, ILD and SiD, follow different philosophies in tracking. We shall briefly describe the SiD and ILD tracking systems, summarise their simulated performance and, in each case, give an overview of the R&D status.

Momentum resolution (~4 T)	$\delta(1/pt) \sim 2 - 5 \times 10^{-5}$/GeV/c all tracking detectors
Solid angle coverage	Up to $\cos\theta \sim 0.98$
Material budget	~0.10 – 0.15 X_0 to the ECAl in r ~0.20 – 0.25 X_0 in z
Performance	~99% all tracking
Background robustness	Full efficiency with 1% occupancy
Background safety factor	Trackers will be prepared for 10-times-worse backgrounds at the linear collider start-up

Table 3.1 An overview of goals for the performance of linear collider tracking.

3.3.1 SiD tracking

The design of the tracking system of the SiD detector is driven by the combined performance of the pixel detector at small radius, the tracker at large radius and the electromagnetic calorimeter for the identification of minimum ionising track stubs. With the choice of a 5-T solenoidal magnetic field, in part chosen to control the electron-positron pair background, the design allows for a compact tracker design. The technology of choice is silicon strip sensors arrayed in five nested cylinders in the central region and four disks following a conical surface with an angle of 5 degrees with respect to the normal to the beamline in each of the end regions for precision tracking and momentum measurement. The geometry of the end caps minimises the material budget to enhance forward tracking. The detectors are single-sided silicon sensors, approximately 10×10 cm^2 with a strip pitch of 50 µm. The end caps utilise two sensors bonded back-to-back for small angle stereo measurements. With an outer cylinder radius of 1.25 metres and a 5-T field, the charged track momentum resolution will be better than $\sigma(1/p_T) = 5 \times 10^{-5}$ (GeV /c)$^{-1}$ for high momentum tracks. *Figure 3.4* shows an isometric view of the SiD tracking system and the material budget as a function of the polar angle.

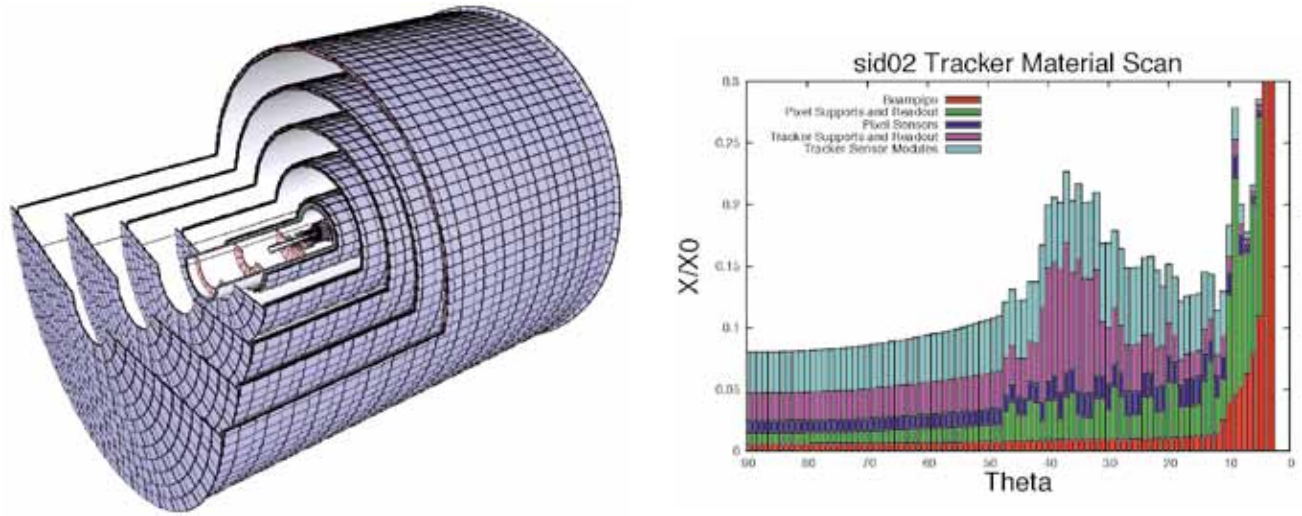

Figure 3.4 Isometric view of the SiD tracking system (left) and total material budget of the tracking system as function of the polar angle (right). The different detector components are indicated. Images: SiD

Status of R&D for SiD tracking

The design of a tracking system at the ILC must minimise the material in front of the calorimeter that might compromise particle-flow jet reconstruction. Furthermore, establishing and maintaining the alignment for the tracker is critical. Even with the largest feasible magnetic field, the tracking volume is quite large, demanding optimised tracker components that facilitate mass production. Finally, the tracker must be robust against beam-related accidents and aging and all these requirements must be maintained within a push-pull scenario.

The silicon modules are supported on a sandwich of pre-impregnated carbon fibre composite around a Rohacell core. The support structures are barrels in the central regions and cones in the forward region. Each support cone is supported off a barrel. Finite element analyses show that these structures meet the static rigidity requirements. It is expected that openings will be cut in the support structures to reduce material once module mounting locations are known. These openings not only reduce the number of radiation lengths, but also reduce the weight to be supported. Openings may also be needed for an optical alignment system. Prototype structures will be built to confirm that the support structures will meet the requirements. Also, dynamic tests will be carried out in a magnetic field with pulsed power.

The tracker employs a modular, hybrid-less design for the silicon readout modules to meet the stringent material budget requirements. This unique design relies on the gold stud bump-bonding of a 1024-channel readout chip directly to the silicon sensor, the signals of which are routed to the readout chip using a double metal layer. Prototype sensors and readout chips with a reduced channel count have been characterised. The readout chips meet the specifications. Initial prototype readout modules have revealed some areas for further study in the bonding of the readout chip and cable to the sensor. Work on the design of a lightweight module frame is in progress.

The bunch structure at the ILC allows for power-pulsing, that is, the readout is current-starved between bunch trains. This makes active cooling unnecessary and allows the tracker to be air-cooled. Ongoing studies demonstrate that the power budget can be met and that the mechanical stability can be maintained with pulsed power in a high magnetic field environment. With judicious routing of power leads, Lorentz forces can be largely cancelled. Such designs, however, need to be simulated and tested to ensure that all design specifications within a 5-T magnetic field with power pulsing can be met. To date studies of signal communication have not been carried out. Such studies are foreseen once full prototype modules and ladders are available.

The unprecedented track momentum resolution demands minimising systematic uncertainties in sub-detector relative alignments. The fact that the two ILC detectors will swap places on the beamline puts a premium on alignment stability and in situ alignment monitoring that does not depend on tracks. Development work is expected to occur to demonstrate that the goals for structural stability will be achieved in a tracker system meeting the material budget. The SiD tracker is considering two alignment methods, one based on frequency-scanning interferometry (FSI) and one based on infrared-transparent silicon sensors (ITSS).

The FSI system incorporates multiple interferometers fed by optical fibres from the same laser sources, where the laser frequency is scanned and fringes counted, to obtain a set of absolute lengths. With a test apparatus precisions better than 100 nanometres (nm) have been attained using a single tunable laser when environmental conditions are carefully controlled. Precisions under uncontrolled conditions (e.g., air currents, temperature fluctuations) were, however, an order of magnitude worse with the single-laser measurements. Hence a dual-laser FSI system is foreseen for the tracker, which employs optical choppers to alternate the beams introduced to the interferometer by the optical fibres. By using lasers that scan over the same wavelength range but in opposite directions during the same short time interval, major systematic uncertainties can be eliminated. It will be important to monitor tracker distortions during the push-pull operations, not only for later track reconstruction, but also to ensure that no damage-inducing stresses are inadvertently applied to the tracker components.

The second method exploits the fact that silicon sensors have a weak absorption of infrared (IR) light. Consecutive layers of silicon sensors are traversed by IR laser beams, which play the role of infinite momentum tracks. Then the same sophisticated alignment algorithms as employed for track alignment with real particles can be applied to achieve relative alignment between modules to better than a few microns. This method employs the tracking sensors themselves, with only a minor modification to make them highly transparent to infrared light. Since IR light produces a measurable signal in the silicon bulk, there is no need for any extra readout electronics. The development of a prototype system that demonstrates the ability to achieve and maintain the required alignment tolerances will be a major focus of future R&D.

3.3.2 ILD tracking

The ILD concept has chosen a combination of continuous tracking and discrete tracking, the former being a TPC central tracker and the latter being layers of silicon detectors. This combination has been chosen to provide a robust system with superb pattern recognition ability due to the large and redundant number of points provided and the complementary strength of silicon and gaseous tracking.

The interaction point is surrounded by a multi-layer pixel-vertex detector (VTX) followed by a system of strip and pixel detectors. In the barrel, two layers of silicon strip inner tracking detectors (SIT) are arranged to bridge the gap between the VTX and the TPC. In the forward region, a system of silicon pixel and silicon strip forward tracking disks (FTD) provides low angle tracking coverage.

A large volume TPC with up to 224 points per track provides continuous tracking for a large volume. The TPC is optimised for excellent three-dimensional point resolution and minimum material in the field cage and in the end plate. It also provides particle identification capabilities based on the energy loss of particles per unit of distance (dE/dx).

A system of Si-strip detectors provides additional high-precision space points, which improve the tracking measurements and provide additional redundancy in the regions between the main tracking volume and the calorimeters. It consists of the silicon internal tracker (SIT) between the vertex detector and TPC, the end cap tracking detector (ETD) behind the end plate of the TPC, and the silicon external tracker (SET) between the TPC and the electromagnetic calorimeter (ECAL) The performance of the ILD tracking system is illustrated in *Figure 3.5*.

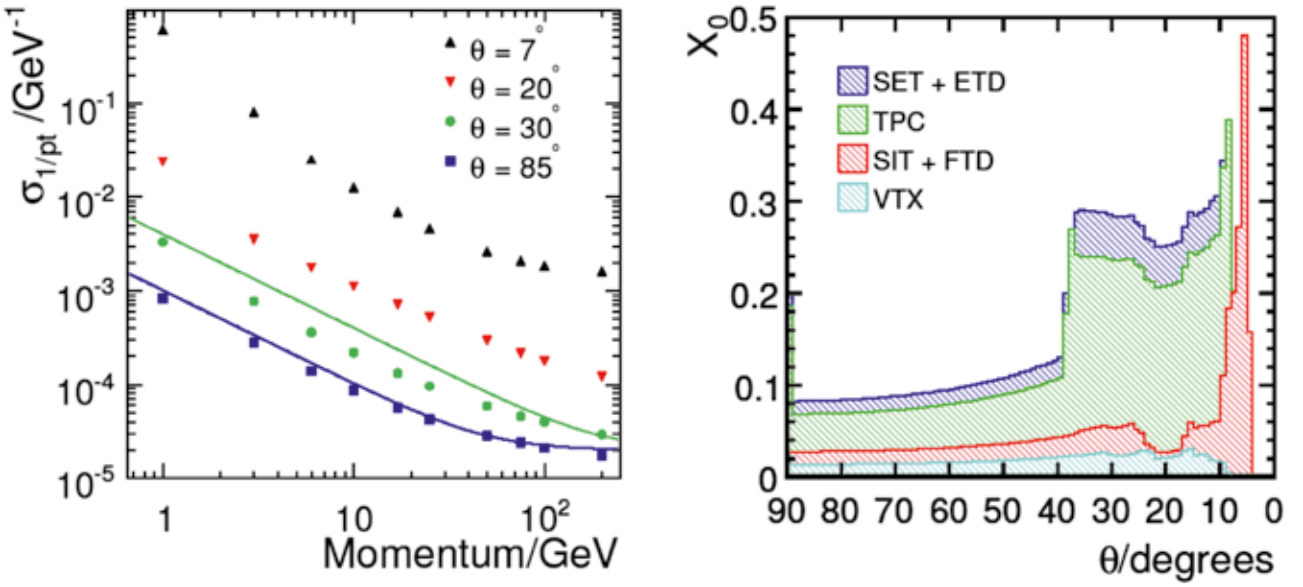

Figure 3.5 Left: transverse momentum resolution in the ILD detector concept for different angles relative to the beam. The lines show the resolution goals parametrised as $\sigma\{1/p_T\} = 2\times10^{-5} \oplus 1\times10^{-3}/(p_T \sin\theta)$. Right: total amount of material in the tracker as a function of the polar angle. Indicated are the different detector components in the ILD tracker. Images: ILD

The time projection chamber in ILD

The TPC for the ILC (see *Figure 3.6)* is based on a lightweight field cage, read out by micro-pattern gas detectors (MPGD) at either end. MPGDs have been chosen since they promise better performance than the more traditional wire chamber readout, are robust, lightweight and comparatively cheap. They lend themselves well to a system with small readout pads as it is needed for a high spatial resolution. In addition MPGD provide a significant suppression of the flow of positive ions back into the drift field, a major obstacle for a TPC, which needs to be operated continuously throughout an ILC bunch train. In addition, the well proven method of a gate will be foreseen to eliminate the remaining backflow.

The international linear collider-TPC collaboration (LC-TPC collaboration) is carrying out a comprehensive research programme to develop and establish the TPC as a possible solution for a tracker at the ILC. During the first phase of the work the fundamental principles of an MPGD-TPC have been established, gas properties have been measured, the achievable point resolution is understood, the resistive anode charge-dispersion technique has been demonstrated, and CMOS pixel readout technology has been demonstrated. The option of wire chamber-based gas amplification has been ruled out and a micro-mesh gaseous detector (or Micromegas, a fine micromesh structure) with standard pads has been ruled out as well.

The second phase of the work is currently ongoing. The main focus here is on the design, construction and operation of a large prototype and is expected to take another two to three years. The main goal of this work is to establish and demonstrate a large TPC readout with MPGDs in a realistic setting and with magnetic field. Both gas electron multiplier (GEM) and Micromegas readout technologies are studied. They are state-of-the-art technologies to detect electrons with gas amplification and fine-grain sensors. An important ingredient will be the demonstration that the field homogeneity can be controlled at the required level. Tests with the large prototype and different readout schemes will continue. The TPC will be upgraded to a lightweight end cap and exposed to electron and possibly hadron beams. A much improved readout system will be tested, one that is more compact and will include facilities for power pulsing. A conceptual design of a TPC will be prepared for the *Detailed Baseline Design Report.* Cabling, power pulsing and active carbon dioxide (CO_2) cooling will be studied as well.
The third phase, the final design and building phase, will commence once the ILC project gets the green light. The three phases described above overlap naturally; for example, certain aspects of the design have already started in preparation for the detailed baseline document.

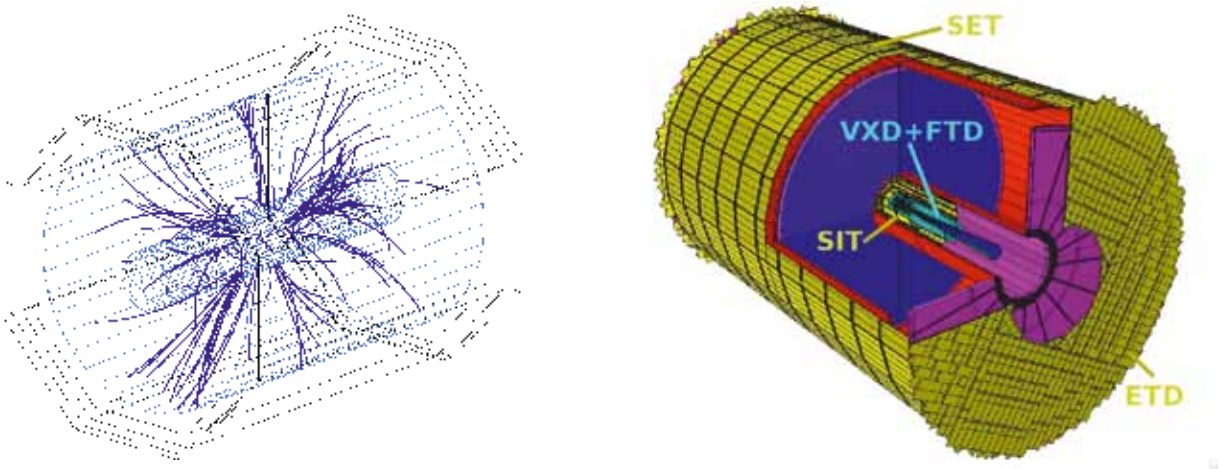

Figure 3.6 Three-dimensional view of the ILD time projection chamber after removal of machine background using a simple algorithm (left) and the silicon tracking system (right). VXD: vertex detector; FTD: forward tracking disks; SIT: silicon internal tracker; ETD: tracker behind the TPC end cap; SET: silcon external tracker. Images: ILD

Silicon tracking in ILD

The silicon tracking system in ILD is a combination of pixel and strip detectors. The forward direction, below the acceptance of the TPC, is covered by a number of pixel disks followed by disks instrumented with crossed-strip detectors. In total, seven stations will provide robust and powerful tracking. In the central region and behind the endplate of the TPC, strip detectors provide high-precision points inside and outside the TPC. The same strip sensor technology and sensor size (except for the FTD disks) is used throughout the system to simplify the system layout and maintenance. A view of the system is shown in *Figure 3.6*.

Significant development work is ongoing to provide sensors and readout systems for this large and complex system. The ladders are realised in deep sub-micron technology. An intense effort is underway to develop edgeless sensors, which would make the tiling of the sensors into a detector much simpler and help reduce the material budget. The integration of the pitch adapter and the readout onto a module made of one or a few sensors are studied to minimise the complexity and the amount of material. Challenging R&D is actively pursued on the front-end readout chip that must fully process the signals from a large number of channels up to and including digitisation. Modern deep sub-micron CMOS technology has been chosen to optimise the performances of the on-detector front-end electronics.

A major goal for the overall design of the system is to provide a lightweight support structure, minimising the material budget but still maintaining the overall tolerances. Studies into the use of new and advanced materials are underway in close cooperation with the Large Hadron Collider (LHC) experiments at CERN, Switzerland, which face similar problems.

Another challenge is to ensure that the system can be aligned quickly and precisely. The chosen scheme uses two different types of laser monitoring systems. One shines an IR laser through the ladders and provides a relative alignment between ladders. Another aligns a complete system relative

to another sub-detector, for example the TPC, through the use of an interferometry system. In addition, the final alignment will be accomplished using tracks from physics events. The capability of the system to provide precise timing will add another powerful tool to help combine information from the silicon tracker and the time projection chamber.

First prototypes of most of the individual parts of the system have been developed and tested with beam. Part of the programme is a combined test of silicon tracking detectors and the time projection chamber in the presence of a magnetic field. The next two years will be devoted to building a complete realistic prototype system, which will be the basis for a realistic conceptual design of the silicon tracking system.

3.4 Calorimetry

3.4.1 Overall design requirements

The baseline designs for the ILD and SiD detectors incorporate the elements needed to successfully implement the particle flow approach, introduced earlier. This imposes a number of basic requirements on the calorimeter systems. The entire central calorimeter system must be contained within the solenoid in order to reliably associate tracks to energy deposits. The electromagnetic and hadronic sections of the calorimeter must have imaging capabilities that allow both efficient track-following and correct assignment of energy clusters to tracks. These requirements imply that the calorimeters must be finely segmented both longitudinally and transversely. In order to ensure that no significant amount of energy can escape detection, the calorimeter system must extend down to small angles with respect to the beam pipe and must be sufficiently deep to prevent significant energy leakage. Since the average penetration depth of a hadronic shower grows with its energy, the calorimeter system must be designed for the highest-energy collisions envisaged.

The mechanical design of the calorimeter must consist of a series of modules of manageable size and weight to ease detector construction. The boundaries between modules must be as small as possible to prevent significant un-instrumented regions. Module boundaries, which do not project onto the interaction point, avoid the non-detection of high-momentum particles. The detectors must have excellent long-term stability and reliability, since access during the data-taking period will be extremely limited, if not impossible.

3.4.2 Electromagnetic calorimeter design requirements

For the efficient identification of individual jet components, it is important that the electromagnetic energy depositions of electrons and photons be as compact as possible to avoid overlaps and confusion. This implies the use of a dense absorber material and minimal active shower sampling gaps between the absorber layers, imposing significant design constraints. The energy resolution of the electromagnetic calorimeter should make a negligible contribution to the overall jet energy resolution. The calorimeter should provide efficient identification of electrons and photons and allow the reconstruction of neutral pions in jets and tau lepton decays to improve jet energy resolution and to discriminate between different tau final states. Due to the narrow size of electromagnetic showers in the ECAL, it is important that module boundaries do not project onto the interaction point.

3.4.3 Hadronic calorimeter requirements

The hadronic calorimeter (HCAL) must be divided into a sufficient number of layers that hadronic showers can be well identified and associated with charged tracks, or identified as a the result of a neutral particle, as appropriate. The radial space for the hadronic calorimeter is therefore divided into alternating layers of steel absorber and active sections, with the need to keep the latter as thin as possible to prevent the increase of lateral shower size and keep the overall detector volume compact. There must also be a fine transverse segmentation to allow efficient charged track following for the particle flow algorithm. Within the detector modules, the active layers should have a good uniformity of response and a reliable monitoring and control system.

3.4.4 The SiD and ILD calorimeter systems

The combined SiD electromagnetic and hadronic calorimeter systems consist of a central barrel part and two end caps (*Figure 3.7)*. The entire barrel system is contained within the volume of the cylindrical superconducting solenoid. The electromagnetic calorimeter has silicon active layers between tungsten absorber layers. The structure has 30 layers in total, the first 20 layers having a thinner absorber than the last ten layers. This configuration attempts to compromise between cost, electromagnetic shower radius, sampling frequency, and shower containment. The total depth is 26 radiation lengths (X_o). The hadronic calorimeter has a depth of 4.5 nuclear interaction lengths (λ), consisting of alternating steel plates and active layers. The baseline choice for the active layers is glass resistive plate chambers, but several other technologies are also being prototyped and evaluated.

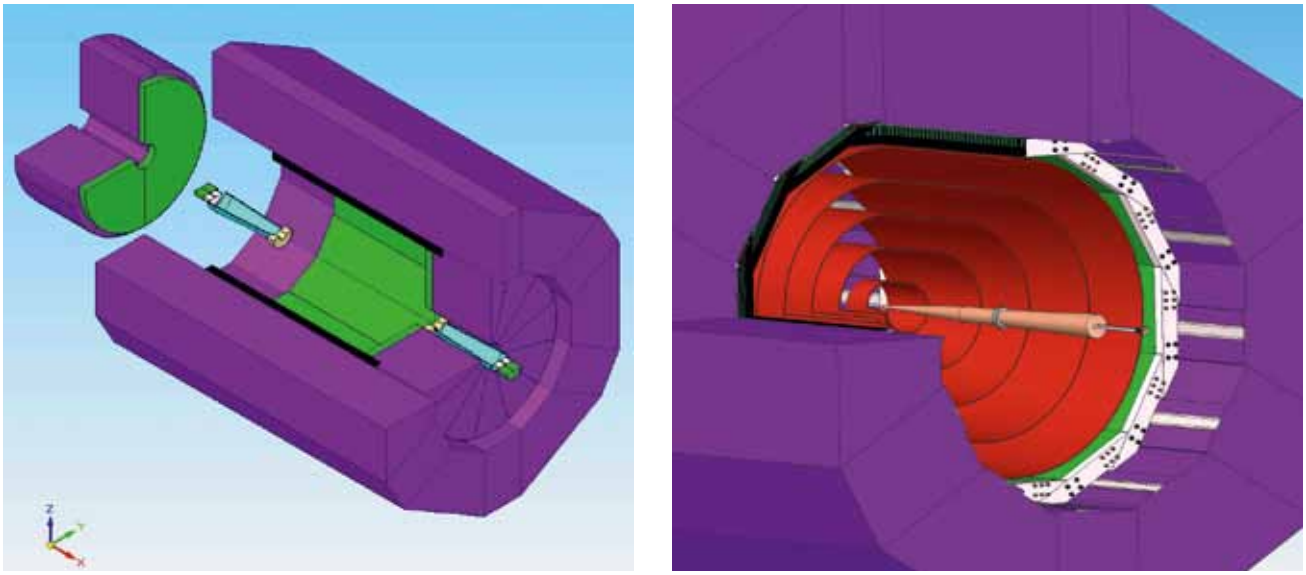

Figure 3.7 The SID calorimeter system. Images: SiD

The hadronic calorimeter is split into three along the beam direction, and into 12 azimuthal sections, giving reasonably sized modules for individual construction while keeping the number of boundaries between modules (and hence dead regions) to a minimum. Each end cap hadronic calorimeter will be in the form of a plug that is split along a vertical median line.

The ILD calorimeter design is guided by similar principles. The main parameters, such as the aspect ratio, inner radius, depth and granularity, have been optimised using a particle flow algorithm package called Pandora. Both electromagnetic and hadronic sections with tungsten and steel, respectively, as absorbers, are situated inside the solenoid as in SiD, however ILD uses a shorter barrel and larger end caps and has an eight-fold azimuthal symmetry. The ECAL (*Figure 3.8)* is segmented into 30 sampling layers corresponding to 24 X_0. The HCAL has 48 layers and a total depth of 5.5 λ, in addition to the ECAL. Several baseline technologies are considered for the instrumentation of the active layers: silicon pad diodes or scintillator strips with a transverse segmentation of 0.5 to 1 cm for the ECAL and 3 x 3 cm^2 scintillator tiles or gaseous devices with a segmentation of 1 x 1 cm^2 for the HCAL.

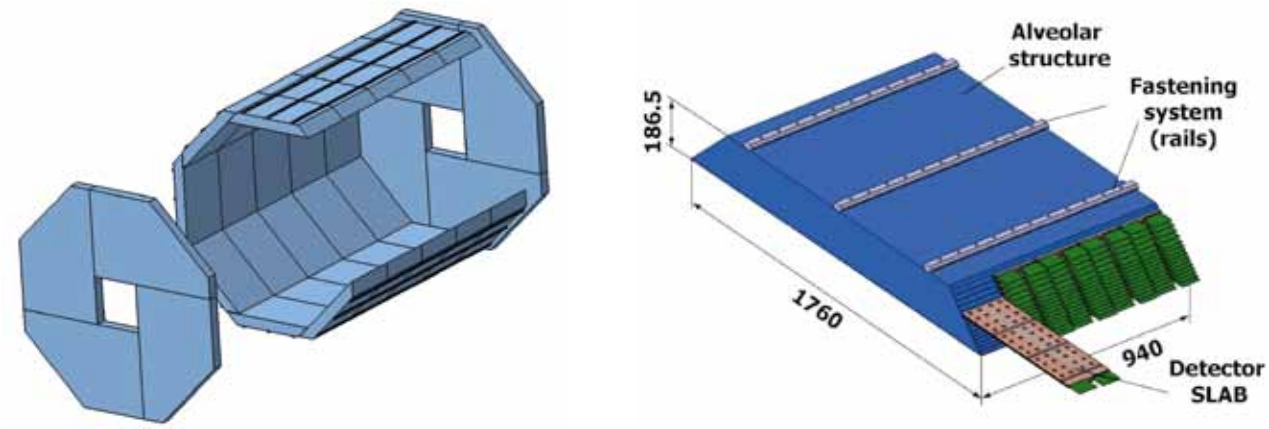

Figure 3.8 The ILD ECAL structure and details of a barrel module. Images: ILD

3.4.5 Electromagnetic calorimeter R&D

The requirements described above have given rise to the design of sampling electromagnetic calorimeters with tungsten absorbers because of its small Moliere radius and short radiation length. The active layers must be thin (to limit the size of the calorimeter's effective Moliere radius) with a highly segmented readout to provide the required transverse granularity.

The CALICE (Calorimeter for Linear Collider Experiment) collaboration presently pursues three technologies for the active part of the calorimeter: one based on matrices of silicon pad sensors, the second on strips of scintillator readout by compact photo-detectors and the third based on silicon pixel sensors with a digital readout.

The silicon-based approach uses matrices of 5 x 5 square millimetre (mm^2) pads made in 300- to 500-micron-thick high-resistivity silicon, fully depleted by a reverse bias voltage of around 200 volts (V). The advantages of this technology are its compactness, the ease of implementing high transverse granularity, and the stability of its response with respect to environmental factors. The scintillator-based option is based on 45 x 5 x 2 mm^3 scintillator strips individually read out by novel Geiger mode multi-pixel photo-sensors, so-called silicon photo-multipliers (SiPM), e.g. multi-pixel photon counter (MPPC) devices (*Figure 3.9).* The small size of the MPPC, its dynamic range and excellent photon-counting capabilities and its insensitivity to magnetic fields make it a very suitable detector for this application. The cost of this approach may be less than for a silicon-based ECAL.

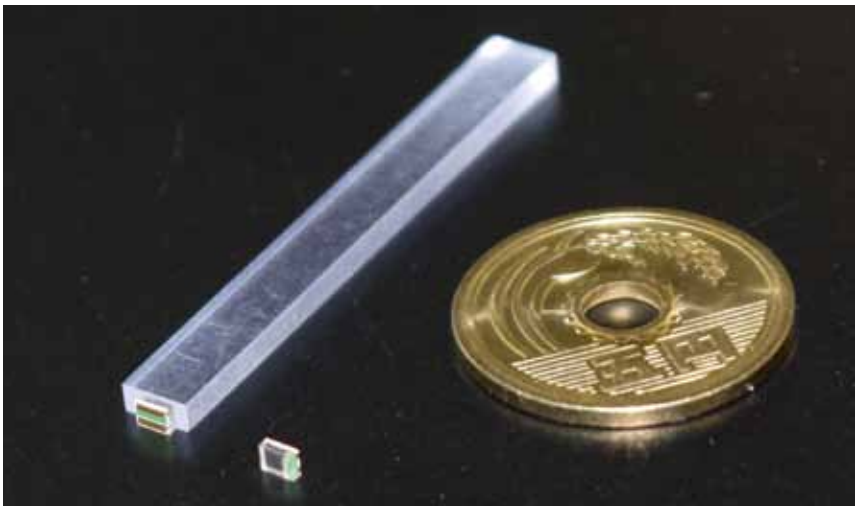

Figure 3.9 5 x 45 x 2 mm^3 scintillator strip and MPPC sensor. Image: CALICE

Prototype calorimeters of these two types have been constructed and tested in particle beams over a number of years. A 30-layer silicon-tungsten (SiW) prototype with almost 10,000 channels in a volume of 18 x 18 x 20 cm^3 has been tested *[3-1]*. A scintillator-based prototype consisting of more than 2,000 scintillator strips in 30 detection layers has also been produced and tested *[3-2]*. The measured performance, in terms of response linearity and energy resolution, of both these prototypes is in line with the expectations from detector simulation and sufficient for the requirements of a detector at a future linear collider.

The groups developing these two technologies are now working closely together on the development of a second-generation prototype, which will address technological questions of the integration of these technologies into a full detector in order to prepare for a detailed detector design. The possibility of a hybrid ECAL design with a mix of scintillator and silicon layers is also under study, with the development of dedicated reconstruction algorithms for such a detector.

Figure 3.10 Mechanical structure of technical prototype. Image: CALICE

A tungsten-carbon fibre composite mechanical structure (a slightly scaled-down version of a barrel module for ILD) has been constructed (*Figure 3.10)*. It will host detection layers based on both detector technologies. Several approaches to leakless water-based detector cooling are being tested. The front-end ASICs designed to read out the PIN detectors and SiPM devices (SKIROC2 and SPIROC2 respectively), including their power-pulsing capabilities, have been produced and are being tested. Studies of the integration process, including the manufacture of dedicated printed circuit boards (PCBs) to host the detection elements and front-end electronics (active sensor units) and their interconnection are also underway (*Figure 3.11)*. Further development of the detection elements (PIN matrices, scintillator strips and MPPCs) are continuing, with a move to 5-mm granularity for improved physics performance, and design developments (working closely with industrial partners) for lower cost and simpler detector construction. The CALICE data acquisition system is being developed to read out these and other calorimeters, and to be scalable to detectors required for a linear collider.

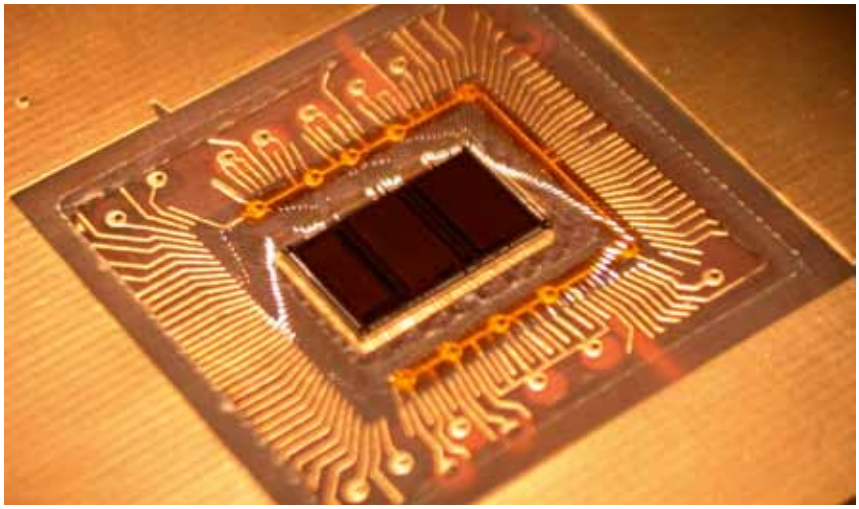

Figure 3.11 SKIROC2 chip bonded on detector PCB (active sensor unit). Image: CALICE

Progress is continuing on understanding the key issues surrounding the development of CMOS sensors, which could be used in a binary pixel readout ECAL. The R&D effort has concentrated on measuring the minimum ionisation particle efficiency of various sensor types and studying the density of particles in the electromagnetic shower downstream of tungsten, using data collected at a series of test beams carried out with pion and electron beams at CERN and DESY. Preliminary results demonstrate the significant improvements afforded by a new CMOS process called INMAPS that was developed during the project *[3-3]*. Work is continuing on the measurement of the electromagnetic shower density, an essential input to the choice of pixel size.

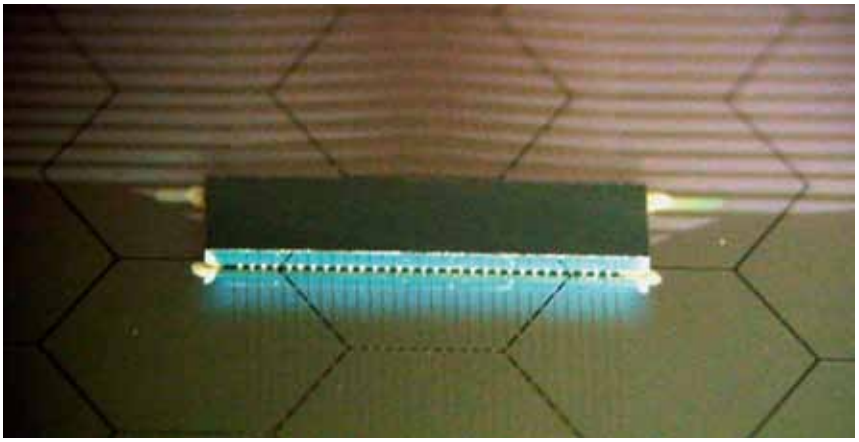

Figure 3.12 A prototype (256-channel) KPiX chip bump-bonded to a sensor. Hexagonal pixels are 13 mm^2. Image: SiD

The SiD ECAL R&D (carried out outside the CALICE collaboration) makes use of innovations in interconnect technologies that combine readout electronics and silicon sensors into a dense, highly segmented imaging electromagnetic calorimeter which, as discussed above, is required to fully exploit the ILC physics potential. The key developments include a fully integrated readout of silicon sensors with 1024 13-mm^2 pixels and interconnect technologies that make small 1- to 1.25-mm readout gaps possible, thus preserving the compact showers in tungsten. The current R&D status is that the technological steps are nearly complete: Having evaluated a series of smaller prototypes, the 1024-channel readout chip (KPiX) is currently in fabrication; the silicon sensors with 13-mm^2 pixels are in hand; and reasonable interconnect technology choices have been identified. After successful system tests, a full-depth module will be constructed for evaluation, which is planned in a test beam at SLAC. *Figure 3.12* is a photograph of a (256-channel) prototype KPiX readout chip affixed to a silicon sensor via bump bonding. *Figure 3.13* shows a flexible Kapton cable being affixed to a prototype sensor. The flex cable, sensor, and KPiX chip fit within the roughly 1-mm gap between tungsten layers.

Figure 3.13 Bonding of a flex cable to a prototype sensor. The cutout is for the KPiX chip. Image: SiD

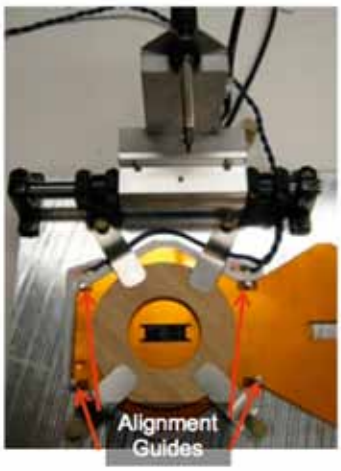

3.4.6 Hadronic calorimeter R&D

The R&D for the hadronic calorimeter of ILD and SiD is pursued in the framework of the worldwide CALICE collaboration. The goals are to establish the new technologies necessary to realise fine granularity, to validate the shower simulations at the detailed level required for particle flow reconstruction and to test these algorithms with real data. Once such a proof of principle is achieved in beam tests of first generation physics prototypes, the system design challenges are tackled with technological prototypes with the aim of demonstrating that the enormous channel densities can be accommodated in a large detector system without large dead spaces for cables, supplies and supports degrading the detector performance.

Both ILD and SiD groups foresee sampling calorimeters with stainless steel as absorbers and are considering different technologies for the active readout layers. These are based either on scintillator tiles of about 3 x 3 cm^2, optically read out by SiPMs (analogue readout, AHCAL) or on gaseous devices with gas amplification micro-structures with even finer 1 x 1 cm^2 segmentation and digital 1- or 2-bit readout (DHCAL). Resistive plate chamber (RPC), gas electron multiplier (GEM) and Micromegas technologies are under study.

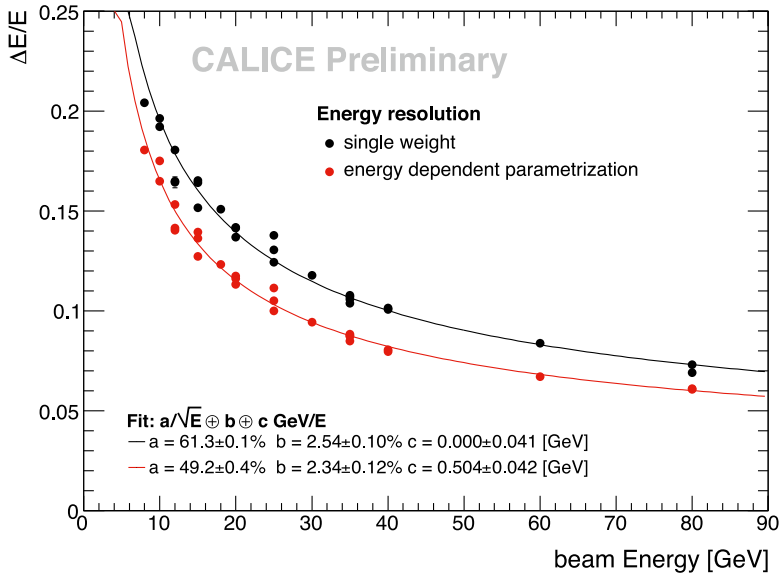

Figure 3.14 Hadronic energy resolution of the scintillator AHCAL prototype, without and with cell energy weighting. Image: CALICE

A cubic-metre-sized prototype of the AHCAL has been extensively tested at CERN and Fermilab in conjunction with silicon tungsten and scintillator tungsten electromagnetic calorimeters. The SiPM technology has proven to be robust and stable and has been chosen for applications in other high-energy physics experiments, for example Belle, CMS and T2K. The calorimeter has performed according to simulation-based expectation, with a resolution for single hadrons of 49%/√E (*Figure 3.14*). The detector shows very good imaging capabilities. For example, tracks are visible inside hadronic showers and used for calibration as well as for detailed feedback to refine the simulation models.

The high granularity and consequent low occupancy allows the use of event mixing techniques to study the performance of the Pandora particle flow algorithm with test beam data. The observed degradation of energy reconstruction for a neutral particle, as the distance to nearby charged particle showers decreases, is well reproduced by simulation; see *Figure 3.15*. This lends strong support to the jet energy performance prediction for the full detector, based on the same algorithm and critically depending on the particle separation power.

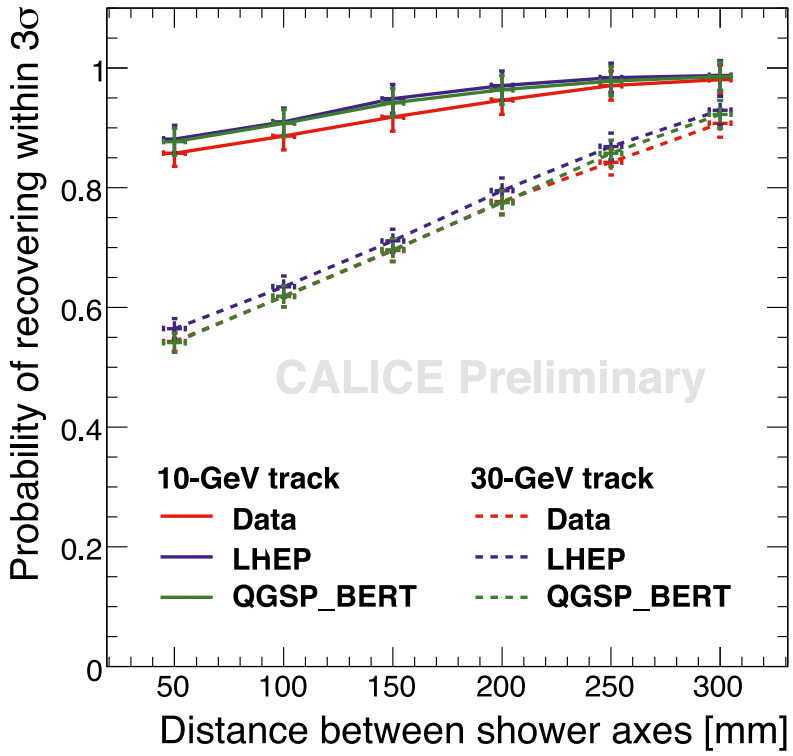

Figure 3.15 Reconstruction quality as function of distance to a nearby shower, in SiW ECAL plus scintillator AHCAL test beam data and simulation. Image: CALICE

An intensive effort is underway to establish the exciting concept of digital calorimetry with gaseous devices for the ILC. Following encouraging performance with a tabletop prototype, the first RPC-based full cubic-metre-sized system, with almost 400,000 channels, was assembled and exposed to hadron beams in the autumn of 2010 for the first time. The imaging resolution of the device is superior, as can be seen from the first events recorded, *Figure 3.16*. A comprehensive test beam programme is in full swing in 2011, including tests in conjunction with the SiW ECAL prototype and different devices. It will deliver the data set to establish the calorimetric and particle flow performance in time for the DBD.

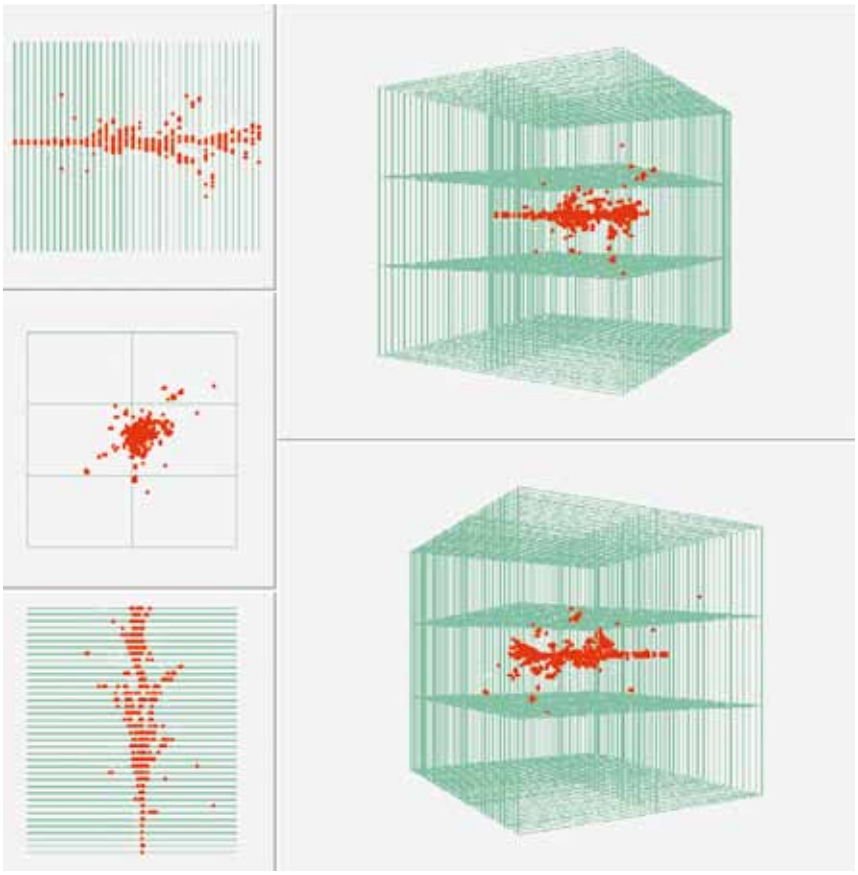

Figure 3.16 Online displays of test beam events in a cubic meter RPC DHCAL prototype. Image: CALICE

In order to handle the high granularity in a full collider detector, the front-end electronics must be integrated into the detector volume and the data be digitised as early as possible. The feasibility depends crucially on the development of ultra-low power, highly integrated micro-electronics ASICs. The 'ROC' chip family, for example, uses common building blocks for the use with different calorimeter technologies for AHCAL, DHCAL and ECAL. The first electronics modules of the second-generation chips have been tested in the beam with tiles and SiPMs as well as with gaseous devices, and full new AHCAL, ECAL and RPC DHCAL prototypes are in preparation.

Glass RPCs are the forerunner in integrating the new, highly integrated power-pulsed readout electronics. It was shown to function well in magnetic fields of more than 3 T. Square-metre planes were tested and a full stack is underway. This will allow tests of 2-bit readouts, expected to improve the resolution for higher particle energies. R&D on other gaseous techniques, GEMs and Micromegas, is being followed with vigour, too. Limited resources currently do not permit exploiting each of them at full cubic-metre scale, but this is also not necessary at this stage. Instead, small stacks and large areas have been successfully tested. Thereby the specific features of the calorimetric response are studied and their understanding in terms of simulations is validated. At the same time for each of them critical technical issues for extrapolating to larger systems are actively addressed.

Conclusion

Altogether, this programme will establish technology options for a feasible particle flow calorimeter with well understood strengths and weaknesses. The next step will be to validate the system performance and interplay of the highly integrated prototypes.

3.5 Very forward calorimeters

Two special calorimeters are foreseen in the very forward region of the ILC detectors - LumiCal for the precise measurement and BeamCal for the fast estimation of the luminosity. For beam tuning a pair monitor is considered, positioned just in front of BeamCal. LumiCal is a precision device with challenging requirements on the mechanics and position control. BeamCal, positioned just outside the beam pipe, is exposed to a large amount of low-energy electron-positron pairs originating from beamsstrahlung. These depositions, useful for a bunch-by-bunch luminosity estimate and the determination of beam parameters, require radiation hard sensors.
The detectors in the very forward region have to tackle relatively high occupancies, requiring dedicated front-end electronics.

3.5.1 Design of the very forward region

A sketch of the very forward region of the ILD detector, as an example, is shown in *Figure 3.17*.

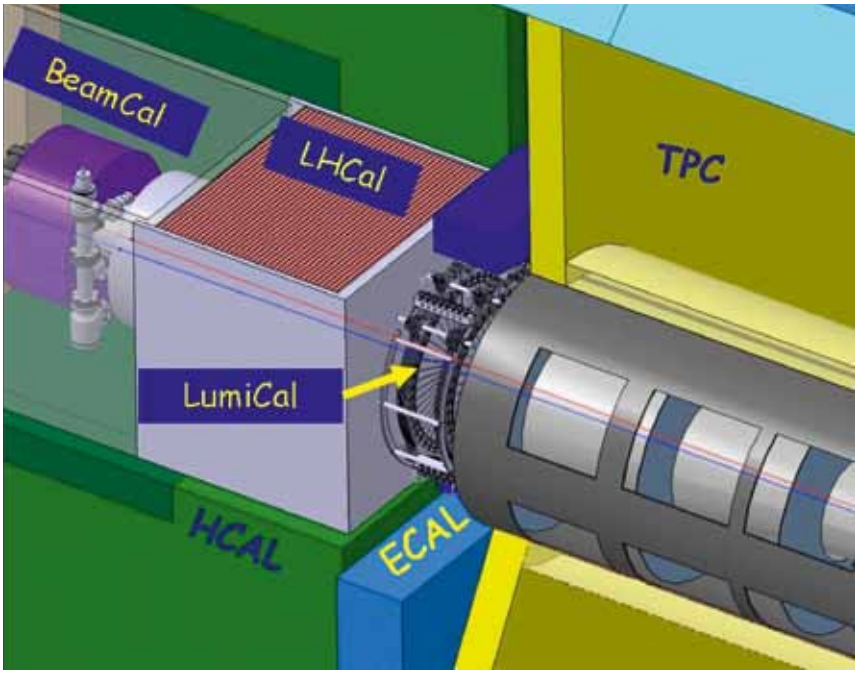

Figure 3.17 The very forward region of the ILD detector. LumiCal, BeamCal and LHCAL are carried by the support tube. Image: ILD

LumiCal and BeamCal are cylindrical electromagnetic calorimeters centred on the outgoing beam. BeamCal is placed just in front of the final focus quadrupole and LumiCal is aligned with the electromagnetic calorimeter endcap.

Both devices are designed as cylindrical sensor-tungsten sandwich calorimeters, consisting of 30 absorber disks, each 3.5 mm thick and corresponding to one radiation length, interspersed with sensor layers. Each sensor layer is segmented radially and azimuthally into pads. The granularity is optimised using Monte Carlo simulation.

Front-end ASICs are positioned at the outer radius of the calorimeters. BeamCal covers polar angles between 5 and 40 milliradians (mrad) and LumiCal between 31 and 77 mrad. The design of the very forward region of the SiD detector is very similar.

3.5.2 Sensor R&D

The challenge of BeamCal is to find sensors tolerating about one megagray (MGy) of dose per year. So far polycrystalline chemical vapour deposition (CVD) diamond sensors of 1 cm^2 and larger sectors of GaAs (gallium arsenide) pad sensors, as shown in *Figure 3.18* (left), have been studied. Since large-area CVD diamond sensors are extremely expensive, they may be used only at the innermost part of BeamCal. At larger radii GaAs sensors appear to be a promising option. Sensor samples produced using the liquid encapsulated Czochralski method and doped with tin and tellurium as shallow donors and chromium as a deep acceptor have been studied in a high-intensity electron beam. The charge collection efficiency is measured as a function of the absorbed dose. It decreases with growing dose; however signals of minimum ionising particles are visible up to a dose of 600 kilograys. The leakage current of a pad at room temperature before irradiation is about 200 nanoamps (nA) at an applied voltage of 50 V. After exposure of a dose of 1.2 MGy, leakage currents of up to a factor 2 larger were found, still tolerable for the application. Prototypes of LumiCal sensors of similar shape have been designed and manufactured by Hamamatsu Photonics. The pitch of the p-type pads on n-type silicon is 1.8 mm. All pads have a leakage current of a few nA and a depletion voltage of about 40 V. The capacitances range from 8 to 20 picofarads.

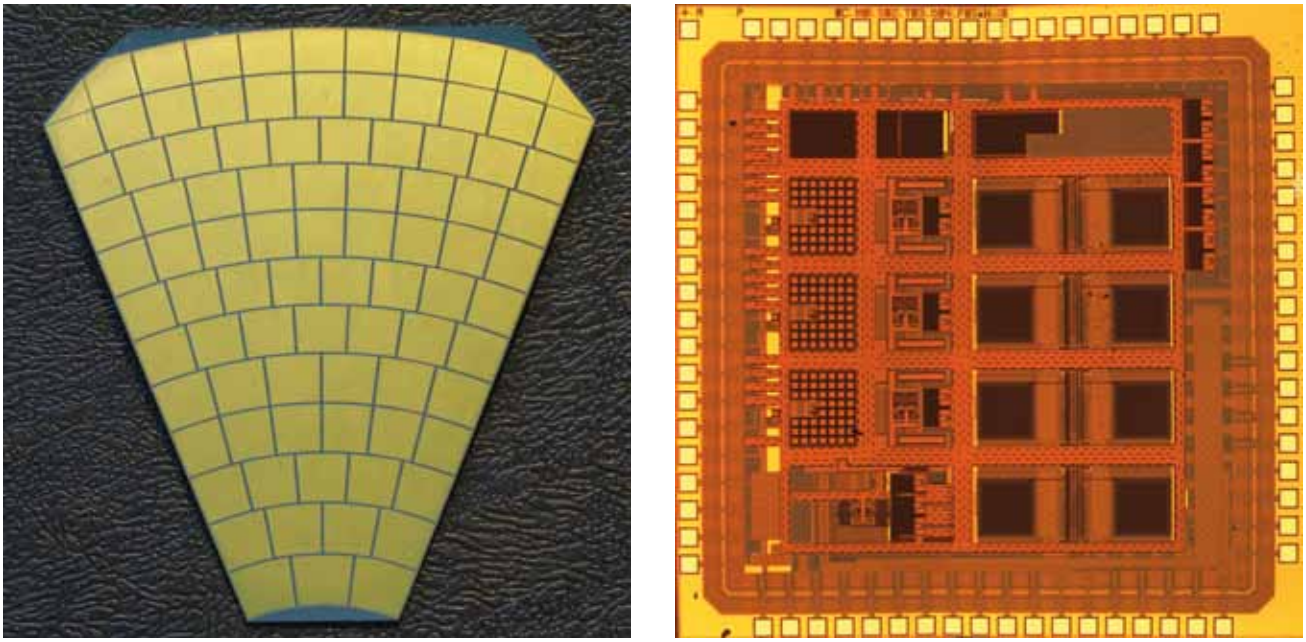

Figure 3.18 A prototype of a GaAs sensor with pads of 8 x 8 mm^2 size (left) and a 4-channel ASIC (right). Left image: G. Shelkov, FCAL, JINR. Right image: A. Abulselme, FCAL, Stanford University

ASIC developments

Since the occupancy in BeamCal and LumiCal is relatively large they must be read out after each bunch crossing. Therefore special front-end and analogue-to-digital converters (ADC) that match the timing of the ILC have been developed. The BeamCal ASICs, designed for 180-nm technology, will be able to handle 32 channels. A prototype, containing 4 channels, is shown in *Figure 3.18* (right). Two modes of operation require a front-end circuit capable of a wide performance envelope: high slew rate for standard data-taking and low noise for calibration. In standard data-taking all data from a full bunch train must be recorded to be read out between bunch trains. Because of its reliability, density and redundancy, a digital memory array will be used to store the data from all collisions in each bunch train. This choice requires a sampling rate of 3.25 megahertz per channel, which is achieved by 10-bit, successive approximation analogue-to-digital converters.

The ASICs for LumiCal, designed in 350-nm CMOS technology, have to tackle in addition a larger range of input capacitances due to a large variation of pad sizes. The chosen front-end architecture comprises a charge-sensitive amplifier, a pole-zero cancellation circuit and a shaper. The ADC is designed using pipeline technology. The first prototype ADC, shown in *Figure 3.19* (left), consists of an input sample and hold circuit, nine pipeline stages and digital correction circuitry. In addition, the power-switching feature is also implemented.

Prototypes have been tested for both BeamCal and LumiCal. The results confirm that the ASICs match the requirements derived from the detector performance necessary for the physics programme.

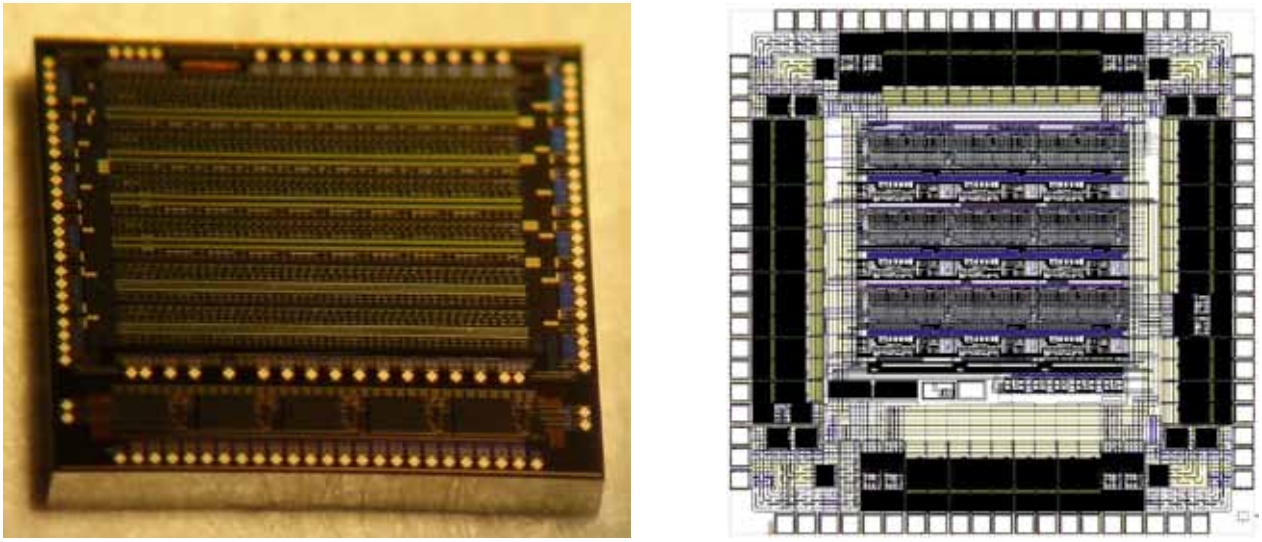

Figure 3.19 Prototypes of the ADC ASIC for LumiCal (left) and for the Pair Monitor (right). Left image: M. Idzik, FCAL, University of Science and Technology, Cracow. Right image: FCAL, Tohoku University.

First fully functional sensor plane

In summer 2010 a sensor for BeamCal and a sensor for LumiCal were assembled with front-end ASICs and investigated in the 4-GeV electron beam at DESY. Several millions of triggers have been recorded, exposing several pads and sensor edges to the beam. Studies of signal-to-noise, cross talk, sensor homogeneity and edge effects are ongoing. Preliminary results, as shown in *Figure 3.20*, are promising.

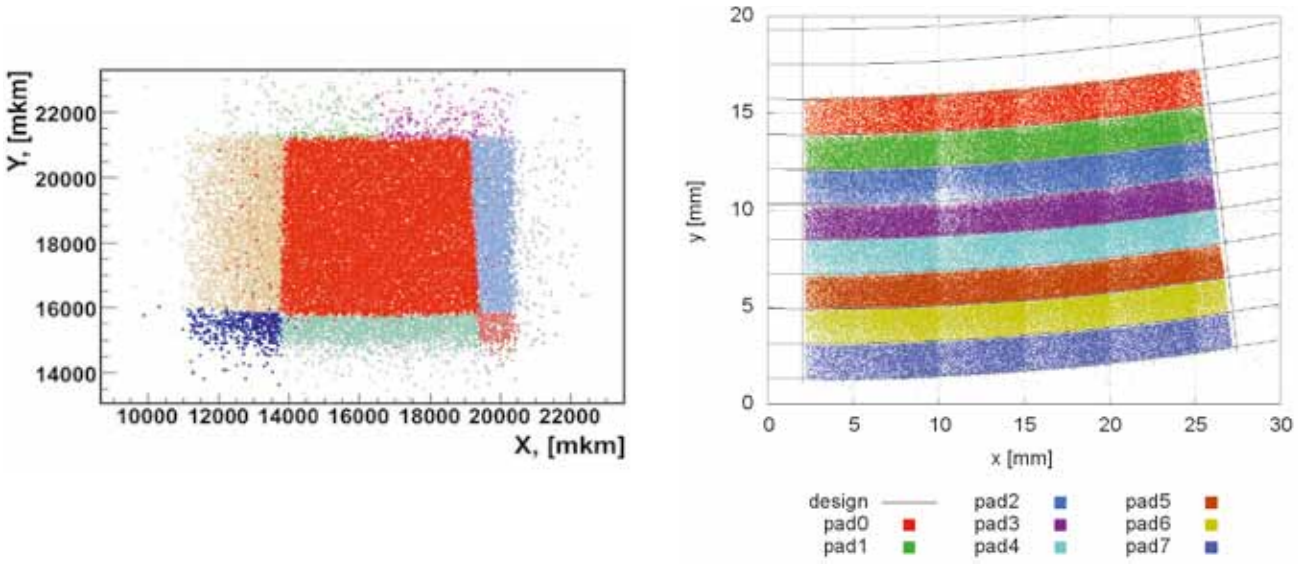

Figure 3.20 Predicted beam particle impact points are compared with the signal on the pad crossed by the beam particle. Left: BeamCal. Right: LumiCal. Each color is assigned to a certain pad. Left image: O. Novgorodova, FCAL, DESY Zeuthen. Right image: S. Kulis, FCAL, University of Science and Technology, Cracow.

3.6 Magnet coil

3.6.1 ILD magnet coil

Since the *Reference Design Report* (RDR), the main progress done on the ILD coil has been to confirm the main coil parameters: design field of 3.5 T in a 6.9-m warm bore and on a 7.35-m coil length to perform 3-D magnetic calculations (including the yoke) and to study various options for the coil design. Starting from the basic ILD design, which is based on the Large Hadron Collider CMS detector configuration, a few possibilities have been studied in detail: improve the magnetic field homogeneity by adding extra current in specific locations of the winding and/or add an anti-DID (detector-integrated dipole, *Figure 3.21)* to compensate the effects of the crossing angle on the beams.

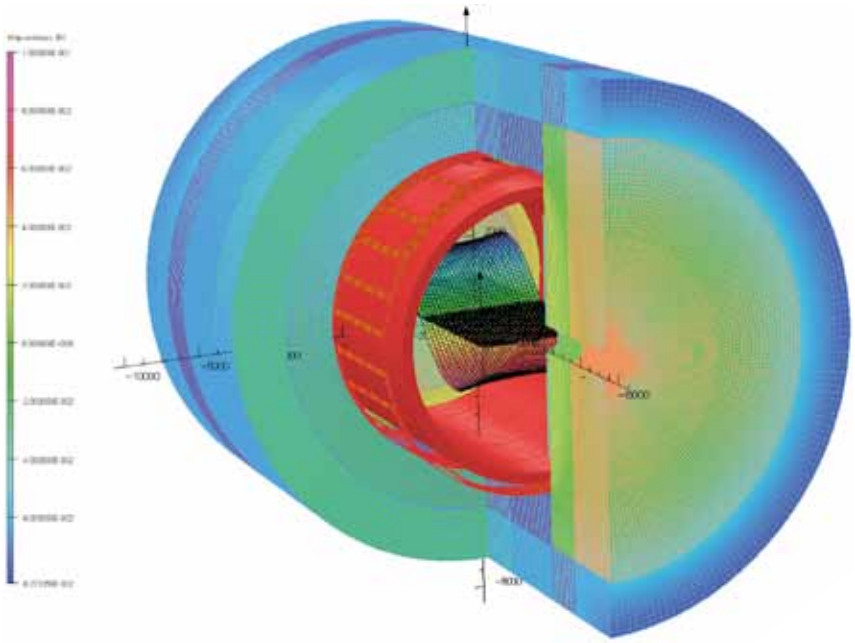

Figure 3.21 Anti-DiD in ILD. Image: Olivier Delferriere

3.6.2 SiD magnet coil

Since the RDR, the SiD superconducting solenoid still retains the CMS solenoid design philosophy and construction techniques, using a slightly modified CMS conductor as its baseline design. Superconducting strand count in the coextruded Rutherford cable was increased from 32 to 40 to accommodate the higher 5-T central field. Many iron flux return configurations have been tested in two dimensions to reduce the fringe field. An Opera 3-D calculation with the DID coil has been completed. Calculations of magnetic field with a 3-D ANSYS program are in progress. These will have the capability to calculate forces and stress on the DID as well as run transient cases to check the viability of using the DID as a quench propagator for the solenoid. Field and force calculations with an iron end cap HCAL were studied. The field homogeneity improvement was found to be insufficient

to pursue this option. Conceptual DID construction and assembly methods have been studied. The solenoid electrical power system, including a water-cooled dump resistor and grounding, was established. Significant work has been expended on examining different conductor stabiliser options and conductor fabrication methods. This work is pursued as a cost- and time-saving effort for solenoid construction.

3.6.3 R&D common programme

An R&D common programme for the improvement of the conductor of the ILD and SiD detector magnets has been proposed and started among various laboratories in Europe, Japan and the US. The main goal is to improve the mechanical behaviour of the conductor without degrading too much the function of the electrical stabiliser. Several ways are foreseen: extrusion with Al/micro-doped alloy, alumina fibres, and carbon nanotube technology.

3.7 The ILD and SiD muon systems

The return yoke for ILD and SiD is instrumented with position sensitive detectors to serve as both a muon filter and a tail catcher. The total area to be instrumented is very significant, with several thousand square metres of area. Technologies that lend themselves to low-cost large-area detectors are therefore under investigation. Particles arriving at the muon system have seen large amounts of material in the calorimeters and encounter significant multiple scattering inside the iron. Spatial resolutions of a few centimetres are therefore sufficient. Occupancies are low, so strip detectors are possible. In the ILD and SiD concepts, solutions exist that extend the technologies for the hadronic calorimeter – either scintillator or resistive plate chambers – to the muon system so that synergies exist for the two systems. Simulation studies have shown that ten or more layers of sensitive detectors yield adequate energy measurements and good muon-detection efficiency. The efficiency to find muons in semi-leptonic bottom decays is shown in *Figure 3.22* (left).

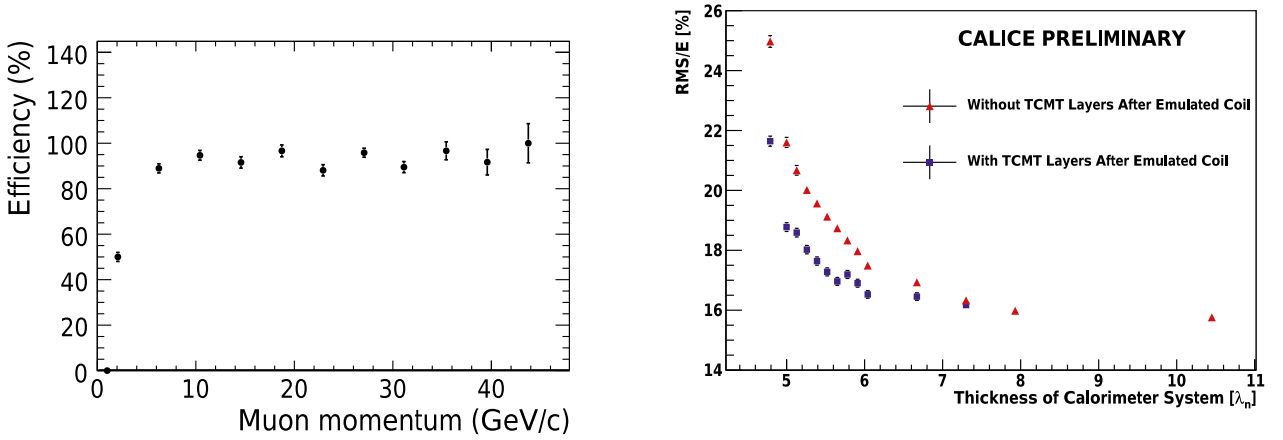

Figure 3.22 Left: muon-finding efficiency in hadronic b-decays as simulated for the ILD detector. Right: resolution improvement for 20-GeV pions using the muon tracker as a tail catcher, measured with CALICE test beam data. The red triangles show the energy resolution as a function of calorimeter thickness. The blue squares show the resolution for a system including a leading calorimeter, an emulated magnet coil, and post-coil sampling with the tail catcher as function of the depth of the forward edge of the emulated coil. The resolution is calculated with the root-mean-square of the energy distribution to account for non-Gaussian tails. The coil is emulated by omitting layers of the tail catcher from the energy measurement. The maximum depth of the full calorimeter system including the tail catcher is 11 proton interaction lengths. Left image: DESY. Right image: CALICE.

The detector R&D that is being pursued has to do with the principles of operation for both resistive plate chambers and readout of wavelength-shifting (WLS) fibres embedded in extruded strip scintillators using pixellated photon detectors (PPDs), or SiPMs.

The R&D on RPCs centres on understanding their long-term efficiencies with about 9-kilovolt direct current voltages applied for long periods of time in a radiation environment, such as is expected in the forward and backward regions of the linear collider interaction region. The strip scintillator/PPD readout R&D has centred on calibration using zero, one and two photoelectron response from spontaneous not-beam-associated signals and on measurement of the attenuation due to subsequent passage of the light pulses through the WLS before they reach the PPD. Because the PPDs have better photoelectron conversion efficiency from light pulses, the observed number of photoelectrons exceeds what is possible with multi-anode photomultiplier vacuum tubes. The list of future R&D includes examples of how to deal with thousands of channels and their specification and background noise in a cost-effective way using integrated circuitry. In the short time we have before the publication of the detailed baseline design, we will need to prioritise our work to attack important problems, such as dealing with many fewer instances of large energy deposits for muons than for hadrons, with the possibility for local tracking of muons.

3.8 Data acquisition

The detectors at the ILC will be built to perform high-precision experiments in a high-luminosity environment. As one of the major components, the data acquisition (DAQ) has to be designed to achieve this by dead-time-free data recording without compromising on possible rare or yet unknown physics processes. Because of the bunched operation mode of the ILC, a DAQ system without a hardware trigger was adopted for both the ILD and the SiD detector concepts *[3-4]*. The data are processed and stored in the front-end readout electronics of the different detectors for a full bunch, that is, for up to 3,000 collisions during a timespan of about 1 millisecond (ms). In the time between bunch trains, on the order of 200 ms, the data are then collected from the front end by an event-building network and are further processed in a software event filter based on commercial processing units. The processed data are finally sent to permanent storage according to physics and calibration needs. This concept will assure the needed flexibility and scalability and will be able to cope with the expected complexity of the physics and detector data without compromising efficiency or performance.

In addition, the ILC physics goals require higher precision in energy and momentum resolution and better impact parameter resolution than any other collider detector built so far. Improved accuracy can only be achieved by a substantially larger number of readout channels than in previous detectors. The increased calculations numbers of readout channels for the ILC detectors will require signal processing and data compression already at the detector electronics level as well as high bandwidth for the event-building network to cope with the data flow. To reduce the power consumption and hence the need for large cooling power, it is proposed to switch off power to parts of the front-end electronics in the time between trains.

For both detector concepts, prototypes of the front-end readout electronics for the different detector technologies have been designed and fabricated *[3-5]* to be used in test beams for verification of the detector design as well as of the electronics design. An essential part of these tests is the demonstration of the power pulsing scheme.

The DAQ systems emerging from the test beam systems began recently to address more and more the issues of system control and integration as well as slow control and monitoring (*Figure 3.23)*. First designs like the EUDAQ and the CALICE DAQ Version 2 or the SiD DAQ try to integrate different detector systems into a common integrated DAQ system.

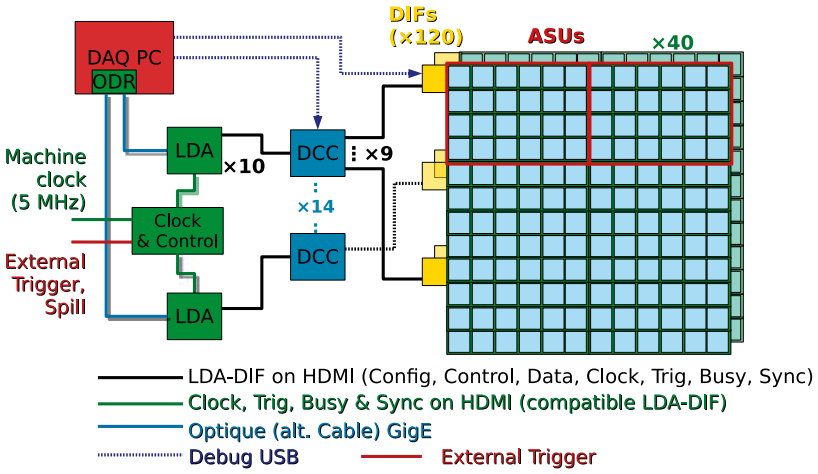

Figure 3.23 Calice DAQ scheme. Only the detector interface is detector-specific. All other components, such as the data concentrator card (DCC), the link data aggregator (LDA) and the off-detector receiver card (ODR) are common. Images: Vincent Boudry

3.9.1 The push-pull system

The push-pull system for the two detectors was only conceptual at the time of RDR's publication, and since then the engineering design has progressed significantly. A time-efficient implementation of the push-pull model of operation sets specific requirements and challenges for many detector and machine systems, in particular the interaction region (IR) magnets, the cryogenics, the alignment system, the beamline shielding, the detector design and the overall integration. The minimal functional requirements and interface specifications for the push-pull IR have been successfully developed and published *[3-4]*, to which all further IR design work on both the detectors and machine sides are constrained.

The push-pull design needs to accommodate two detector concepts, ILD and SiD, that are different in their design, dimensions and mechanical characteristics (such as mechanical rigidity). The different sizes provide particular challenges for the beamline shielding elements, referred to as the 'pacman' shielding. An example of a design of the pacman shielding that ensures compatibility with both detectors is illustrated in *Figure 3.24*.

3.9 The machine-detector interface

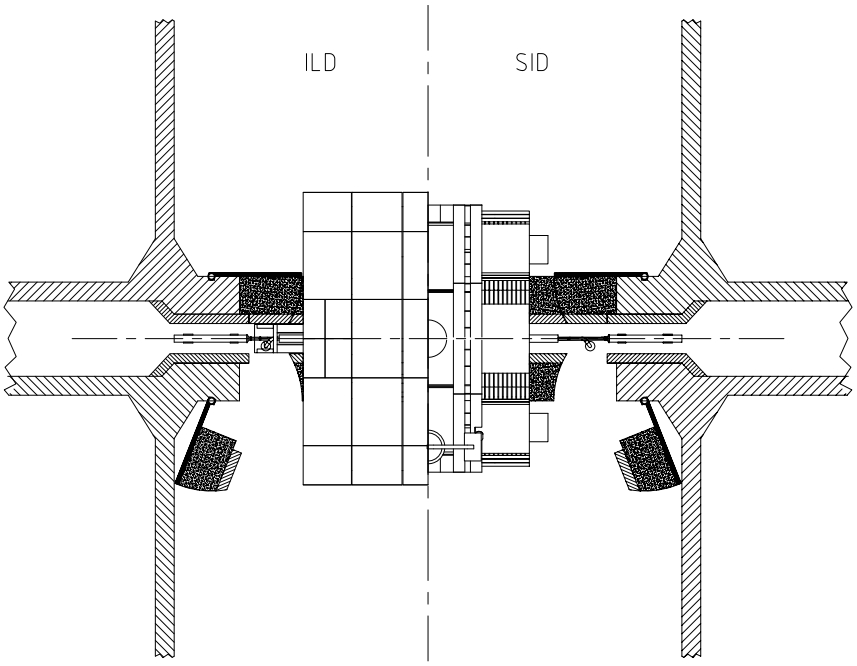

Figure 3.24 Design of the beamline shielding compatible with two detectors of different sizes. Image: Marco Oriunno

The detector motion and support system has to be designed to ensure reliable push-pull operation, allowing a hundred moves over the life of the experiment, while preserving internal alignment of the detector's internal components and ensuring accuracy of detector positioning. The motion system must be designed to preserve structural integrity of the collider hall floor and walls. Moreover, the motion and support system must be compatible with the tens-of-nanometre-level vibration stability of the detector. If situated in seismic regions, the system must also be compatible with earthquake safety standards. Two different approaches for the detector support system are currently being considered, a roller and a platform-based system.

The approach for the design of the detector motion system, and in particular the use of a platform, is currently being investigated. The criteria for selection of the common design will be based on engineering considerations and on vibration stability analysis of the entire system (detector together with its support and motion system). The selection is planned to happen in the near future.

SiD in a push-pull configuration

The more compact and rigid SiD detector can naturally be supported by an eight-leg structure as shown on *Figure 3.25* or sit upon a rigid platform. As its half-height is 1.7 m less than that of ILD, either extra-long legs or an extra thick platform will be required. With the magnetic field turned on and the end cap doors sucked into the central barrel, SiD is very stiff. The last quadrupole lens package, QD0, is designed to rest on a magnetically insensitive mover system, which in turn rests on cylinder-shaped cutouts in the doors, which are only marginally larger than the diameter of the QD0 cryostat. This design emphasises maximal hermeticity and rapid push-pull detector exchange. The forward calorimeter (FCAL) package (LumiCal,

BeamCal and masking) will be a logical cantilevered extension of the QD0 cryostat. A frequency-scanning interferometer (FSI)-based alignment system will align the opposing QD0/FCAL packages to the tunnel-mounted QF1 cryostats that complete the final doublet telescope and ensure precision LumiCal positioning with respect to the interaction point. The same FSI system will guarantee vertex and tracking detector alignment after each push-pull operation without the need to reacquire beam-based alignment data. This design requires that all mechanical systems mounted on the detector be vibration-free. While still under study, interaction point vacuum is assumed achievable via QD0 cryo-pumping without external pumps or non-evaporative getter (NEG) coating systems.

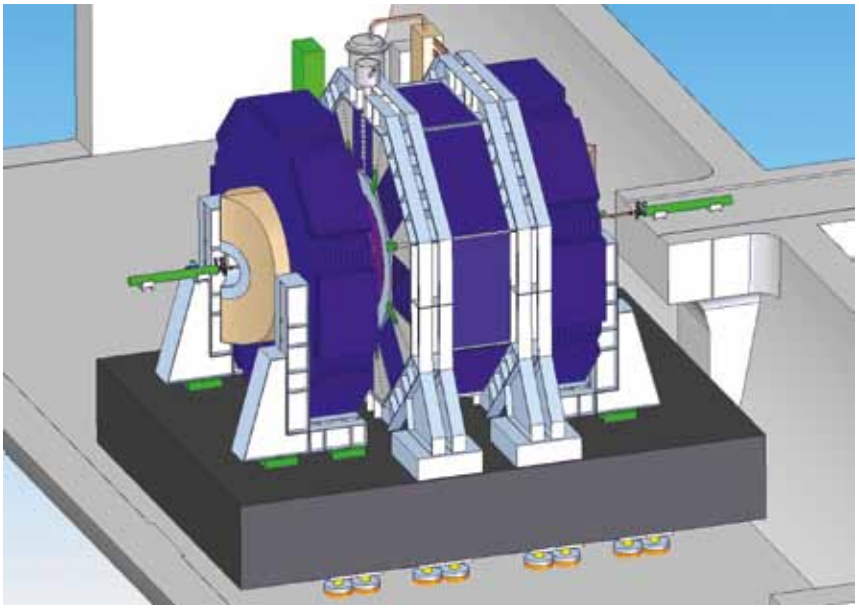

Figure 3.25 Possible detector motion system for the SiD. Image: Marco Oriunno

ILD in a push-pull configuration

The ILD detector is somewhat larger than SiD and is also designed to be assembled from slices in a similar way to the Large Hadron Collider CMS detector. The ILD detector motion system foresees the use of a rigid platform on which the entire detector can be placed. The platform will preserve detector alignment and will distribute the load evenly onto the floor. Such an approach is illustrated in *Figure 3.26.* The platform will carry also some of the detector services like electronic racks. Cables and cryogenic lines will be routed to the platform in flexible cable chains that move in trenches underneath the platform itself. The platform itself will move on air pads that allow linear and rotational movements on the floor. In combination with a simple positive indexing mechanism, the platform with the detector can be positioned quickly within the required precision of 1 mm with respect to the beam axis.

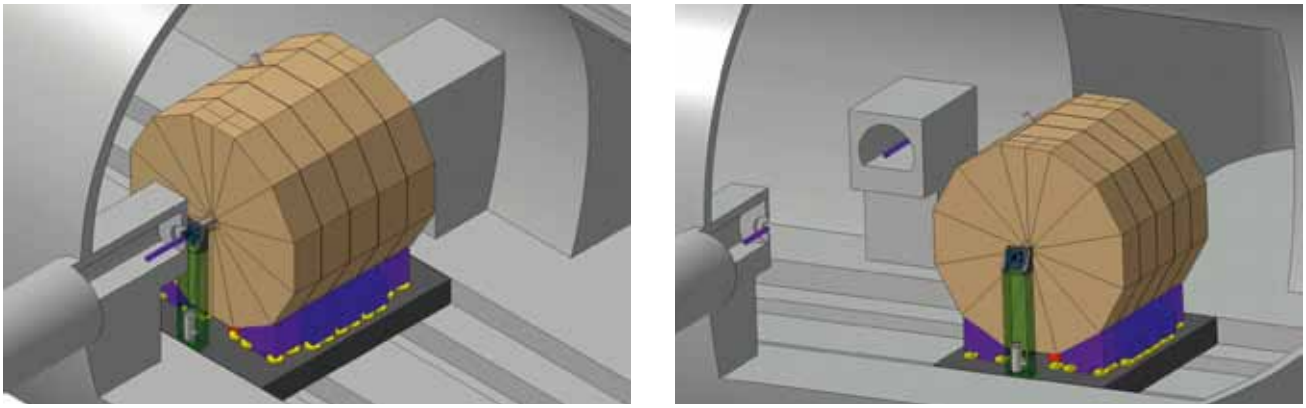

Figure 3.26 Possible platform support concept for the ILD. Left: on the beamline. Right: off the beamline. Images: Marco Oriunno

3.9.2 Vibration analysis

The main causes of luminosity losses in the beam delivery system are the naturally occurring ground motion, mechanical vibration sources and wake field effects. The most acute effects are the relative jitter of the final focussing magnets, which need mechanical stabilisation at about the 50-nm level, with the residual effect being compensated by beam feedback systems for collision optimisation. Mechanical vibrations generated by technical systems, such as HVAC and cryogenics, will be mitigated by design, placing them in appropriate locations of the experimental area. Ground vibrations are site-dependent and a careful design of the detector support and final focussing system is required. A comprehensive database of ground motion vibrations for different sites around the world that host accelerator facilities is available. The ILD and SiD collaborations are working together towards the simulation and benchmarking of the respective detectors in order to guarantee the required level of stability. Preliminary results show that both detectors can achieve the goals by means of mechanical passive stabilisation of the QD0 systems, in conjunction with the interaction point feedback system. Further studies are necessary to understand the coupling with the QF1 magnets, which will be mechanically independent from the QD0 during the push-pull operations.

A possible solution for the transport of the detectors in the push-pull is a reinforced concrete platform. The stability requirements of a platform solution are under study and a first mechanical design is in progress. Because of the intrinsic uncertainty related to the nonlinearity and the damping factors of large reinforced concrete structures, an experimental benchmark with comparable structures was required. An experimental characterisation of the dynamic behaviour of the large reinforced concrete shielding slab of the CMS access shaft, which is so far the closest existing example of a push-pull platform, has been made.

References

[3-1] CALICE collaboration, Design and Electronics Commissioning of the Physics Prototype of a Si-W Electromagnetic Calorimeter for the International Linear Collider, 2008_JINST_3_P08001; CALICE collaboration, Response of the CALICE Si-W Electromagnetic Calorimeter Physics Prototype to Electrons, NIM A608 (2009) 372.

[3-2] S. Uozumi, "Performance of the Scintillator-Strip Electromagnetic Calorimeter Prototype for the Linear Collider Experiment," talk at CALOR2010, Beijing.

[3-3] P. Dauncey, "Performance of CMOS sensors for a digital electromagnetic calorimeter," PoS (ICHEP 2010) 502.

[3-4] B. Parker et al., ILC-Note-2009-050.

04

PHYSICS AND SIMULATION UPDATES

4.1 Software

The ILD (International Large Detector) simulation has been performed with a model implemented in a full simulation framework called Mokka. The model used for the Letter of Intent (LOI) study is shown in *Figure 4.1*. Most of the sub-detectors in this model have been implemented, including a significant amount of engineering detail such as material structures, electronics and cabling as well as dead materials and cracks with detailed cell structures of calorimeters. This provides a reasonable estimate of the material budget, which is crucial for a realistic demonstration of detector performances. The update of the model is now in progress for the detailed baseline design (DBD). The new features to be implemented in the new model include additions of services and support structures between sub-detectors, catching up the evolution of the computer-aided design (CAD) model of ILD and implementations of wafer and support structures of silicon trackers, which had been approximated by cylinder and disks in the current ILD model.

Simulated ILD events have been reconstructed by a set of realistic event reconstruction programs called Marlin. Reconstruction processors in Marlin include the Kalman filter-based charged track reconstruction processors of Marlin Reco, PandoraPFA processor for reconstructions of particle flow objects, and LCFIVertexing for flavour tagging through reconstructions of secondary and tertiary vertices. According to our study, these programs perform charged particle reconstruction with efficiency better than 99% in top-antitop pair events with background hits overlaid, with jet energy resolution of 3% for jets with energy between 100 to 200 gigaelectronvolts (GeV), and with excellent flavour tagging efficiency. Improvements of reconstruction and analysis tools are in progress following the update of simulator model for the Detailed Baseline Design (DBD) report.

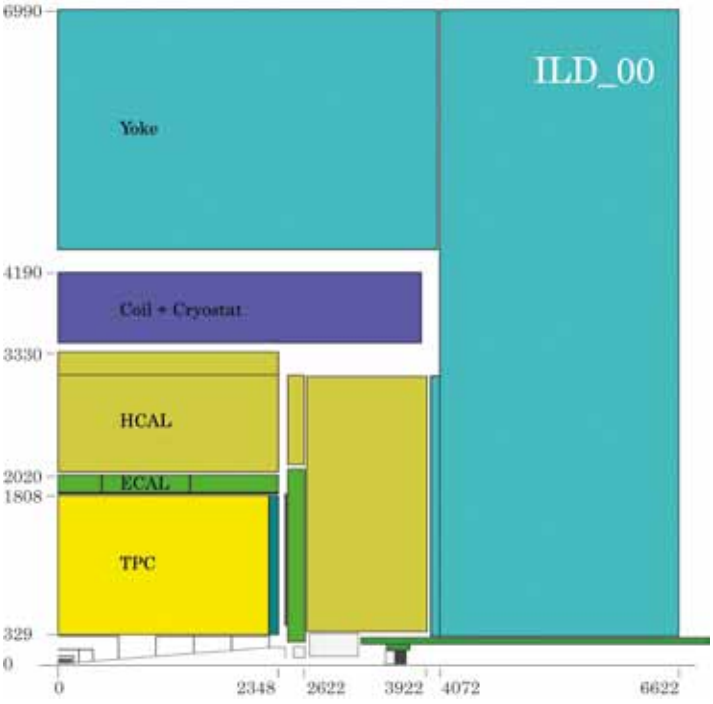

Figure 4.1 The ILD detector model as implemented in Mokka. From the inside to the outside, the detector components are the vertex detector, silicon strip inner tracker, time projection chamber (TPC), silicon external tracker, electromagnetic calorimeter (ECAL), hadronic calorimeter (HCAL), and yoke. In the forward region the forward tracking disks, endcap tracking detector, LumiCal (LCAL), LHCAL and BeamCal (BCAL) are shown. Image: Akiya Miyamoto

Using the fast and flexible detector simulation package developed by the American Linear Collider Simulation and Reconstruction Physics Group, more than 50 different detector designs were modeled before selecting the baseline design for SiD (Silicon Detector). Since that time, the fully detailed geometry has been implemented in a model called sidloi3. All of the tracker elements are therefore modelled as planar silicon wafers with their attendant support structures. The readout geometry is simplified, but reflects the gross amount and general distribution of the materials. The calorimeters are modelled as polygonal staves in the barrel region or planes in the end caps with interleaved readouts. The complexity of this detector model does not lend itself to a simple textual description. We therefore present a few figures to give an indication of the detail implemented in this model. See *Figure 4.2*.

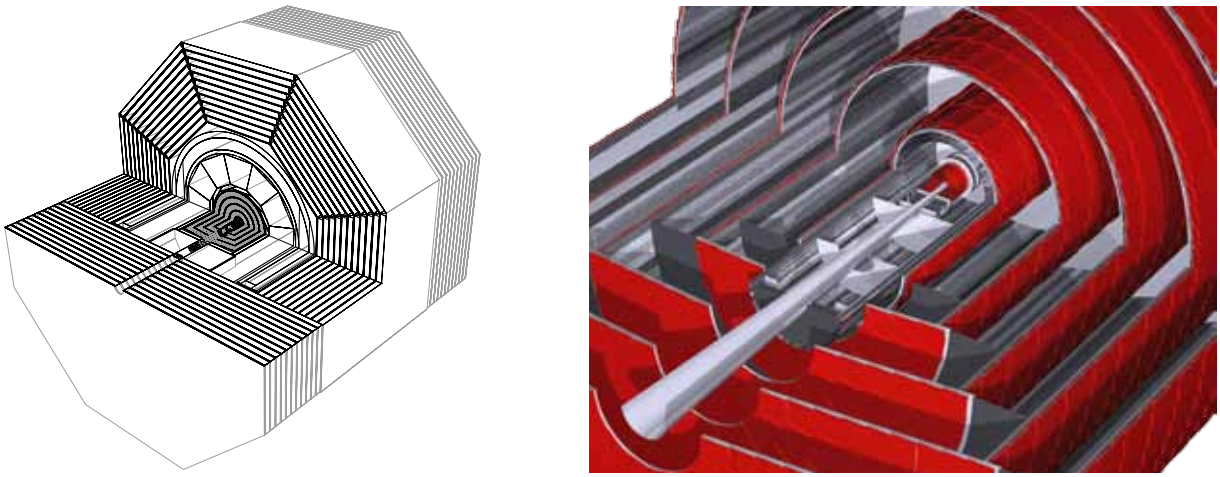

Figure 4.2 SiD as implemented in the simulation program showing the complexity of the design implemented for the DBD studies. Left: complete detector. Right: tracker. Images: Norman Graf

Digitisation involves a detailed simulation of the ionisation generation in the sensitive layer of the sensor, charge collection, signal formation and signal processing. This has two major goals during the detector design phase: optimising sensor parameters and comparing different sensors, and providing an estimation of the full detector performance. Very detailed but flexible simulation of the response of silicon detectors is possible, including variable readout dimensions (e.g. pixels or strips), various media, electric and magnetic field maps, detailed energy loss simulation using specialised code, electronics response, including electronics noise or inefficiencies, propagation of the signal to readout and digitisation of the signal. The reconstruction software has been modified as necessary to accommodate the changes in geometry, and the tracking continues to show excellent efficiency and resolution. A binding between the simulation output and the PandoraPFA package has also been released. Production simulation and reconstruction will take place on the worldwide network of computers (namely, 'Grid') using a submission tool called Dirac

4.2 Benchmark modes

The physics case for the ILC operating at a centre-of-mass energy of 500 GeV and its complementarity to that of the Large Hadron Collider has been well established (see documents on Tesla Test Facility R&D *[4-1]*, the *Reference Design Report* (RDR) *[4-2]*, and studies on ILC-LHC physics cases *[4-3]*). However, realising the full potential of the ILC places stringent requirements on the performance of the detectors. Compared to the previous generation of electron-positron machines (LEP at CERN and SLC at SLAC National Accelerator Laboratory) the detector at the ILC needs to deliver an order of magnitude better momentum resolution, a factor two to three better jet energy resolution and a factor three better impact parameter resolution. Since the *Reference Design Report,* much of the work of the detector and physics community has focussed on demonstrating that the full physics reach of the ILC can be achieved based on detailed simulations of the ILD and SiD detector concept designs. In order to demonstrate the physics reach with realistic detector simulations and a full event reconstruction chain, several physics benchmark processes were identified and studied in detail. These studies, summarised below and described in detail in the ILD *[4-4]* and SiD *[4-5]* LOI documents, were rigourously reviewed by the International Detector Advisory Group. As a result of this process, it was demonstrated that the full physics potential of the ILC could be realised with realistic and technically feasible detector designs operating in the ILC beam conditions. It should be noted, however, that the prime motivation for the study of the benchmark modes is to demonstrate the capabilities of detectors; they are not intended as a list of physics highlights of ILC.

The physics benchmark channels were studied for both the ILD and SiD detector concepts with both concepts leading to broadly similar physics sensitivities. The highlights of these studies are described below. For reasons of space, for each physics benchmark process, only the studies from one of ILD or SiD is shown. In all cases, all Standard Model (SM) backgrounds were simulated and included in the analysis.

4.2.1 Higgs production and mass measurement

The precise determination of the properties of the Higgs boson (H) is one of the main goals of the ILC regardless of its nature, whether it fits in the SM or is described by some other model. Of particular importance are the Higgs boson mass, m_H, and its branching ratios. Electroweak data and direct limits from searches at LEP and at the Tevatron favour a relatively low value for m_H. Hence the ILC benchmark studies assumed m_H = 120 GeV. To assess the physics reach a data sample of 250 inverse femtobarns (fb^{-1}) recorded at a centre-of-mass energy of E_{CM} = 250 GeV was assumed. In this case, the dominant Higgs production process is that of Higgsstrahlung, $e^+e^- \rightarrow HZ$. A particularly clean signature is obtained for the case where $Z \rightarrow \mu^+\mu^-$ and $Z \rightarrow e^+e^-$. Here the distribution of the invariant mass recoiling against the reconstructed Z provides a precise measurement of m_H, independent of the Higgs decay mode. In particular, the $\mu^+\mu^-X$ final state provides a particularly precise measurement as the e^+e^-X channel suffers from larger experimental uncertainties due to bremsstrahlung. It should be noted that it is the capability to precisely reconstruct the recoil mass distribution from $Z \rightarrow \mu^+\mu^-$ that defines the momentum resolution requirement for an ILC detector.

The ILD analysis is outlined below. The first stage in the event selection is the identification of leptonically decaying Z bosons. Candidate lepton tracks with transverse momentum (p_T) greater than 15 GeV, are identified. Candidate leptonic Z decays are then selected from oppositely charged pairs of identified leptons using a mass window around m_Z. Background from $e^+e^- \rightarrow$ leptons is rejected using cuts on transverse momentum of the di-lepton system and the acoplanarity of the two tracks. Additional cuts are used to reject background from lepton pair production with initial and final state radiation. Backgrounds from $e^+e^- \rightarrow ZZ$ and $e^+e^- \rightarrow WW$ are suppressed using a multivariate likelihood based on the acoplanarity, the polar angle, the transverse momentum and the invariant mass of the di-lepton system.

The reconstructed recoil mass distributions, calculated assuming the ZH is produced with four-momentum (E_{CM}, 0, 0, 0), are shown in *Figure 4.3*. In the e^+e^-X-channel final state radiation and Bremsstrahlung photons are identified and used in the calculation of the $e^+e^-(ng)$ recoil mass. Fits to signal and background components are used to extract m_H. Based on this model-independent analysis of Higgs production in the ILD detector, it is shown that m_H can be determined with a statistical precision of 40 megaelectronvolts (MeV) (80 MeV) from the m^+m^-X (e^+e^-X) channel. When the two channels are combined, an uncertainty of 32 MeV is obtained. The corresponding model-independent uncertainty on the Higgs production cross-section is 2.6%. Similar results were obtained from SiD. It should be emphasised that these measurements only used the information from the leptonic decay products of the Z and are independent of the Higgs decay mode. As such this analysis technique could be applied even if the Higgs decayed invisibly.

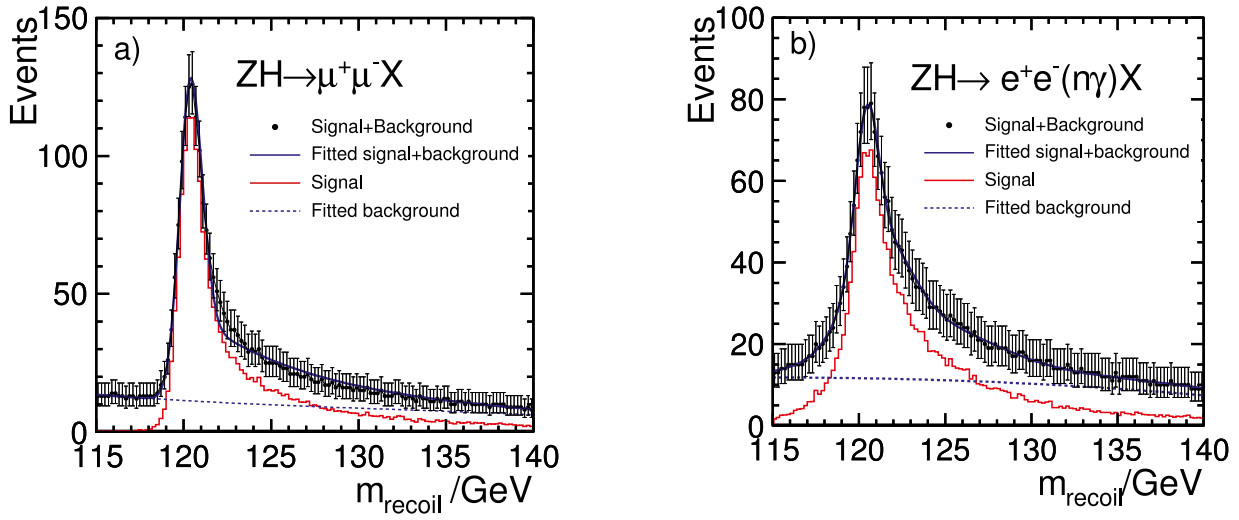

Figure 4.3 Results of the model-independent analysis of the Higgsstrahlung process $e^+e^- \rightarrow HZ$ in which $Z \rightarrow \mu^+\mu^-$ (left) and b $Z \rightarrow e^+e^-$(ng) (right). The results are shown for $P(e^+, e^-)$ = (+30 %, -80 %) beam polarisation. Images: Mark Thomson

It is worth noting that for the m^+m^-X channel the width of the recoil mass peak is dominated by the beam energy spread. In the above study Gaussian beam energy spreads of 0.28% and 0.18% are assumed for the incoming electron and positron beams respectively. For ILD the detector response leads to the broadening of the recoil mass peak from 560 MeV to 650 MeV. The contribution from momentum resolution is therefore estimated to be 330 MeV. Although the effect of the detector resolution is not negligible, the dominant contribution to the observed width arises from the incoming beam energy spread rather than the detector response. This is no coincidence; the measurement of m_H from the $\mu^+\mu^-X$ recoil mass distribution determines the momentum resolution requirement for a detector at the ILC.

4.2.2 Higgs branching fractions

A precise measurement of the absolute branching ratios of the Higgs bosons is an important test of the Higgs boson hypothesis and provides a window into effects beyond the SM. With an SM branching ratio of 3%, the decay of a 120-GeV Higgs boson into a pair of charm quarks challenges the flavour tagging and calorimeter capabilities of an ILC detector.

At E_{CM} = 250 GeV, a 120-GeV Higgs boson is produced primarily through $e^+e^- \rightarrow ZH$, where the largest branching fraction (BF) Z boson decay modes are $Z \rightarrow \nu\nu$ and $Z \rightarrow qq$, q = u,d,s,c,b. The main signal event topology therefore consists of either two or four jets, with at least two of the jets originating from charm quarks. The primary background arises from $e^+e^- \rightarrow qq$, $e^+e^- \rightarrow ZZ$ and $e^+e^- \rightarrow WW$ events. In addition, the $H \rightarrow cc$ decays have to be separated from $H \rightarrow bb$ decays (SM BF = 68%) or $H \rightarrow gg$ (SM BF = 5%). The SiD analysis, based on an assumed integrated luminosity of 250 fb^{-1} with initial state polarisations of +80% for the electron beam and -30% for the positron beam, is presented here. ILD obtained similar results. Events are first classified into the candidate decay topology. Events with reconstructed charged leptons of energy greater than 15 GeV are rejected. If the visible energy lies between 90 and 160 GeV the event is classified as a candidate $H\nu\nu$; events with visible energy above 170 GeV are classified a candidate Hqq. The candidate $H\nu\nu$ (Hqq) are forced into two (four) jet topologies using the Durham algorithm. Cuts are then applied to reduce the main non-Higgs SM backgrounds. The cut variables include the H candidate di-jet invariant mass, the number of charged tracks in a jet, the event thrust, the angle of the thrust axis with respect to the beamline, the angle between the two jets from the Z candidate and the maximum energy of any isolated photon.

Finally, for the surviving events in each of the final state topologies, two neural net (NN) variables are calculated. The first, to reject non-Higgs background, is trained using all Higgs decays as signal and all SM processes as background ($NN_{SM\text{-}Higgs}$). The second, which identifies $H \rightarrow cc$ decays, is trained using $H \rightarrow cc$ as signal and all other Higgs decays as background ($NN_{Higgs\text{-}signal}$). The input variables to the neural nets include all cut variables as well as three different charm flavour-tag variables. *Figure 4.4* shows, for the four-jet analysis, the distributions for one of the three flavour tag variables and the neural net variable $NN_{Higgs\text{-}signal}$. For 250 fb^{-1} a total 1292 (1930) events survive the final cuts of $NN_{SM\text{-}Higgs\,1} > 0.2$ and $NN_{Higgs\text{-}signal} > 0.3$ in

the two- (four-) jet selections. The purity of the final sample is about 40% with the background being roughly equally divided between Higgsstrahlung process with H → bb and other SM processes. The H → cc branching fraction is obtained by dividing the measured signal cross-section by the total. For the analysis described above, the simulated H → cc branching fraction is determined to be 3.3 ± 0.4% and 3.3 ± 0.2% for the Z → νν and Z → qq respectively.

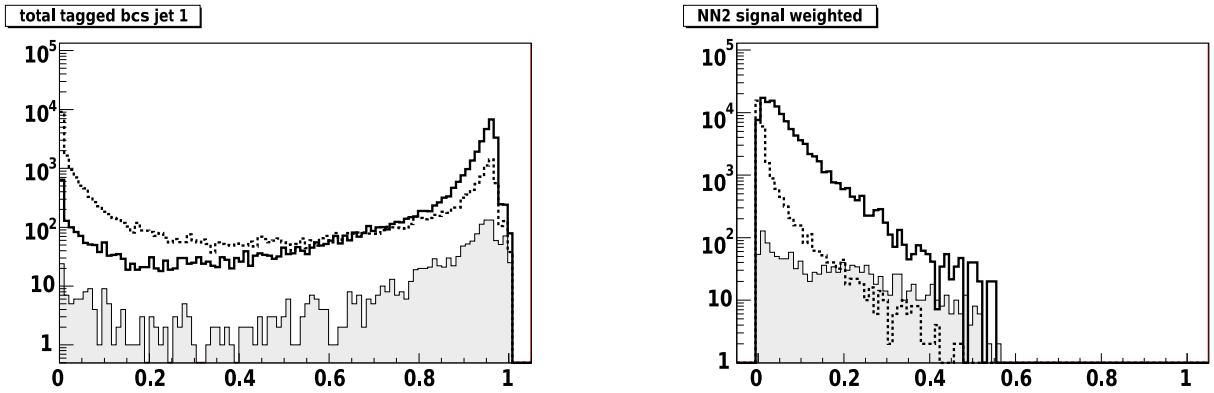

Figure 4.4 Distributions of flavour tag variable 'charm with only b-quark background' (left) and $NN_{Higgs\text{-}signal}$ (right) for hadronic mode events. The solid curves are the Standard Model background, dashed are background Higgsstrahlung events, and filled histograms are ZH → qqcc. Images: Mark Thomson

4.2.3 Top mass measurement from direct reconstruction

Top physics will form an important part of the scientific programme at the ILC. In particular, the top mass, m_t, and top width, Γ_t, can be determined with high precision. The measurement of m_t and Γ_t from the direct reconstruction of $e^+e^- \rightarrow t\bar{t}$ events was studied for the detector LOIs. Similar results were obtained by ILD and SiD. The results with the full ILD detector simulation and event reconstruction are shown here. Two main decay topologies were considered by ILD: fully hadronic, $t\bar{t} \rightarrow (bqq)(bqq)$ and semi-leptonic, $t\bar{t} \rightarrow (bqq)(bln)$, decay topologies. Results were obtained for an integrated luminosity of 500 fb^{-1} at E_{CM} = 500 GeV.

The analysis depends on excellent jet energy resolution and high-performance flavour tagging. In the ILD study, events with an isolated lepton are considered to be candidates for the semi-leptonic analysis; otherwise they are assumed to be candidates for the fully hadronic analysis branch. In the fully hadronic branch, the event is reconstructed as six jets that are combined to form W bosons and, when combined with a b quark jet, top quarks. The two b-jets originating directly from the top quark decays are identified using the flavour-tagging information. The four remaining jets are considered as the decay products of the two Ws. The combination of the four jets into two di-jets that gives the smallest value of $|m_{ij}-m_W|+|m_{kl}-m_W|$ is chosen to form the two Ws (where m_{ij} and m_{kl} are the di-jet masses for a given jet pairing). Out of two possible combinations to pair the W bosons with the b-jets, the one that yields the smallest mass difference is chosen.

The first step in the semi-leptonic branch is to remove the identified lepton and to force the remainder of the event into four jets. The two b-jets are identified using flavour-tagging information. The two remaining jets are assigned to the hadronically decaying W. The identified lepton and the neutrino are assigned to the leptonically decaying W boson, with the three-momentum of the neutrino defined as the missing momentum. The chosen pairing of the W bosons with the b-jets is that which yields the smallest reconstructed top mass difference. For each analysis branch, background events are rejected using a multi-variate likelihood technique. Finally, a kinematic fit is applied in order to improve the final top mass resolution. The reconstructed mass distributions in the two event topologies are shown in *Figure 4.5*.

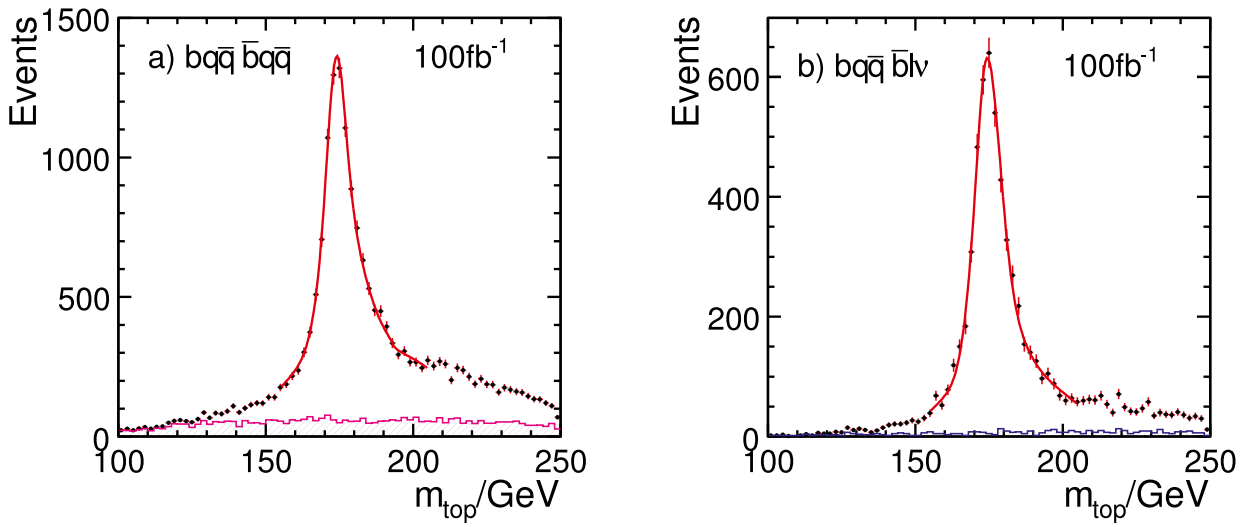

Figure 4.5 Reconstructed top mass distributions in fully hadronic and semi-leptonic events as simulated and reconstructed in the ILD detector concept. Images: Mark Thomson

For an integrated luminosity of 500 fb^{-1} it was shown that the cross-section (s) of $e^+e^- \rightarrow tt$ can be determined with a statistical uncertainty of 0.4% using the fully hadronic decays only. The invariant mass spectra are fitted with the convolution of a Breit-Wigner function and an asymmetric double Gaussian, the latter representing the detector resolution. The combinatoric background and the background from other processes are described by a 2nd-order polynomial. For an integrated luminosity of 500 fb^{-1} leads to uncertainties of 30 MeV on m_t and 22 MeV on Γ_t. Both ILD and SiD also studied the prospect to measure the top quark forward-backward asymmetry; a precision of about 2% was demonstrated.

4.2.4 Tau decay identification and tau polarisation in $e^+e^- \rightarrow \tau^+\tau^-$

The analysis of full energy tau leptons at E_{CM} = 500 GeV would be an important part of the physics programme at the ILC if, for example, a Z' is discovered at the LHC. Through interference with the Z/g* amplitudes, the couplings of the Z' to left- and right-handed tau leptons can be determined by measuring the tau angular distribution and polarisation. As a detector benchmark the identification of 250-GeV tau leptons and their decay modes pushes the tracker and calorimeter capabilities of the detector. Tightly collimated low-multiplicity jets must be reconstructed in terms of the underlying charged hadron and π^0 constituents. It provides a challenging test for particle flow reconstruction.

The SiD event selection for full energy tau pair events requires 2 and 6 charged tracks and that the visible energy be in the range of 100 to 450 GeV. Jet clustering is applied to the reconstructed particles and exactly two jets, each with $|\cos\theta| < 0.95$ where θ is the polar angle with respect to the beam axis, are required. The opening angle between the two jets must be more than 178^o. Events with two muons or two electrons are rejected. This procedure selects 72% of tau pair events where the energy of each tau is at least 240 GeV. The SM background is 2.4% of the selected event sample. For 250 fb^{-1}, the tau polarisation can be measured with a statistical precision of 0.28%. The forward-backward asymmetry, A_{FB}, is measured by fitting the t^- angular distribution, with the result A_{FB}=0.5038 ± 0.0021 for 250 fb^{-1} (assuming 80% left-handed electron polarisation and 30% right-handed positron polarisation).

The SiD particle flow algorithm was modified to identify tau decay modes. All calorimeter hits were clustered and assigned to the nearest tau jet. Photon identification was performed. All remaining clusters were assigned to tracks. The total calorimeter energy assigned to the track was required to be consistent with the track momentum. Neutral pions were formed from pairs of photons satisfying 60 MeV < m_{gg} < 180 MeV. The purity and efficiency of the tau decay mode identification is summarised in *Table 4.1*.

Table 4.1 Tau decay mode purity and efficiency

Decay mode	Correct ID	Wrong ID	ID eff	ID purity	SM bgnd
$e\nu\nu$	39602	920	0.991	0.977	1703
$\mu\nu\nu$	39561	439	0.993	0.989	1436
$\pi\nu$	28876	2612	0.993	0.917	516
$\rho\nu$	55931	8094	0.790	0.874	1054
$a_1\nu$, $a_1 \rightarrow \pi^+\pi^0\pi^0$	18259	11140	0.732	0.621	847
$a_1\nu$, $a_1 \rightarrow \pi^+\pi^-\pi^-$	21579	2275	0.914	0.905	141

The optimal observable technique is used to measure the mean tau polarisation, P_t, using the $e\nu\nu$, $\mu\nu\nu$, $\pi\nu$, and $\rho\nu$ decay modes giving P_t = -0.611 ± 0.009, where the error is purely statistical. Similar decay mode identification efficiencies and measurement statistical precisions were obtained by the ILD concept group.

4.2.5 SUSY gaugino mass reconstruction

The above benchmark processes represent precision tests of the Standard Model including the Higgs sector. In addition, the ILC has sensitivity to many Beyond the Standard Model processes. One much discussed extension to SM is supersymmetry (SUSY). As part of the physics benchmark studies, both ILD and SID investigated the SUSY 'point 5' scenario with non-universal soft SUSY-breaking contributions to the Higgs masses. In this model the lowest mass chargino, $\chi_1^{\pm}$, and the second lightest neutralino, χ_2^0, are not only nearly mass degenerate, but decay predominantly into $W^{\pm}\chi_1^0$ and $Z\chi_1^0$, respectively. For this SUSY benchmark point, the gaugino masses are: $m(\chi_1^0)$ = 115.7 GeV, $m(\chi_1^{\pm})$ = 216.5 GeV, $m(\chi_2^0)$ = 216.7 GeV, and $m(\chi_3^0)$ = 380 GeV. The SUSY point-5 scenario was chosen solely because it provides a suitable benchmark test of the di-jet mass reconstruction capability of a detector at the ILC. From an experimental point of view the reconstruction of the gaugino masses is particularly challenging as both $e^+e^- \rightarrow \chi_1^+\chi_1^- \rightarrow W^+W^-\chi_1^0\chi_1^0 \rightarrow qqqq\chi_1^0\chi_1^0$ and $e^+e^- \rightarrow \chi_2^0\chi_2^0 \rightarrow ZZ\chi_1^0\chi_1^0 \rightarrow qqqq\chi_1^0\chi_1^0$ result in final states consisting of four jets and missing energy. Distinguishing between these two processes requires the ability to accurately reconstruct the di-jet invariant mass distribution from the decays of W and Z bosons. This capability drives the jet energy requirement for the ILC detectors.

The event selection starts by forcing events into four jets. A cut-based pre-selection retains events consistent with a four-jet plus missing energy topology. All three possible di-jet associations to two bosons are considered. A kinematic fit that constrains the two boson masses to be equal is applied; in terms of mass resolution this is essentially equivalent to taking the average mass of the two di-jet systems. After a number of cuts used to reject the majority of the SM background, ILD obtained the mass distribution shown in *Figure 4.6*, left. The contributions from WW and ZZ final states are clearly distinguishable. By cutting the invariant mass, samples of $e^+e^- \rightarrow \chi_1^+\chi_1^- \rightarrow W^+W^-\chi_1^0\chi_1^0$ and $e^+e^- \rightarrow \chi_2^0\chi_2^0 \rightarrow ZZ\chi_1^0\chi_1^0$ can be isolated. The gaugino masses are then reconstructed from the endpoints of the energy reconstructed energy spectra of the reconstructed W and Z, as shown in *Figure 4.6*, right. For the analysis of simulated events in the ILD detector, statistical precisions of 2.4 GeV, 0.9 GeV, and 0.8 GeV are obtained for the masses of the $\chi_1^{\pm}$, χ_2^0 and χ_1^0 respectively.

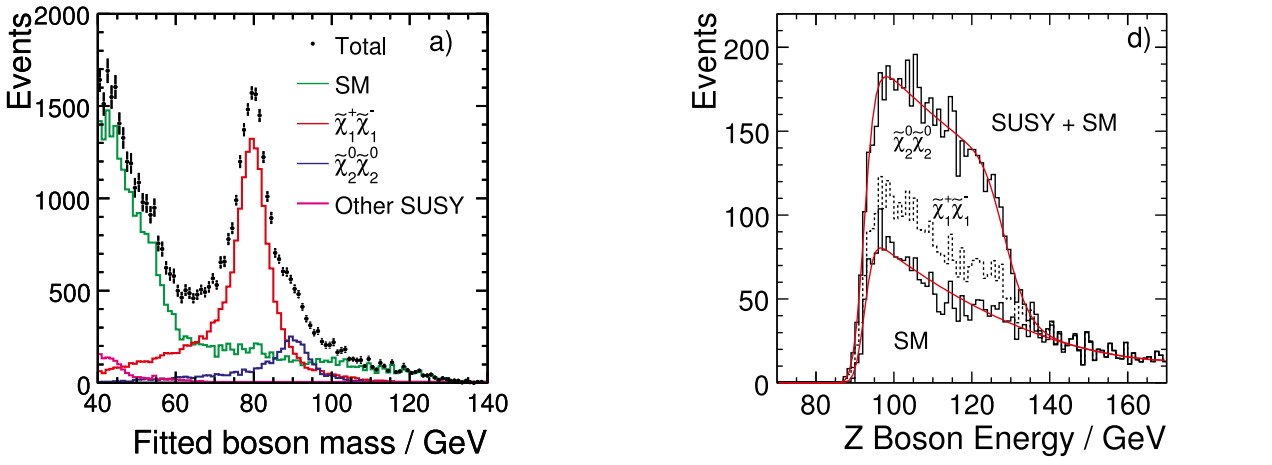

Figure 4.6 Left: distribution of reconstructed di-jet invariant masses from gauge boson decays in chargino and neutralino production. Right: reconstructed energy of select Z bosons and a fit to determine the χ_2^0 and χ_1^0 masses. Images: Mark Thomson

4.2.6 Squark production

In addition to the ILC benchmark channels both SiD and ILD studied a number of other physics processes. One such example is the study of squark production. Measurements of the neutralino relic density point to a small mass difference between the next-to-lightest SUSY particle (NLSP) and the lightest neutralino, assuming that the lightest neutralino makes up most of the dark matter in the universe. Motivated by this, SiD studied the case that the b squark was the NLSP and considered four different b squark and neutralino mass points of ($m_{bsquark,}$ $m_{neutralino}$) = (230,210); (240,210); (230,220); (240,220) GeV. The b squark mass determines the b squark pair production cross-section of 1.3 fb, 0.4 fb for b squark masses of 230 GeV and 240 GeV, respectively, at E_{CM} = 500 GeV. The mass difference between the b squark and neutralino determines the energy of the b-jets, which, for the model parameters considered here, are less than 30 GeV. At these b-jet energies the b-tagging efficiency is relatively low (10-30%).

The analysis proceeds by applying the Durham k_T jet algorithm with k_T^{min} = 10 GeV to the reconstructed particles. Events are required to have exactly two jets. The SM background is suppressed by requiring that the total visible energy be less than 80 GeV and by applying cuts on the event acoplanarity, jet polar angles and the number of reconstructed particles. In addition an event is rejected if a photon or electron with an energy greater than 300 MeV is detected in the SiD luminosity calorimeter. Following the selection cuts, a neural net algorithm is applied using the above cut variables as well as the total number of charged particles and a b-jet flavour tag variable. *Figure 4.7* shows the NN output for signal and background. Also shown is the statistical significance of the signal, $S/(S+B)^{1/2}$, for the mass point ($m_{bsquark,}$ $m_{neutralino}$) = (230,210) GeV as a function of the number of signal events passing the final NN cut as the NN cut is varied. A luminosity of 1,000 fb^{-1} is assumed. The other mass points ($m_{bsquark,}$ $m_{neutralino}$) = (240,210); (230,220); (240,220) GeV can all be excluded at the 95% confidence level.

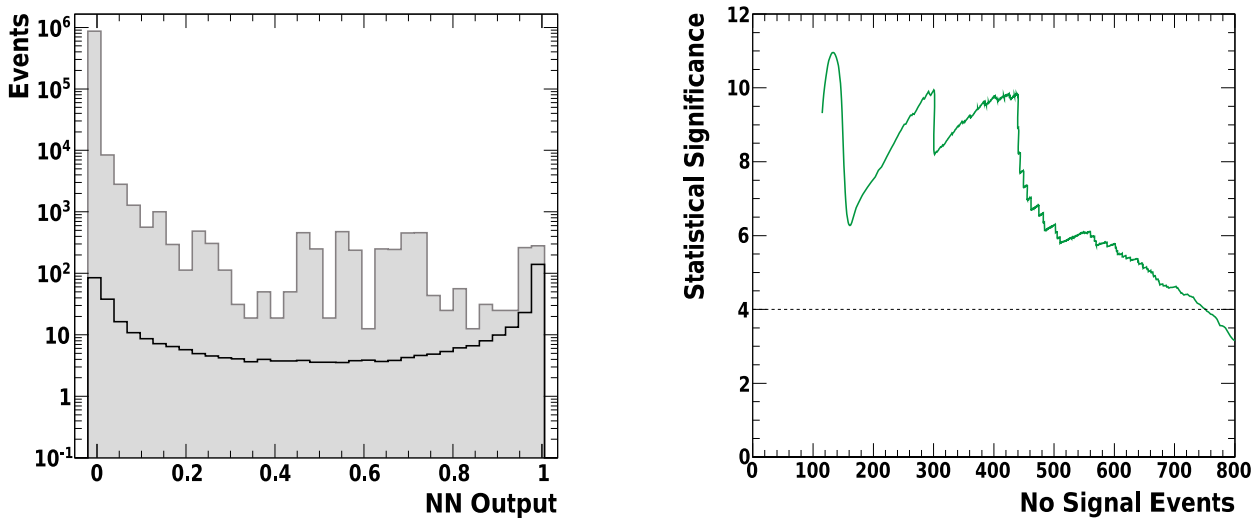

Figure 4.7 Left: final neural net output for the b squark mass of 230 GeV and lightest neutralino mass of 210 GeV (black) and SM background (filled histogram). Right: statistical significance versus the number of signal events passing the final NN cut as the NN cut is varied. Large variations are due to SM events with large weights. Images: SiD

4.2.7 Strong electroweak symmetry breaking

If strong electroweak symmetry breaking is realised in nature, the study of the WW scattering processes is particularly important. At the ILC the WW → WW and WW → ZZ vertices can be probed via the processes $e^+e^- \rightarrow qqq\nu\nu$ where the final state quarks arise from the decays of two W bosons or two Z bosons. Separating the two processes through the reconstruction of 4 jets requires an excellent di-jet mass reconstruction and thus provides a test of the jet energy resolution of an ILC detector. While not an official benchmark channel, this process was studied in detailed by the ILD concept group at E_{CM} = 1 TeV.

The analysis is relatively straightforward. Cuts are applied to remove the majority of the SM background, then events are forced into four jets and of the three possible jet-pairings, the one that minimises the product of $|m_{ij}-m_{W/Z}|$ and $|m_{kl}-m_{W/Z}|$ is chosen. The two processes WW → WW and WW → ZZ are separated using the reconstructed invariant mass distributions shown in *Figure 4.8*. The contributions from the WW$\nu\nu$ and ZZ$\nu\nu$ final states are clearly resolved as a result of the excellent jet energy resolution of the ILD detector. Fits to the anomalous quartic (4^{th}-order) gauge boson couplings (a_4 and a_5) were obtained from a binned maximum likelihood fit to the two-dimensional distribution of the boson polar angle in the reference frame of boson pair and the jet polar angle in the reference frame of each boson, giving a 90% confidence level sensitivity of $-1.38 < a_4 < +1.10$ and $-0.92 < a_5 < +0.77$.

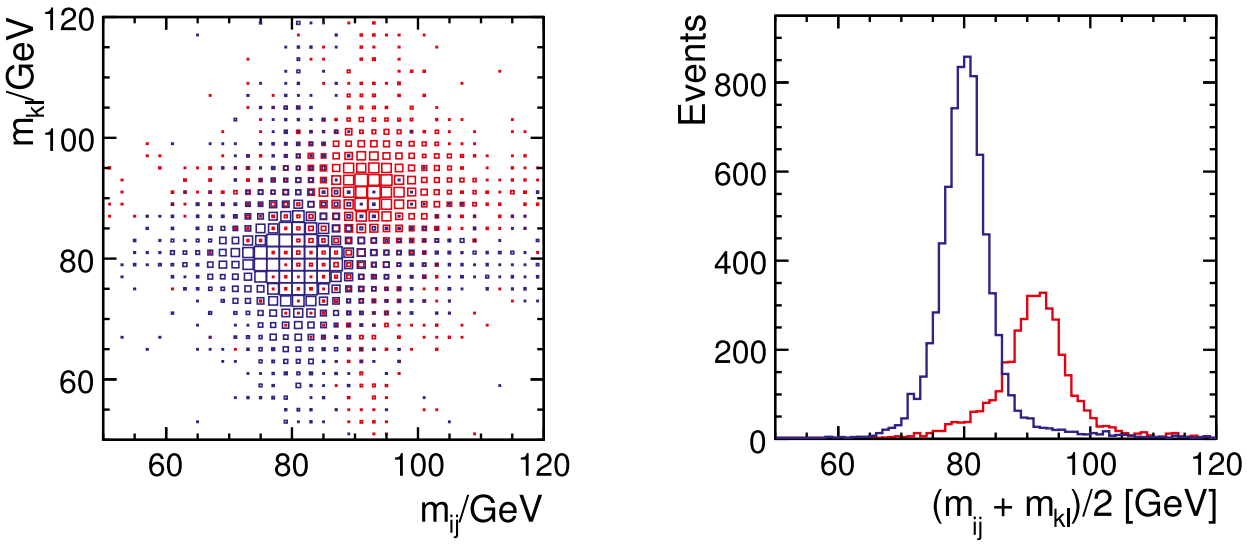

Figure 4.8 Left: the two di-jet masses. Right: the mean di-jet mass in $e^+e^- \to qqqqvv$ simulated events reconstructed in the ILD detector. Images: Mark Thomson

Towards the detailed baseline designs

As shown above, both the ILD and SiD detector concepts meet the basic requirements to carry out the ILC physics programme expected at energies up to 500 GeV. It should be emphasised that this has been demonstrated with full simulations and with full Standard Model backgrounds. Some 50 million events were generated at 250 GeV and 500 GeV, which amounted to more than 50 terabytes of simulated data for each for the two detector concepts. This is an unprecedented achievement for detector optimisation studies in the 0th stage.

The two LOI detector concept groups are now trying to further the level of realism in their detector simulations by implementing details of the detector system including various detector services such as power lines, cooling lines, and support structures, which had been represented only as a bulk of dead material with a density averaged over a relatively wide region. They are also planning to overlay beam-induced backgrounds in a more realistic way. These improvements will not only enhance the precision of the detector simulations, which is already very good, but also help establish the validity of the detector concepts at higher energies, say at 1 TeV.

It is very difficult to predict the physics scenarios at 1 TeV, since the terascale physics will take more concrete shape only after the discoveries at the LHC. Nevertheless, we need to prepare ourselves for the machine upgrade to 1 TeV by considering typical situations where the different aspects of the detector performance will have to be tested. For this purpose a new set of benchmark processes, primarily meant for the detector validation at 1 TeV, is being decided. The new set will include complicated final states such as those from $e^+e^- \to ttH$, eight jets or six jets plus an isolated lepton, as well as final states populating more in the forward-backward regions such as from $e^+e^- \to \nu\nu H$ and $e^+e^- \to WW$. There will be also some 500-GeV processes for the comparisons with the LOI studies. The results from these simulation studies will comprise the main body of the analysis section of the DBD document.

4.3.1 Standard Model physics

Higgs self-coupling

Most aspects of the SM Higgs physics are part of the benchmarks. However, one important and very challenging aspect is the Higgs self-coupling. The observation and measurement of coupling can be seen as the ultimate test of whether an observed Higgs particle is the SM Higgs or something different. It is potentially measurable from the final state ZHH. However, the results of the LOI studies were inconclusive. The expected cross-section is very low, and the background from $t\bar{t}$ is large. The aim of the current studies is to bring together expertise from all needed topics (jet-finding, flavour-tagging, kinematic fitting, theory) into a ZHH task-force and thereby be in the position to have definite answer on the feasibility of such a measurement by the DBD.

Top physics

Another SM topic only partly covered by the benchmarks is top physics. Here ongoing studies will address couplings, mass and forward-backward asymmetries. The last was addressed as a benchmark for the LOI. The LOI benchmark analysis was more aimed at detector performance studies, and thus it concentrated on fully hadronic decays to see if a detector can handle highly complicated events. A more sensitive mode is when one top decays semi-leptonically. In this mode, there is no ambiguity in separating top from anti-top, and a study on it with full simulation has been initiated.
Furthermore, recent theoretical advances shows that there is a very important quantum chromodynamic enhancement of the top pair cross-section near threshold. The implications of this effect are now under study, including the development of an event-generator that takes this effect into account. It is quite probable that the result of such a study will be to indicate a different running scenario than what was previously assumed to be optimal. For example, it seems probable that the study of the top-Higgs coupling can very well be done at E_{CM} = 500 GeV, contrary to what is assumed for the benchmark study of the channel (to be done at 1 TeV). With one inverse attobarn (ab^{-1}) of integrated luminosity at 500 GeV, a significant signal of the top-Yukawa coupling could be attained.

Gauge bosons

While WW production at 1 TeV is a benchmark study, the ZZ, Weν and Zee channels are being studied at 1 TeV. In addition, the LOI studies on the ILC capabilities to measure deviations from the SM predictions for triple-gauge couplings are being continued, in particular the impact of the modified beam parameters.

4.3 Ongoing physics analyses beyond benchmark reactions

4.3.2 New physics

Supersymmetry

Supersymmetry (SUSY) may provide a rich spectrum of kinematically accessible new particles at the ILC. It might also yield new sources of violation of conservation laws, for example, charge parity violation or flavour violation. New particles might be short- or long-lived, depending on the SUSY breaking mechanism and whether R-parity is conserved or not. Hence, various SUSY scenarios are under study.

The signals for SUSY consist of a complex mixture of dominant and subdominant processes, often with identical visible final states. An extended study of the popular SPS1a' is planned. In SPS1a', which is an mSUGRA-type model, all sleptons, neutralinos up to χ_3 and the lighter chargino can be produced at a 500-GeV ILC. For the LOI, certain channels were studied (smuons and staus), but no evaluation of the complete exploration was done. In particular, the combined precision on the lightest supersymmetric particle (LSP) mass from all channels is quite important to estimate, as it tends to enter into many other measurements.

A study of the possibly existing long-lived, heavy, charged particles, in particular the long-lived staus, is also ongoing. These types of models are particularly interesting because they are of the type that the LHC quite likely would be able to observe at an early stage.

Another class of SUSY models under study is bi-linear R-parity-violating SUSY. In such models, the neutral fermions (neutrinos) mix with the neutral bosinos (neutralinos), yielding a relation between neutrino masses and SUSY, and LSP decays to Standard Model particles. The LSP lifetime is long, so the decay vertex is expected to be well separated from production vertex.

Another search, extended beyond the LOI study, is a model-independent weakly interacting massive particle (WIMP) search in $e^+e^- \rightarrow n\gamma$ + invisible. WIMPs are possible candidates for dark matter. The SUSY LSP is a WIMP, but many other new physics models also predict the existence of such objects. Different models predict different spins of the WIMPs, different Lorentz structures and different decay modes. If they can pair annihilate into e^+e^-, then the reverse process can be detected at the International Linear Collider. In this case the two neutral (undetected) WIMPs are accompanied by an initial state radiation (ISR) from the incoming electron or positron, giving a photon recoil mass distribution that has a characteristic onset. The location of the onset and shape of the recoil mass distribution depends on the WIMP mass and spin. Experimentally, the WIMP signal has to be resolved from the large irreducible ISR background from $e^+e^- \rightarrow \nu\nu+n\gamma$ events. Assuming that the total cross-section for WIMP pair annihilation into SM fermion pairs is known from cosmological observations, the ILC sensitivity can be expressed in terms of the WIMP pair branching fraction into e^+e^-. It is found that the WIMP can be detected over a wide range of theory assumptions.

Other new physics: little Higgs and extra dimensions

Several non-SUSY models of new physics are also under study:

1. The little Higgs model shares several features with SUSY: It predicts a number of new states, some of which might be directly observable at a 500-GeV linear collider. If the model predicts that T-parity is conserved – some little Higgs models do, some don't – the lightest of these new T-odd states is stable and is a WIMP-type dark matter candidate. However, the quantum numbers of the new states are different from the SUSY case: In the simplest little Higgs model, the new states occur when extending the SM SU(2) doublets to SU(3) triplets so that the new states are left-handed quarks and leptons. One also obtains new heavy gauge bosons, and typically the heavy photon A_H is the WIMP. Ongoing studies of a scenario with a little Higgs model with T-parity have analysed heavy photon and SM particles, so a simultaneous fit of the masses of W_H , Z_H and A_H gives the vacuum expectation value <f>, which in turn implies that the ILC can determine the relic abundance to a level comparable to what the Planck mission will be able to do from the observation of the cosmic microwave background.
2. Models with extra dimensions are also being studied. In particular, the possibility of the existence of a 100-GeV-scale right-handed neutrino (N) has been considered. In the SM, the lightness of the neutrino can be understood by the seesaw mechanism, but then the N must be ultra-heavy. However, in compact extra-dimensional models, this is not so: An N would not need to be heavier than 100 GeV to explain the lightness of the ordinary neutrino. In addition, an infinite number of such states is expected as Kaluza-Klein (KK) excitations. At the ILC, the N could be produced together with an SM neutrino. In the decay process, the N is expected to have interacted with the Higgs field – transforming it to a virtual ν, which then decays to a W or a Z and an ordinary lepton. Due to neutrino mixing (the Pontecorvo-Maki-Nakagawa-Sakata mixing matrix), the ordinary lepton does not need to have the same flavour as the neutrino initially produced together with the N. If the N decays via a W*, all decay products will be observable and it can be fully reconstructed. A case where the masses of the first three KK modes are 150, 450 and 750 GeV, respectively, has been studied at E_{CM} = 500 and 1000 GeV. The cross-sections depend on the model of neutrino mixing, but the first KK mode would be observable in any case, while all three would be so at 1 TeV. In addition, by studying the number of events with different final state leptons, it would be possible to separate different models.

References

[4-1] T. Behnke et al., TESLA Technical Design Report, DESY 2001-011, ECFA 2001-209, March 2001.

[4-2] ILC project, International Linear Collider Reference Design Report, 2007, ILC-REPORT-2007-001.

[4-3] LHC/LC study group, G. Weiglein et al., Phys. Rept. 426, 47 (2006).

[4-4] The International Large Detector, Letter of Intent, March 2009, DESY 2009-87, KEK 2009-6.

[4-5] SiD Letter of Intent, March 2009, https://silicondetector.org/display/SiD/LOI.

05

COMMON TASK GROUPS

5.1 The Machine-Detector Interface Common Task Group

The Machine-Detector Interface (MDI) Common Task Group (CTG) has been established to deal with all topics that are common to the machine and the detector design. Strong interdependencies exist at a linear collider between both push-pull detectors and between the detectors and the machine itself. Therefore the MDI CTG is a forum of information exchange for the SiD (Silicon Detector) and the ILD (International Large Detector) as well as for the respective groups of the ILC machine design team. The task group currently comprises six members, three from ILD and three from SiD, and usually meets together with the technical area leaders of the ILC beam delivery system[4] to enable a well functioning communication on common work and related information between all three parties.

The paramount challenge in the design of the interaction region of the ILC is the development of an engineering design for a realistic push-pull system. The idea of using one common beam line with two interchangeable detectors has never been realised at a major particle collider so far, so it is new territory for all involved experts.

[4] Current members: K. Buesser (convener, DESY, ILD), P. Burrows (deputy convener, Oxford, SiD), Alain Hervé (University of Wisconsin, ILD), T. Markiewicz (SLAC, SiD), M. Oriunno (SLAC, SiD), T. Tauchi (KEK, ILD); regular guest: A. Seryi (Oxford, GDE-BDS)

5.1.1 Design process

Figure 5.1 displays the flow diagram of the path towards an engineering design of the interaction region. The starting point is a set of functional requirements that define the ground rules for a friendly coexistence of two detectors and the machine in the push-pull scenario. These ground rules have been worked out in the discussions of the MDI CTG together with the ILC Global Design Effort (GDE) Beam Delivery System Group (BDS) and have been published in the Interaction Region Interface Document *[5-1]*.

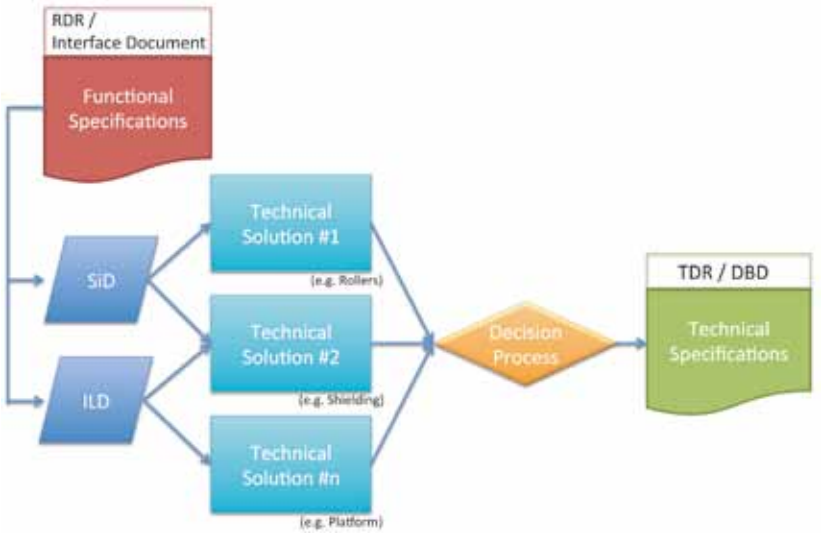

Figure 5.1 Towards an engineering design. Image: Karsten Buesser

The detector concept groups are designing technical solutions for the detector integration with the interaction region that need to fulfil these functional requirements. While some of those technical solutions might be common from the start for both detectors, for example, a common design of the shielding in the underground hall, some might be different, such as the design of the detector motion systems where SiD prefers a rollers and ILD a platform. In the end, the technical solutions need to be evolved so that a decision could be taken for the common design. The detailed engineering requirements form then the basis of the *Technical Design Report* and the detailed baseline design (DBD).

The MDI CTG started this process after the publication of the ILC *Reference Design Report* (RDR). Major milestones were the publication of the interaction region Interface Document and the Letters of Intent (LOI) of the detector concepts in 2009.

5.1.2 Interaction Region Interface Document

The Interaction Region Interface Document is a major deliverable of the MDI CTG. It was published in 2009 and has the approval of the detector concepts and also of the GDE project managers. The document lists requirements that stem from the technical and physical boundary conditions of the machine design. It includes geometrical boundaries, like the required floor space of the underground experimental hall or the height of the beam above the floor. It also covers safety and working requirements like limits on the allowed magnetic fields or about the radiation environment. Emphasis has been placed on the requirements defined by the ILC beam operations. Vacuum conditions and the requirements on the support and alignment of the final focus magnets are of paramount importance to a successful operation of the ILC.

5.1.3 Push-pull design study

The technical work on the engineering design and the technical specifications of the interaction region are the focus of the MDI group since the publication and validation of the Letters of Intent. The most important topic is the engineering design of a realistic push-pull system for both detectors. As the required engineering resources are not controlled by the MDI CTG, but exist mainly within the detector concept and machine groups, a comprehensive work plan needed to be established in close cooperation with the participating laboratories and universities. Following a request by the ILC Steering Committee, which offered help in finding additional resources, the MDI/Beam Delivery System (BDS) Group has developed a work plan for a design study on the push-pull system. An important milestone will be the choice of a common detector motion system (platform or rollers) that is envisaged for the first half of 2011.[5] *Figure 5.2* shows a possible underground hall layout with the detectors in push-pull configuration with rollers and with platforms.

[5] In March 2011, it was decided that the detector motion system will use platforms.

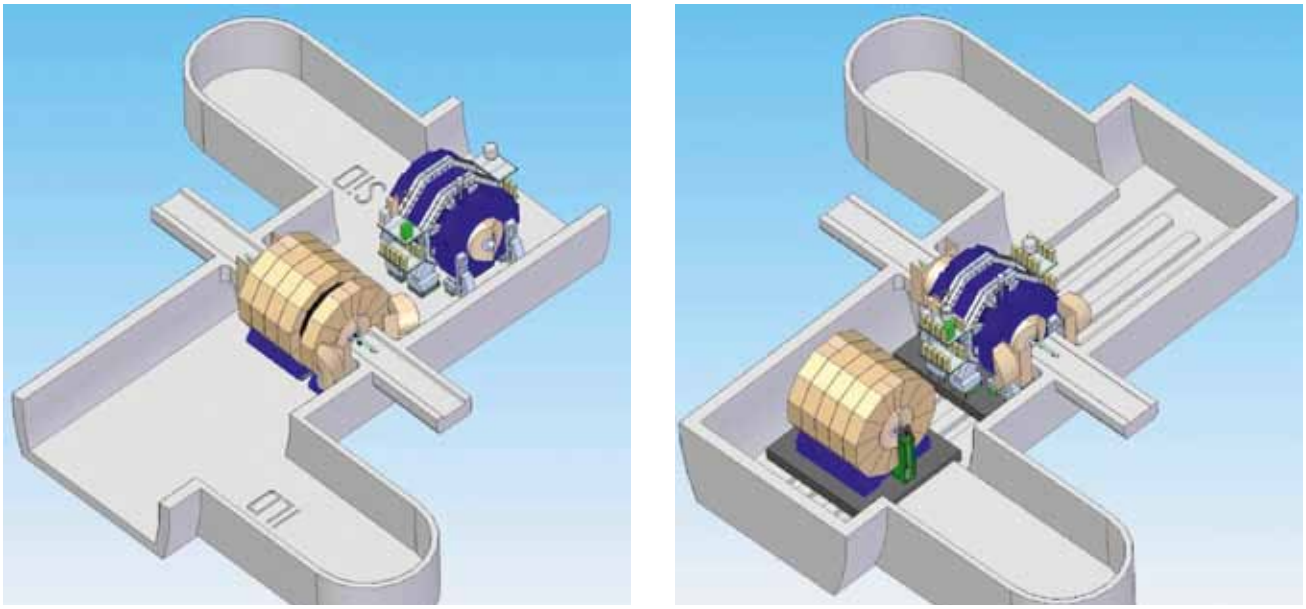

Figure 5.2 Underground hall with both detectors in push-pull configuration: roller-based system (left) and platform-based system (right). Image: Marco Oriunno

5.2 Engineering Tools Common Task Group

As the two detectors concepts, ILD and SiD, will be placed in a common experimental area and will share some services and constraints, it is necessary to ensure the compatibility of their engineering tools and that they are working with the same basis data. This is the purpose of the Engineering Tools CTG.

An additional goal of the Engineering Tools CTG is to propose and validate the use of the future ILC common tools.

The group concentrated its work on the selection of a document server specifically devoted to the repository and exchange of engineering documents in a consistent way with the International Linear Collider's existing tools. This system is to be used as a support tool for the coordination of the engineering process and will facilitate the informational workflow during of the lifecycle of the project within the constraints of an international project.

Thus the decision was to follow the recommendations of GDE and to use the ILC EDMS (electronic document management system), led by the DESY EDMS team *(Figure 5.3)*.

Figure 5.3 Foreseen system breakdown structure for the detectors EDMS

An adequate system breakdown structure describing the main components of the two detectors has been created and is to be implemented on the ILC EDMS with a common level corresponding to the design of the two detectors in the experimental hall.

This common node should contain 2-D drawings for both detectors in order to have reference dimensions and ease the studies concerning the experimental hall (cavern design, motion system, services). It will become the repository to exchange technical notes and data for detectors common studies.

5.3 The Detector R&D Common Task Group

The Detector R&D CTG was created out of a desire to work across the detector concept groups and coordinate activities between these groups and the horizontal detector R&D collaborations, such as CALICE (CAlorimetry for the LInear Collider with Electrons) and LC-TPC (A Time Projection Chamber for a future Linear Collider). It was realised that many issues in the area of detector development are common and are better addressed, not in a competitive, but in a collaborative common framework. This holds especially true for the area of detector R&D. The proposed detectors for the ILC call for highly sophisticated technologies that have not yet reached a level of maturity to prove that the concept can be employed in a large-scale experiment. Moreover, the resources dedicated to the detector R&D are scarce. The Detector R&D CTG was formed to coordinate cooperation of detector R&D among various parties and to maintain contact with detector R&D collaborations. The synergistic and mutually supportive efforts in the area of detector R&D are illustrated in *Figure 5.4*. A shared test beam infrastructure is used to independently characterize silicon detectors and a time projection tracking chamber, where each will benefit from the studies of the other.

The Detector R&D CTG is composed of representatives from the ILC collaborations, the horizontal detector R&D collaborations and dedicated detector technology groups. The group acts as a forum for all detector development that is being carried out within the ILC community, facilitating their communication. Furthermore, the group acts as a strong advocate of support for its activities and the research activities of its members. It is also a resource of the ILC management that can be called upon to carry out specific tasks, such as surveys in certain areas of R&D as well as reporting at various advisory and review panels.

The overarching goal of the Detector R&D CTG is to help the concept groups be ready by 2012 to make a realistic proposal for detectors that can execute the precision-physics programme. Collaboration readiness means that the technologies are well understood and proven to be scalable; it does not imply a fully engineered design. Because of the structure of the collaborations and their funding this group does not coordinate existing activities of the separate R&D collaborations.

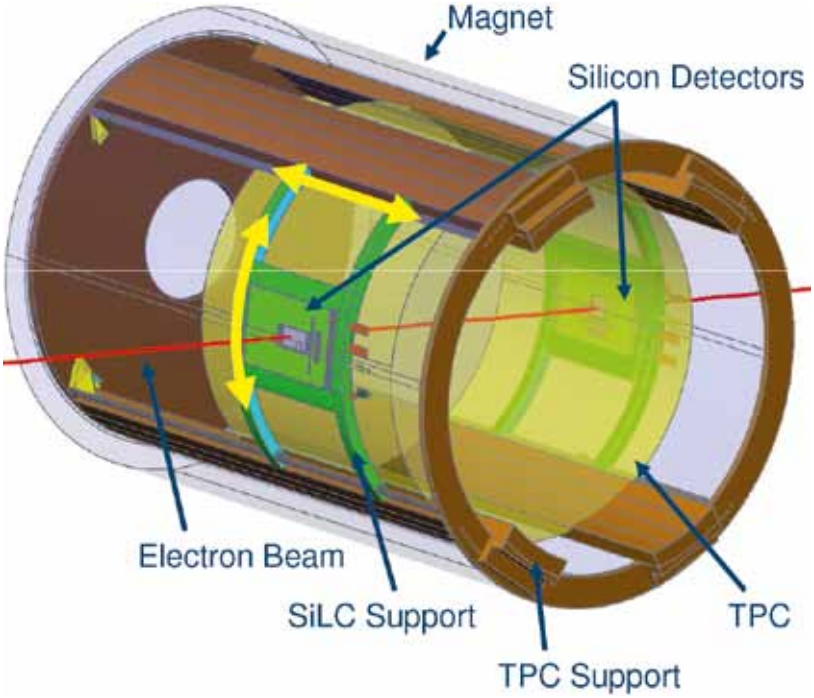

Figure 5.4 Example of a synergistic effort between different detector development efforts characterising a silicon and time projection chamber tracking system in a shared test beam infrastructure. Image: SILC Collaboration

The support for the development of new detector technologies has fluctuated significantly over the last few years. The R&D is often considered to be far enough in advance of any defined future project that the importance and need for this effort has struggled, and continues to struggle, to be formally recognised by the agencies. As a result, the funding situation has been relatively unstable and the size of the community engaged in the project has ebbed and waned with the real and perceived level of support. The detector development programme currently faces an immediate problem beyond 2012. Efforts could be severely curtailed or even stopped beyond 2012, which would be a significant loss of its decade-long investment in the development of new technologies. The Detector R&D CTG continues to strongly argue for stable strong support for its activities beyond 2012.

A sustained, stable and strategic investment in the area of detector development is critical, not only for the ILC, but for the viability of the field as a whole. Many R&D initiatives from within the ILC detector groups have already found their way into other projects, some beyond high-energy physics. For example, the DEPFET sensor technology for an ILC vertex detector is currently being deployed for the Belle-II vertex detector at KEK in Japan and is also being considered for a large-area Cherenkov telescope studying air showers. The development work for a micro-pattern-gas detector time projection chamber (TPC) has been implemented in the TPC for the T2K experiment at Japan's J-PARC, shown in *Figure 5.5*. Large-scale application of silicon photomultipliers was proven for the first time in the context of R&D for the ILD concept detector and has subsequently been chosen for the T2K detector and the upgrades of the CMS detector of LHC at CERN and the Belle kaon and muon end cap identification system. Another example is the 3-D vertically integrated silicon technology, which is being considered for the CMS upgrade experiment. The development of CMOS pixel detectors has found its way into nuclear and heavy-ion physics experiments. The Detector R&D CTG made a systematic survey of these spin-off cases *[5-2]*. The field of particle physics is a highly integrated field and the importance of investments in the development of new detector technologies and detector systems for any facility is unquestioned for the sustained viability of the field. The Detector R&D CTG has recently proposed that a plan be developed to coordinate the detector R&D on a broad international basis, leading to a more stable, coherent, efficient and cost-effective way to carry out research and development for future projects.

Figure 5.5 Micromegas readout plane for the near detector of the T2K experiment, the development of which fully originated out of R&D carried out for the ILC. Image: T2K Collaboration

Two other lepton colliders, albeit with a different timescale than the ILC, are being considered, namely the Compact Linear Collider (CLIC) and the muon collider. The Detector R&D CTG tries to maintain close links with the activities related to these projects, given the large overlap in technical requirements. When topics can be identified that serve all the projects, common workshops are organised. There is in particular an active participation of physicists performing CLIC-related detector studies within the CALICE, LC-TPC and forward calorimetry FCAL collaborations.

To provide infrastructure to the community is another area that the Detector R&D CTG tries to address. Beam tests of prototype detectors are an essential element in bringing a technology from the concept stage to the detector stage. Facilities for beam tests are scarce and are subsequently heavily subscribed. The Detector R&D CTG provides the individual detector groups a forum to optimise use of all available resources, and to discuss areas of concern.

5.4 Software Common Task Group

The Software CTG is charged with coordinating tools and databases common to the detector concepts and code compatibility for simulation studies. It is also charged with working on any common software issues for ILC detector studies. For the detailed baseline design studies, the Research Director has requested that the ILD and SiD groups develop a realistic detector simulation model, including faults and limitations, and perform simulation and re-analysis of some LOI benchmark processes and analyses of newly defined processes at 1 TeV, including realistic backgrounds. This is the main target of current software activities in SiD and ILD and making this effort coherent is the goal of the Software CTG *[5-3]*.

For the LOI, the common generator samples were produced primarily at SLAC; small signal samples were produced at DESY and KEK. The Standard Model samples were produced using an event generation program, Whizard *[5-4, 5-5]* at the centre-of-mass energy of 250 and 500 GeV. The processes consisted of final states of 2 to 6 fermions and 0 to 4 gammas (γ) by collisions of e^+e^-, $e^{+/-}\gamma$ and γγ. We adopted StdHep *[5-6]* as the common file format. Using the same input event samples has been extremely useful to understand the results of the benchmark studies, especially when differences were seen.

For DBD studies, new samples have to be generated for benchmark studies with updated generator code. In order to share the work involved in the generator code preparation and the sample production, a generator sub-working group was formed in early 2010. A member from the CLIC study group joined soon thereafter, and thus the group is now working together as the Linear Collider Generator Group. The group agreed to use Whizard 1.95 and Pythia 6.422 for the DBD samples with some minor exceptions. The interface to Whizard 1.95 for linear collider physics has been updated, which includes a proper treatment of the polarisation in τ decay, use of the CKM matrix, preparation of a luminosity function for new ILC beam parameters, and use of LEP-tuned parameters for quark fragmentation. New features such as storing initial particles' information, colour flow and spin information in output files and the ability to generate many processes at once will be implemented soon. The systematic production of the generator samples will start in 2011.

For easy communication at the software level and sharing of software tools among the linear collider community, a common persistence format and a common event data model are essential. To this end, Linear Collider Input/Output (LCIO) *[5-7]* has been developed and has been used by ILD and SiD for the infrastructure of their simulation and reconstruction. LCIO has been used since the pre-LOI period, which led to the successful development and use of cross-concept group software packages such as PandoraPFA *[5-8]* and LCFIVertexing *[5-9]*.

When the LOI studies were completed in 2009, requests from users were collected, and an effort to upgrade LCIO from version 1.0 to 2.0 was launched. A list of new features planned includes (1) random access to event data, (2) the support of ROOT dictionary and IO with ROOT format, (3) extension of track data model for 2-D devices and improved treatment of kink and curl tracks, (4) preservation of additional generator information such as spin, colour and others. Features (1) and (2) have been implemented and (3) is in preparation, involving discussions among software experts. LCIO version 1.51 was released in autumn 2010, and a release of version 2.0 is expected in 2011.

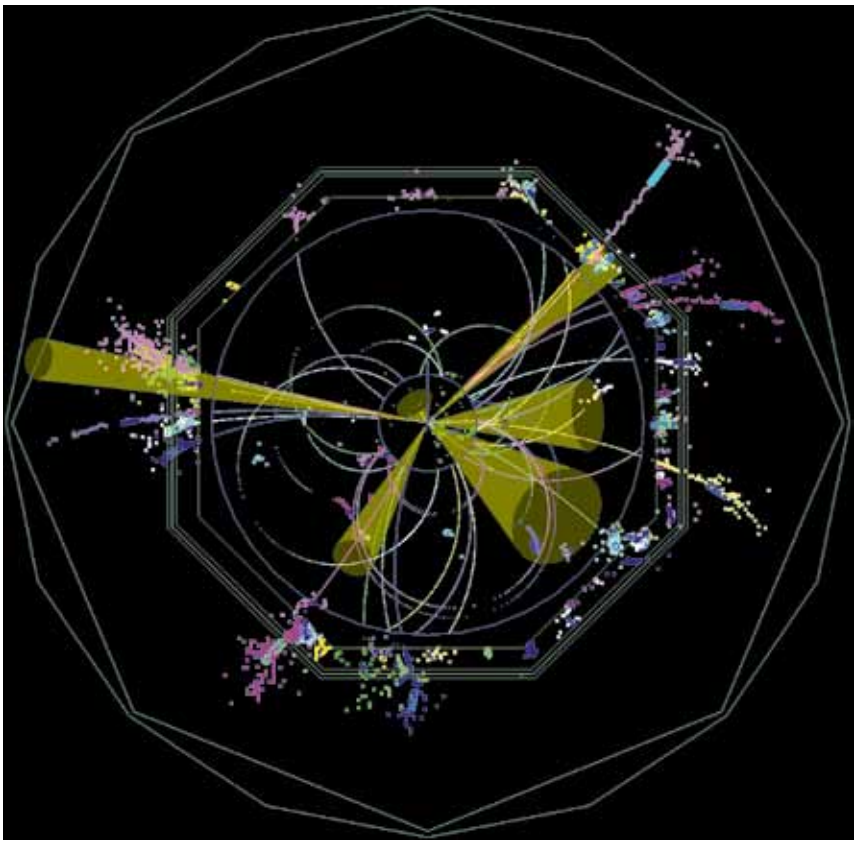

Figure 5.6 A typical 6-jet event simulated and reconstructed by the ILD software. Calorimeter and tracker hits grouped to the same particle flow objects are painted with the same colour and reconstructed jets are indicated by cones. Image: ILD

Despite differences between the detector concepts, ILD and SiD use many of the same software tools. The Software CTG acts as a contact between the two groups on software tools, such as geometry infrastructure, particle flow analysis (PFA), vertexing and kinematical fitting. Faced with the request from the Research Directorate to implement detailed detector models for simulation, the two detector groups desired a program with unified geometry tools to support detector simulations, event reconstruction and physics analyses. Such a program has been underway since 2010 in Europe under the aegis of the Advanced European Infrastructures for Detectors at Accelerators, including people outside the ILC community. The PandoraPFA program, which performs PFA very efficiently, has been rewritten to make it more modular and less framework- and geometry-dependent. It has been used to analyse SiD events simulated by the new SiD geometry for DBD study. A typical 6-jet event simulated and reconstructed by ILD is shown in *Figure 5.6*. The LCFIVertexing package has been widely used in the linear collider community to bring out the best performance of vertex detectors in ILC experiments. The code was originally developed in the UK, but it is now maintained by a Japanese group and work is in progress to improve the performance, especially in multi-jet environments. In order to encourage the broader use of common software tools, communication among people participating in software developments is crucial. In addition to presentations at various workshops, the Software CTG organised a dedicated linear collider software meeting in May 2009 at CERN and a second in July 2010 at DESY. It plans to continue these meetings in the coming years.

5.5 Physics Common Task Group

The Physics CTG was added to the Physics and Experiments Board in the autumn of 2008. The purpose of this group is to develop the understanding of the physics goals and opportunities of the ILC, building on the work done for the physics volume of the *Reference Design Report.* One goal of this group is to assess changes in the ILC capabilities as a result of changes in the design and schedule of the machine. However, its main purpose is to take into account progress in our understanding of elementary particle physics, especially from results from the Large Hadron Collider experiments. It is often said that the ILC will follow the LHC and build on the discoveries made by that machine. Ideally, this connection should be made in concrete and specific terms. This is the primary goal of the Physics CTG.

The LHC is now well into the early phase of its operation. It has been running at an energy 3.5 times that achieved by the Tevatron collider at Fermilab, and the event samples analysed so far by the LHC experiments are approaching those of the Tevatron experiments. The search for the rare events that signal the appearance of the Higgs boson and other new particles has just begun. As the data samples increase, the search for new particles will sharpen. The Physics CTG has been preparing for this search by enumerating scenarios for new physics that can be discovered relatively early in the LHC programme and analysing the experiments at the ILC that these discoveries will call for. Though the Higgs boson will be relatively difficult to discover if its mass is below 130 GeV, as preferred by other data, there is a significant chance that the Higgs boson will be seen before the end of 2012. The current estimate of the sensitivity of the LHC to the Standard Model Higgs boson is shown in *Figure 5.7.*

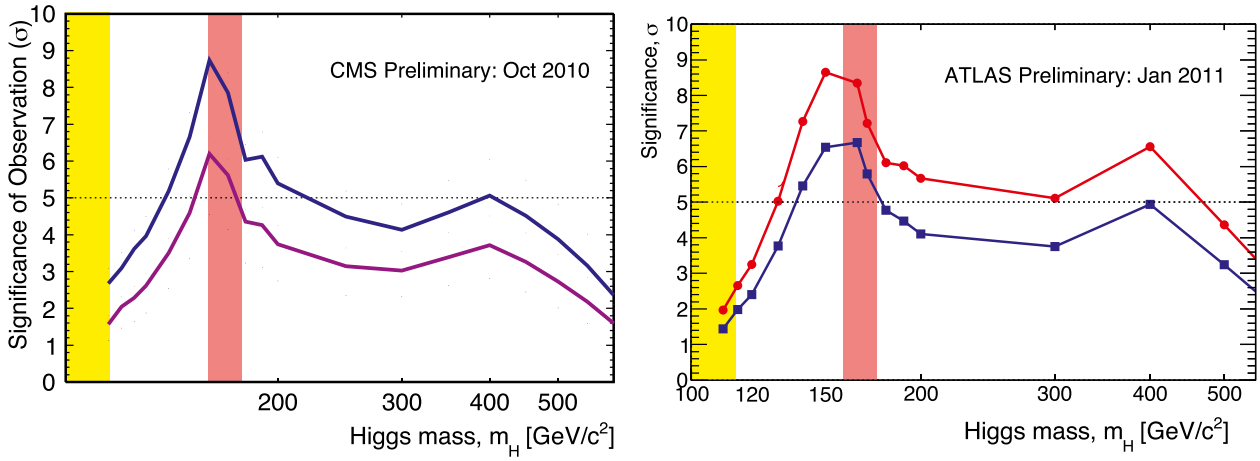

Figure 5.7 Expected significance of the observation of the Standard Model Higgs boson as a function of the mass of that particle, as estimated by the CMS and ATLAS collaborations for different levels of integrated luminosity at the LHC *[5-10, 5-11].* Observation at 5 sigmas is the conventional criterion for a particle discovery. The curves give the estimates for 2 inverse femtobarns (fb^{-1}) (purple), 5 fb^{-1} (blue), and 10 fb^{-1} (red). The vertical bands are the exclusion regions for the Standard Model Higgs boson by the Tevatron as of early 2011 (red) and LEP (yellow). Each experiment accumulated over 5 fb^{-1} of data in 2011. Left image: CMS. Right image: ATLAS.

The Physics CTG has also carried out a number of other studies for the ILC programme. It has discussed the programme of a photon collider based on the ILC in the light of new understanding of constraints on the properties of the Higgs boson and the LHC capabilities for Higgs boson measurements. The group has also participated in the analysis of the SB2009 revision of the ILC baseline design, emphasising in particular the maintenance of the ILC capabilities for precision measurement. It has discussed progress in the ILC capabilities for Higgs boson studies and, in particular, the measurement of the characteristic self-coupling of the Higgs boson field. It has also participated, with members of the Software CTG and representatives of the two concept groups, in defining the new full simulation studies that should be done for the 2012 detailed baseline design.

References

[5-1] ILC-Note-2009-050.

[5-2] ILC-REPORT-2011-034, http://ilcdoc.linearcollider.org/record/35252.

[5-3] http://www.linearcollider.org/wiki/doku.php?id=swctwg:swctwg_home.

[5-4] W. Kilian, T. Ohl, J. Reuter, WHIZARD: Simulating Multi-Particle Processes at LHC and ILC, http://arxiv.org/abs/0708.4233.

[5-5] M. Moretti, T. Ohl, J. Reuter, O'Mega: An Optimizing matrix element generator, LC-TOOL-2001-040-rev, http://arxiv.org/abs/hep-ph/0102195.

[5-6] http://cepa.fnal.gov/psm/stdhep/.

[5-7] LCIO: A Persistency framework for linear collider simulation studies. F. Gaede, T. Behnke, N. Graf, T. Johnson, In the Proceedings of 2003 Conference for Computing in High-Energy and Nuclear Physics (CHEP 03), La Jolla, California, 24-28 Mar 2003, pp TUKT001. e-Print: physics/0306114.

[5-8] Particle Flow Calorimetry and the PandoraPFA Algorithm, M. A. Thomson, NIMA 611 (2009) 25-40.

[5-9] The LCFIVertex package: Vertexing, flavour tagging and vertex charge reconstruction with an ILC vertex detector, D. Bailey, et al., NIMA 610 (2009) 573-589.

[5-10] CMS Note 2010/008 and http://twiki.cern.ch/twiki/bin/view/CMSPublic/PhysicsResultsHIG.

[5-11] ATLAS collaboration, report ATL-PHY-PUB-2011-001 (2011), http://cdsweb.cern.ch/record/1323856/.

06

WORKING GROUPS

6.1 SB2009 Working Group

The value of energy variability of the linear collider, enabling threshold scans, has been emphasised as critical as long as the linear collider has been advocated. The ILC Steering Committee (ILCSC) 'scope document' *[6-1]* included variable energy operation and good luminosity in its specification of the linear collider requirements.

To meet these crucial requirements, the Global Design Effort (GDE) developed the design presented in the *Reference Design Report* (RDR), with energy variability over the 200- to 500- gigaelectronvolt (GeV) centre-of-mass energy range and with electron polarisation of at least 80%.

Last year, in preparing for the next major design phase, moving from the RDR to the *Technical Design Report* at the end of 2012, the GDE initiated a process to evolve the ILC design to improve the optimisation of cost to performance-to-risk with major changes that will improve these tradeoffs. An early set of these changes in the form of a straw man baseline, SB2009, was presented in a plenary session at the September 2009 Linear Collider Workshop of the Americas in Albuquerque, USA (ALCPG) *[6-2]*.

In the months following the Albuquerque meeting, the specific parameters of SB2009 were presented. Two sets of parameters were presented, one assuming travelling focus operation at the interaction point, achieving a luminosity of 10^{34} $cm^{-2}s^{-1}$ at 500-GeV centre-of-mass energy, and parameters without the travelling focus. Among the changes from assumed RDR parameters were reduced low centre-of-mass energy luminosities, increased beamsstrahlung and associated background pairs and increased energy beam spread. Research Director Sakue Yamada established a physics and detectors SB2009 Working Group to study the impact of the design changes on the physics performance, convened by Jim Brau. The working group membership includes T. Barklow, M. Berggren, J. Brau, K. Buesser, K. Fujii, N. Graf, J. Hewett, T. Markiewicz, T. Maruyama, D. Miller, A. Miyamoto, Y. Okada, M. Thomson and G. Weiglein, and has benefitted from contributions by P. Grannis and H. Li. The Working Group identified issues of concern and risk for the physics programme and developed a plan of studies to measure the impact. The most significant concern was the reduced luminosity for lower energies, as illustrated in *Figure 6.1*.

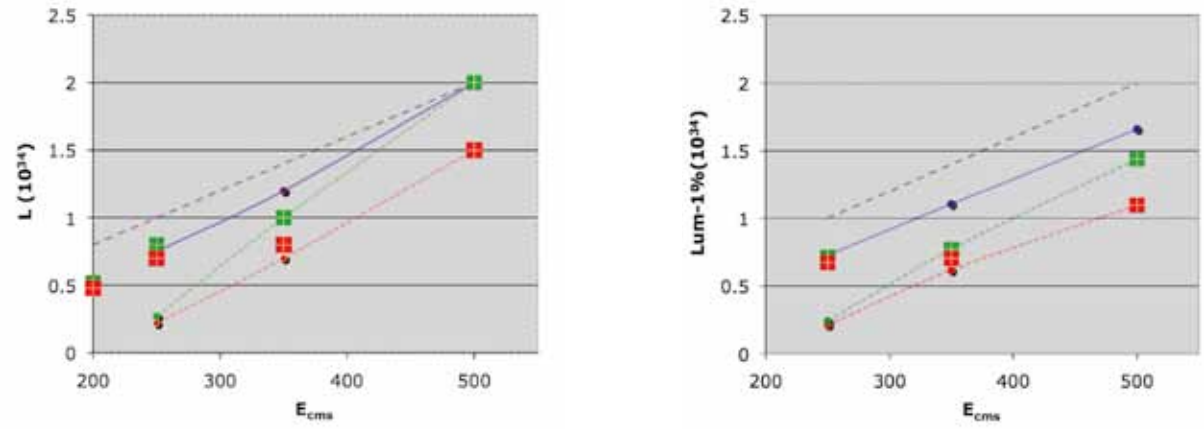

Figure 6.1 Left: luminosity versus centre-of-mass energy (ECMS). Right: luminosity restricted to the peak at full energy allowing less than 1% loss of the full collision energy. Red squares: New ILC, no travelling focus. Green squares: New ILC, travelling focus. Red dots: 2009 straw man ILC, no travelling focus. Green dots: 2009 straw man ILC, travelling focus. Violet dots: 2007 RDR. Dashed line: reference line showing luminosity proportional to energy. The RDR parameters are unofficial. SB2009 parameters were presented in 2009. Parameters labeled 'New ILC' were determined in 2010 following the Beijing Linear Collider Workshop. Image: Jim Brau

In the early months of 2010, leading up to the Beijing Linear Collider Workshop (March 2010), the study group prepared analyses of a few benchmarks. These established quantitatively that the low-energy performance of SB2009 had a serious negative impact on optimal performance at lower energies, such as at and just above the threshold for Z-Higgs (210 to 350 GeV), an assumed key operating point for the measurement of Higgs properties. The optimal operating point for the Z mass measurement appeared to be 350 GeV, rather than the 250 GeV assumed for the RDR parameters. Threshold scans for new lower mass states were also significantly affected.

The studies included:

1. Backgrounds (M. Berggren , T. Maruyama)
2. Higgs mass and cross-section measurements (H. Li)
3. Stau measurements (M. Berggren)
4. Low-mass SUSY scenario (P. Grannis)

Figure 6.2 shows the resulting electron-positron pair distributions *[6-3]*. The SB2009 parameters were found to have a small impact on the margin between the pairs and beam pipe. Compared to the RDR parameters, the total energy per bunch crossing in pairs for SB2009 was found to increase from 215 teraelectronvolts (TeV) to 635 TeV with the travelling focus. The number of electrons and positrons increased from 85,500 to 203,000, with average energies increased from 2.5 GeV to 3.1 GeV. A related study showed increased, but manageable, backgrounds in the vertex detector *[6-4]*.

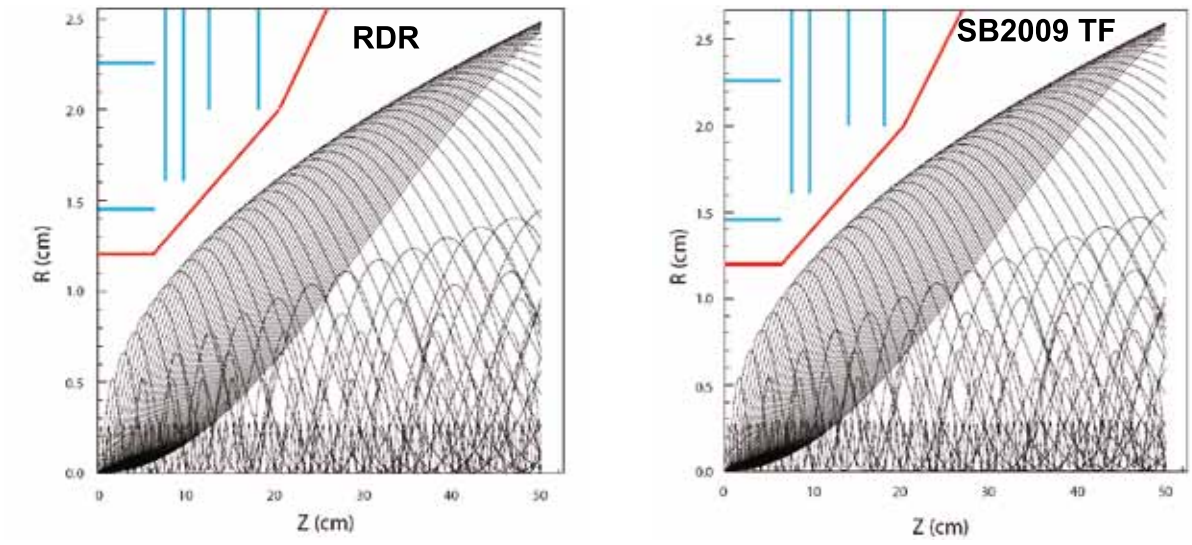

Figure 6.2 Distribution of beam pairs near the interaction point relative to the SiD beam pipe and vertex detector for the RDR beam parameters (left) and SB2009 with travelling focus (right). Image: Takashi Maruyama

The results of these studies were also presented at the Beijing Linear Collider Workshop.

Responding to these comments from the physics community, the GDE began investigating concepts that could improve the low-energy luminosity by increasing the operating rate of the design above the nominal 5 hertz and by improving the final quad doublet focusing system. These new designs matured over the summer months of 2010, and in the autumn of 2010 the GDE provided new baseline (NB) parameters to the SB2009 Working Group.

The Working Group repeated its studies of physics performance, noting that the new parameter set largely restored the performance of the RDR. The Higgs mass and cross-section measurement study *[6-5]* are summarised in *Table 6.1*. The operation at each energy is normalised to correspond to a constant period of time. The Higgs mass precision is improved from 43 to 29 megaelectronvolts (MeV) compared to the RDR when operating at 250 GeV with the travelling focus. The cross-section precision is also improved from 3.9% to 3.4%.

Beam parameters	L_{int} (fb^{-1})	ε	S/B	M_H (GeV)	σ (fb) (δσ/σ)
RDR 250	188	55%	62%	120.001 ± 0.043	11.63 ± 0.45 (3.9%)
RDR 350	300	51%	92%	120.010 ± 0.087	7.13 ± 0.28 (4.0%)
NB w/o TF 250	175	61%	62%	120.002 ± 0.034	11.67 ± 0.42 (3.6%)
NB w/o TF 350	200	52%	84%	120.003 ± 0.106	7.09 ± 0.35 (4.9%)
NB w/ TF 250	200	63%	59%	120.002 ± 0.029	11.68 ± 0.40 (3.4%)
NB w/ TF 350	250	51%	89%	120.005 ± 0.093	7.09 ± 0.31 (4.4%)

Table 6.1 Results based on NB beam parameters, assuming a beam polarisation of e^-: –80%; e^+: +30%, compared with those of RDR beam parameters. *[6-5]*

Higgs branching ratio studies have also been completed *[6-6]*.

A study of staus at the SPS1a' point (a supersymmetry benchmark point *[6-7]*) was repeated with the new beam parameters *[6-8]*. Three impacts of the SB2009 parameters were evaluated: increased background pairs in the BeamCal (beam calorimeter) could induce more γγ background; the overlaid beam background on the signal could reduce efficiency; and with a reduced number of events in the peak and a more spread-out peak, the precision of the mass measurement could be affected. The study found a degradation of 15 to 20% in mass and cross-section errors operating at the full 500-GeV centre-of-mass energy.

A run scenario study for the first 1,000 inverse femtobarns of data at the 500-GeV ILC first performed in 2002 was repeated with the new beam parameters. A SUSY working point (Snowmass 2001 SM2, *[6-9]*), although ruled out by current data to some level, has a very rich spectrum of supersymmetric particles, or sparticles, that are accessible at the 500-GeV (and below) ILC. The SUSY portion of the programme was composed of runs at the full 500-GeV energy to produce all accessible sparticle pairs and obtain a rough estimate of the masses through measurements of endpoint energies of observable final state particles, followed by dedicated scans across the thresholds for several of the sparticle pairs to obtain a more accurate determination. The importance of a $t\bar{t}$ threshold scan and of the critical need to measure the Higgs boson properties was recognised in the study. The selected energies of operation included a run above 500 GeV aimed at studying the $\tilde{\chi}_1^+\tilde{\chi}_2^-$ reaction, assuming that a tradeoff between energy and luminosity could be achieved. It also included a run with electron-electron operation to study the sharp threshold for selectron R-pair production. Both of these were included in part as a reminder that such special operating conditions may be required by the physics. The details are provided in *[6-10]*.

Table 6.2 presents the estimated sparticle mass precisions (in GeV) for luminosities at approximately the full centre-of-mass energy (labelled E_{CM} scaling), the RDR parameter sets, and the new baseline parameters (labelled NB). NB precisions are presented with and without the travelling focus (TF) and assume use of the full luminosity (full L), or just the luminosity within 1% of the full collision energy (peak L).

As expected, the changes in sparticle mass precision expected in the RDR parameter set differ little from those with the E_{CM} luminosity scaling. The precisions are typically only a few percent worse than with E_{CM} scaling, and at worst are roughly 10% larger. Similarly the full luminosity with travelling focus new baseline parameters (NB TF full L) at any energy show little degradation of mass precision. But the mass precisions degrade by up to around 25 to 30% for the other parameter sets, either considering only the luminosity within 1% of the nominal energy (NB TF peak L), without travelling focus (NB no TF full L), or just peak luminosity without travelling focus (NB no TF peak L).

Table 6.2 Estimated total sparticle mass precisions (in GeV) for all parameter sets considered, including cases with no travelling focus and the cases considering only the luminosity within 1% of the nominal energy (peak L).

sparticle	E_{CM} scaling	RDR	NB TF full L	NB TF peak L	NB no TF full L	NB no TF peak L
$selectron_R$	0.02	0.02	0.02	0.02	0.02	0.02
$selectron_L$	0.20	0.21	0.21	0.25	0.25	0.28
$smuon_R$	0.07	0.07	0.07	0.08	0.08	0.09
$smuon_L$	0.51	0.52	0.53	0.62	0.61	0.70
$stau_1$	0.64	0.82	0.73	0.78	0.78	0.81
$stau_2$	1.10	1.25	1.25	1.34	1.35	1.39
$sneutrino_e$	~1	~1	~1	~1	~1	~1
$sneutrino_\mu$	~7	~7	~7	~7	~7	~7
$sneutrino_\tau$	--	--	--	--	--	--
$\tilde{\chi}_1^0$	0.07	0.07	0.07	0.08	0.08	0.09
$\tilde{\chi}_2^0$	0.12	0.14	0.14	0.15	0.15	0.15
$\tilde{\chi}_3^0$	8.50	8.50	8.50	10.02	9.81	11.49
$\tilde{\chi}_4^0$	--	--	--	--	--	--
$\tilde{\chi}_1^+$	0.18	0.19	0.21	0.24	0.24	0.25
$\tilde{\chi}_2^+$	4.00	4.00	4.00	4.71	4.62	5.41

6.2 CLIC-ILC collaborations on detectors

One of the seven working groups was created in 2008 to foster cooperation between the Compact Linear Collider (CLIC) Study and ILC detector collaborations and was under the responsibility of S. Yamada and F. Richard from the ILC side. It is fair to say that before this initiative was taken, many contacts occurred between the CLIC physics and detector study and the two LOI detector groups, SiD (Silicon Detector) and ILD (International Large Detector). CLIC has signed Memoranda of Understanding (MOUs) with several international R&D detector collaborations, in particular CALICE (CAlorimeter for the LInear Collider with Electrons), LC-TPC (a Time Projection Chamber for a future Linear Collider) and FCAL (Forward CALorimetry). CLIC has also developed active contacts with the ILC software group, adopting the reconstruction strategy developed around the particle flow ideas.

This bottom-up approach is sound and should continue. It was proposed to provide ILCSC with an overall picture of the ongoing collaborations and to organise a joint working group on CLIC-ILC general detector issues composed of the main players.

This joint group has met on a bimonthly basis since March 2010 and has produced a chart summarising its primary actions. The group is composed of: S. Yamada (Research Directorate chair), L. Linssen (CLIC/CERN co-chair), M. Demarteau (R&D panel of the RD, SiD), F. Richard (RD Executive Committee, ILD)[6], F. Sefkow (CALICE / ILD nominated by CLIC), M. Stanitzki (SiD), M. Thomson (ILD).

[6] In January 2011 F. Richard was replaced by J. Fuster.

6.2.1 From ILC to CLIC detectors

CLIC has adapted the two ILC detector concepts for its current conceptual design phase. As with the ILC, the CLIC detectors SiD and ILD would also be operated in a push-pull scheme. However, CLIC researchers have identified some specific aspects of the detector scheme that justify significant variances with respect to the SiD and ILD standard versions.

CLIC requires increased HCAL (hadron calorimeter) absorption length to contain more energetic jets produced in the multi-TeV regime. Since the radius of the superconducting solenoid coil cannot be significantly increased, CLIC has chosen to use a tungsten absorber for the barrel HCAL, which gives a higher stopping power for the same thickness. This allows for a calorimeter depth of 7.5 λwithout any significant change in the inner bore radius of the solenoid. CLIC has also increased the depth of the steel HCAL end cap of the two detectors. To reduce cell occupancies in the vertex detector due to background from incoherent pairs, the inner radius of the vertex barrel was increased to 31 millimetres (mm) and 27 mm for CLIC_ILD and CLIC_SiD respectively. In view of the higher rates from beam-induced background and the more stringent stability requirements for the forward focusing quadrupole at CLIC, important design changes were implemented in the very forward region of both detectors. A vertical cut of the CLIC_ILD and CLIC_SiD detectors as presented in the CLIC conceptual design report is shown in *Figure 6.3*.

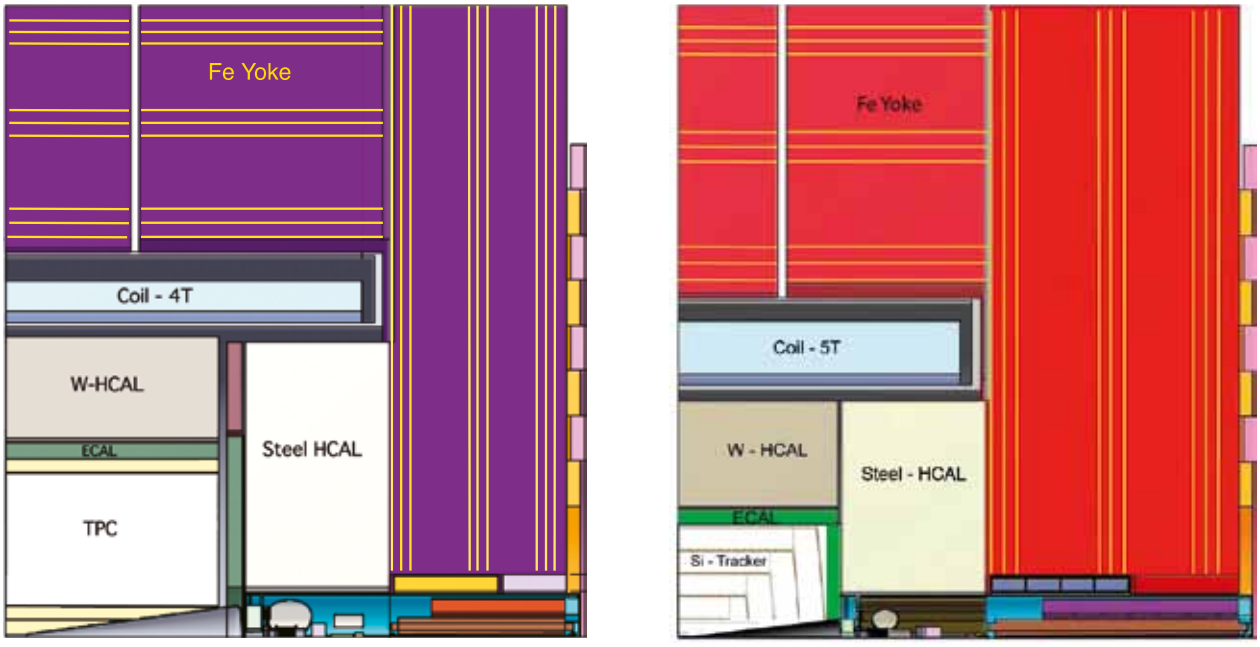

Figure 6.3 ILD (left) and SiD (right) versions used for the CLIC Conceptual Design Report. Image: CLIC CDR

With these modifications, the particle flow algorithm used for the CLIC_ILD version gives very good performances as shown below in *Table 6.3* and *Figure 6.4*.

E_{jet}	root-mean-squared 90%/E_{jet}
45 GeV	3.7%
100 GeV	3.0%
250 GeV	3.0%
500 GeV	3.2%
1 TeV	3.5%
1.5 TeV	3.6%

Table 6.3 Jet energy resolution for various jet energies in the barrel region of the CLIC_ILD detector

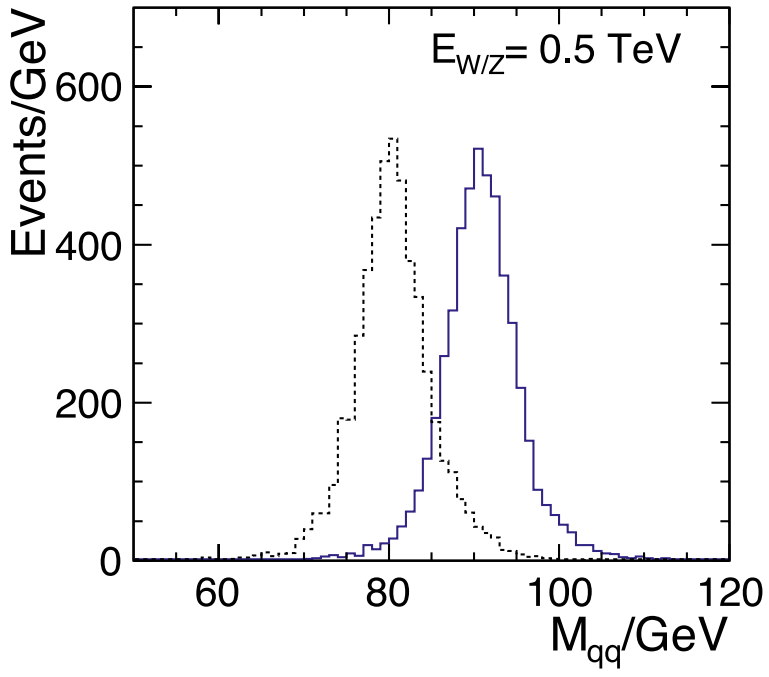

Figure 6.4 Jet-jet mass separation for 500-GeV W and Z decays. Image: Mark Thomson

An essential difference between CLIC and ILC lies in the time structure. While ILC has several hundred nanoseconds (ns) between bunch crossings, CLIC works with bunch crossings separated by only 0.5 ns over a 312-ns bunch train duration for CLIC operating at 3 TeV. The ability to separate interesting physics events from beam-induced background imposes very challenging timing requirements on the various sub-detectors. As described in the CLIC Conceptual Design Report, the calorimeters with fine granularity allow for a very effective background suppression at CLIC by applying precise timing cuts on reconstructed particle flow objects. Therefore supplementary R&D is needed for the readout of the CLIC detectors, with time-stamping capabilities of 10 ns for ECAL (electromagnetic calorimeter) and for all silicon tracking and vertex detectors, while a 1-ns hit time resolution will be required for HCAL. Needless to say, ILC would also benefit from such improvements.

6.2.2 Content of CLIC-ILC collaborations

The main topics covered are:

- Core software development: frameworks, geometry description, tracking, particle flow algorithms, event overlays, grid tools
- Beam-induced background studies
- Detector performance studies and detector optimisation for high energies (at 3-TeV and 1-TeV centre-of-mass energies), for example, for particle flow and tracking
- Event generation and physics benchmarking
- Engineering studies and cost assessment
- Solenoid studies and conductor R&D (with CMS (Compact Muon Solenoid) expertise)
- Electronics developments (CERN expertise)
- HCAL beam tests (tungsten absorbers)

The CLIC-ILC collaboration proceeds through mini-workshops, gathering specialists from both collider groups:

- Software workshop: Following the May 2009 workshop, a follow-up workshop was held on 5 July 2010 at DESY. Contacts: F. Gaede, N. Graf, A. Miyamoto, D. Schlatter.
- Monte Carlo generators: a member of the CLIC study has recently joined the ILC common data sample subgroup. This is an ongoing cooperation, so no new initiative from this working group is required. Contacts: T. Barklow, M. Berggren, A. Miyamoto, S. Poss.
- Power delivery and power pulsing: a common ILC-CLIC workshop was held at Orsay in May 2011.
- Extended ILC-CLIC collaboration on push-pull and experimental hall: in this area common meetings take place on a regular basis.

ILD and SiD are also very actively collaborating on the CLIC Conceptual Design Report on detectors, in particular by providing more than half of the editors.

CALICE has performed beam tests on hadron calorimetry with a tungsten absorber using the analog HCAL developed for ILC.

Figure 6.5 Test setup for the CLIC W-HCAL. Left image: *CERN Bulletin*. Right image: CERN LCD.

6.2.3 Common workshops

An important step in the CLIC-ILC collaboration has been the October 2010 workshop organised at CERN, Switzerland, under the European Committee for Future Accelerators Study of Physics and Detectors for a Linear Collider. For the first time, both CLIC and the ILC were equal partners in organising the event, which covered all linear collider activities: theory, instrumentation, machine and machine-detector interfaces.
There were approximately 500 registered participants with a large fraction of non-European attendees *[6-11]*.

Future annual linear collider collaboration meetings, under the responsibility of the Worldwide Study Organizing Committee, will cover all ILC and CLIC aspects. The latest meeting took place in Granada, Spain, from 26 – 30 September 2011.

References

[6-1] "Parameters for the Linear Collider" document (URL - http://www.fnal.gov/directorate/icfa/para-Nov20-final.pdf), updated 20 November 2006.

[6-2] N. Walker, "Design Considerations for the ILC," (URL - http://ilcagenda.linearcollider.org/materialDisplay.py?contribId=29&sessionId=2&materialId=slides&confId=3461), Sep 28, 2009.

[6-3] T. Maruyama, "SiD beampipe and pairs edge," private communication, 16 March 2010.

[6-4] M. Berggren, "Beam pair-background in with SB2009 and RDR from GuineaPig," Jan 15, 2010.

[6-5] H. Li, "Impacts of the New Baseline ILC Design on the Higgs Recoil Mass Analysis Based on a Fast Simulation of the ILD," 10 October 2010.

[6-6] H. Ono, "ZH branching ratio study @ 350 GeV," 19 October 2010.

[6-7] J.A. Aguilar-Saavedra et al, Eur. Phy. J C46 (2006) 43.

[6-8] M. Berggren, private communication, March 7, 2010; P. Bechtle et al., "Prospects for the study of the stau-system in SPS1a' at the ILC," DESY-09-124, July 2009.

[6-9] B.C. Allanach et al, hep-ph/0202233

[6-10] P. Grannis, "Sparticle mass precision with revised ILC luminosity estimate," revised 10 December 2010; arXiv:hep-ex/0211002.

[6-11] International Workshop on Linear Colliders 2010, 18-22 October 2010, Geneva, Switzerland, https://espace.cern.ch/LC2010/default.aspx.

07

APPENDIX

ACKNOWLEDGEMENT

We acknowledge the support of BMWF, Austria; MinObr, Belarus; FNRS and FWO, Belgium; NSERC, Canada; NSFC, China; MPO CR and VSC CR, Czech Republic; FP7 European Commission, FP6 European Commission, European Union; HIP, Finland; CNRS/IN2P3, CEA-DSM/IRFU, France; BMBF, DFG, HGF, MPG and AvH Foundation, Germany; DAE and DST, India; ISF, Israel; INFN, Italy; MEXT and JSPS, Japan; CRI (MST) and MOST/ KOSEF, Korea; FOM and NWO, The Netherlands; NFR, Norway; MNSW, Poland; ANCS, Romania; MES of Russia and ROSATOM, Russian Federation; MON, Serbia and Montenegro; MSSR, Slovakia; MICINN and CPAN, Spain; SRC, Sweden; STFC, United Kingdom; DOE and NSF, United States of America.

AUTHOR LIST

Tim Barklow
SLAC, USA

Ties Behnke
DESY, Germany

Mikael Berggren
DESY, Germany

James E. Brau
University of Oregon, USA

Karsten Buesser
DESY, Germany

Philip Burrows
University of Oxford, UK

Marty Breidenbach
SLAC, USA

Catherine Clerc
LLR, École polytechnique, CNRS / IN2P3, France

Wes Craddock
SLAC, USA

Marcel Demarteau
ANL, USA

Guenter Eckerlin
DESY, Germany

Gene Fisk
Fermilab, USA

Ray Frey
University of Oregon, USA

Keisuke Fujii
KEK, Japan

Norman Graf
SLAC, USA

Gunther Haller
SLAC, USA

Daniel Jeans
LLR, École polytechnique, CNRS / IN2P3, France

Francois Kircher
CEA, France

Wolfgang Lohmann
DESY, Germany

Tom Markiewicz
SLAC, USA

Takeshi Maruyama
SLAC, USA

Akiya Miyamoto
KEK, Japan

Michael Peskin
SLAC, USA

Francois Richard
LAL, Université Paris-Sud, CNRS / IN2P3, France

Bruce Schumm
UCSC, USA

Felix Sefkow
DESY, Germany

Yasuhiro Sugimoto
KEK, Japan

Mark Thomson
University of Cambridge, UK

Jan Timmermans
DESY, Germany and NIKHEF, The Netherlands

Andrew White
UTA, US

Sakue Yamada
KEK and University of Tokyo, Japan

Vishnu Zutshi
NIU, USA

Members of Physics and Experiment Board

Ties Behnke (ILD)
James Brau (Regional Contact for Americas)
Karsten Buesser (Machine Detector Interface CTG)
Katherine Clerc (Engineering Tool CTG)
Marcel Demarteau (Detector R&D CTG)
Juan Fuster (Regional Contact for Europe, since February 2011)
John Jaros (SiD)
Akiya Miyamoto (Software CTG)
Michael Peskin (Physics CTG)
Francois Richard (Regional Contact for Europe, till January 2011)
Yasuhiro Sugimoto (ILD)
Sakue Yamada (Research Director)
Hitoshi Yamamoto (Regional Contact for Asia)
Andrew White (SiD)

Members of the Common Task Groups

Machine Detector Interface CTG

Karsten Buesser (convener)
Philip Burrows (deputy)
Marco Oriunno
Toshiaki Tauchi

Engineering Tool

Catherine Clerc (convener)
Kurt Krempetz
Marco Oriunno (deputy)
Hiroshi Yamaoka

Detector R&D

Dhiman Chakraborty
Marcel Demarteau (convener)
John Hauptman
Ronald Lipton
Wolfgang Lohmann
Timothy Nelson
Burkhard Schmidt
Aurore Savoy-Navarro
Felix Sefkow
Tohru Takeshita
Jan Timmermans
Andrew White
Marc Winter

Software

Frank Gaede
Norman Graf (deputy)
Tony Johnson
Akiya Miyamoto (convener)

Physics

Tim Barklow
Stewart Boogert
Seong Youl Choi
Klaus Desch
Keisuke Fujii (deputy)
Youanning Gao
Heather Logan
Klaus Moenig
Andrei Nomerotski
Michael Peskin (convener)
Aurore Savoy-Navarro
Georg Weiglein (deputy)
Jae Yu

LETTERS OF INTENT SIGNATORIES

The following are signatories to the Letters of Intent of the ILD groups. Names are listed as given in the official signatories list. Institute names are abbreviated to save space.

ILD (International Large Detector)

Toshinori Abe[142], Jason M. Abernathy[145], Halina Abramowicz[101], Marek Adamus[3], Bernardo Adeva[43], Konstantin Afanaciev[5], Juan Antonio Aguilar-Saavedra[111], Carmen Alabau Pons[39], Enrique Calvo Alamillo[13], Hartwig Albrecht[16], Ladislav Andrieck[71], Marc Anduze[63], Steve J. Aplin[16], Yasuo Arai[53], Masaki Asano[143], David Attie[49], Derek J. Attree[109], David Bailey[135], Juan Pablo Balbuena[41], Markus Ball[39], James Ballin[32], Mauricio Barbi[138], Roger Barlow[14, 135], Christoph Bartels[16, 128], Valeria Bartsch[109], Daniela Bassignana[41], Richard Bates[127], Sudeb Battacharya[92], Jerome Baudot[47, 114], Philip Bechtle[16], Jeannine Beck[16], Moritz Beckmann[16, 25], Marc Bedjidian[48], Ties Behnke[16], Khaled Belkadhi[63], Alain Bellerive[9], Stan Bentvelsen[81], Thomas Bergauer[86], C. Mikael U. Berggren[16], Matthias Bergholz[7, 17], Werner Bernreuther[88], Marc Besancon[49], Auguste Besson[47, 114], Bipul Bhuyan[33], Otmar Biebel[69], Burak Bilki[131], Grahame Blair[89], Johannes Bluemlein[17], Li Bo[106], Veronique Boisvert[89], A. Bondar[8], Giovanni Bonvicini[154], Eduard Boos[64], Vincent Boudry[63], Bernard Bouquet[60], Joël Bouvier[68], Ivanka Bozovic-Jelisavcic[151], Jean-Claude Brient[63], Ian Brock[108], Andrea Brogna[47, 114], Peter Buchholz[150], Karsten Buesser[16], Antonio Bulgheroni[35], Jochen Bürger[16], John Butler[6], Craig Buttar[127], A. F. Buzulutskov[8], Massimo Caccia[35, 115], Stefano Caiazza[16, 128], Alessandro Calcaterra[59], Allen Caldwell[71], Stephane L. C. Callier[60], Alan J. Campbell[16], Michael Campbell[10], Chiara Cappellini[35, 115], Cristina Carloganu[66], Nuno Castro[111], Maria Elena Castro Carballo[17], Marina Chadeeva[45], Dhiman Chakraborty[83], Paoti Chang[79], Alexandre Charpy[67], Hongfang Chen[139], Shaomin Chen[106], Xun Chen[71], Byunggu Cheon[26], Suyong Choi[98], B. C. Choudhary[124], Sandra Christen[16, 128], Jacek Ciborowski[134, 146], Catalin Ciobanu[67], Gilles Claus[47, 114], Catherine Clerc[63], Cornelia Coca[28], Paul Colas[49], Auke Colijn[81], Claude Colledani[47, 114], Christophe Combaret[48], Rémi Cornat[63], Patrick Cornebise[60], François Corriveau[72], Jaroslav Cvach[44], Michal Czakon[147], Nicola D'Ascenzo[16, 84], Wilfrid Da Silva[67], Olivier Dadoun[60], Mogens Dam[123], Chris Damerell[90], Witold Daniluk[102], Mikhail Daniolv[45], Guillaume Daubard[67], Dörte David[16], Jacques David[67], Wim De Boer[10, 116], Nicolo De Groot[42, 81], Paul De Jong[81], Sijbrand De Jong[42, 81], Christophe De La Taille[60], Rita De Masi[47], Albert De Roeck[10], David Decotigny[63], Klaus Dehmelt[16], Eric Delagnes[49], Zhi Deng[106], Klaus Desch[108], Angel Dieguez[110], Ralf Diener[16], Mihai-Octavian Dima[28], Günther Dissertori[19], Madhu S. Dixit[9, 105], Zdenek Dolezal[11], Ralph Dollan[29], Boris A. Dologoshein[73], Andrei Dorokhov[47, 114], Philippe Doublet[60], Tony Doyle[127], Guy Doziere[47, 114], Marko Dragicevic[86], Zbynek Drasal[11], Vladimir Drugakov[5], Jordi Duarte Campderrós[40], Frédéric Dulucq[60], Laurentiu Alexandru Dumitru[28], Daniel Dzahini[68], Helmut Eberl[86], Guenter Eckerlin[16], Wolfgang Ehrenfeld[16], Gerald Eigen[117], Lars Eklund[127], Eckhard Elsen[16], Konrad Elsener[10], Igor Emeliantchik[5], Jan Engels[16], Christophe Evrard[67], Riccardo Fabbri[16], Gerard Faber[19], Michele Faucci Gianelli[60, 89], Angeles Faus-Golfe[39], Nils Feege[16, 128], Cunfeng Feng[94], Jozef Ferencei[96], Marcos Fernandez Garcia[40], Frank Filthaut[42, 81], Ivor Fleck[150], Manfred Fleischer[16], Celeste Fleta[41], Julien L. Fleury[60], Jean-Charles Fontaine[112], Brian Foster[137], Nicolas Fourches[49], Mary-Cruz Fouz[13], Sebastian Frank[86], Ariane Frey[24], Mickael Frotin[63], Hirofumi Fujii[53], Keisuke Fujii[53], Junpei Fujimoto[53], Yowichi Fujita[53], Takahiro Fusayasu[75], Juan Fuster[39],

Andrea Gaddi[10], Frank Gaede[16], Alexei Galkin[84], Valery Galkin[84], Abraham Gallas[43], Laurent Gallin-Martel[68], Diego Gamba[38], Yuanning Gao[106], Luis Garrido Beltran[110], Erika Garutti[16], Franck Gastaldi[63], Bakul Gaur[150], Pascal Gay[66], Andreas Gellrich[16], Jean-Francois Genat[67, 122], Simonetta Gentile[37], Hubert Gerwig[10], Lawrence Gibbons[15], Elena Ginina[86], Julien Giraud[68], Giuseppe Giraudo[38], Leonid Gladilin[64], Joel Goldstein[119], Francisco Javier González Sánchez[40], Filimon Gournaris[109], Tim Greenshaw[133], Z. D. Greenwood[65], Christian Grefe[10, 108], Ingrid-Maria Gregor[16], Gérald Grenier[48], Philippe Gris[66], Denis Grondin[68], Martin Grunewald[126], Grzegorz Grzelak[146], Atul Gurtu[99], Tobias Haas[16], Stephan Haensel[86], Csaba Hajdu[30], Lea Hallermann[16, 128], Liang Han[139], Peter H. Hansen[123], Takanori Hara[53], Kristian Harder[90], Anthony Hartin[16], Tomiyoshi Haruyama[53], Martin Harz[16], Yoji Hasegawa[95], Michael Hauschild[10], Qing He[87], Vincent Hedbeg[70], David Hedin[83], Isa Heinze[16, 128], Christian Helebrant[16, 128], Hans Henschel[17], Carsten Hensel[24], Ralf Hertenberger[69], Alain Hervé[19], Takeo Higuchi[53], Abdelkader Himmi[47, 114], Kazurayama Hironori[103], Hana Hlucha[86], Bart Hommels[121], Yasuyuki Horii[103], Dezso Horvath[30], Jean-Yves Hostachy[68], Wei-Shu Hou[79], Christine Hu-Guo[47, 114], Xingtao Huang[94], Jean Francois Huppert[67], Yasuhiro Ide[95], Marek Idzik[1], Carmen Iglesias Escudero[43], Alexandr Ignatenko[5], Olga Igonkina[81], Hirokazu Ikeda[50], Katsumasa Ikematsu[53], Yukiko Ikemoto[53], Toshinori Ikuno[144], Didier Imbault[67], Andreas Imhof[128], Marc Imhoff[47, 114], Ronen Ingbir[101], Eiji Inoue[53], Giomataris Ioannis[49], Akimasa Ishikawa[55], Kennosuke Itagaki[103], Kazutoshi Ito[103], Hideo Itoh[53], Masaya Iwabuchi[97], Go Iwai[53], Toshiyuki Iwamoto[142], Editha P. Jacosalem[74], Richard Jaramillo Echeverria[40], Daniel T. D. Jeans[63], Fanfan Jing[106], Ge Jing[139], Stevan Jokic[151], Leif Jonsson[70], Matthieu Joré[60], Tatjana Jovin[151], Daniela Käfer[16], Fumiyoshi Kajino[57], Yusuke Kamai[103], Jochen Kaminski[108], Yoshio Kamiya[142], Alexander Kaplan[16, 129], Frédéric Kapusta[67], Deepak Kar[100], Dean Karlen[105, 145], Nobu Katayama[53], Eriko Kato[103], Yukihiro Kato[54], Alexander Kaukher[149], Kiyotomo Kawagoe[55], Hiroki Kawahara[142], Masanori Kawai[53], Takeo Kawasaki[80], Sameen Ahmed Khan[93], Robert Kieffer[48], Eryk Kielar[102], Wolfgang Kiesenhofer[86], Christian M. Kiesling[71], Martin Killenberg[108], Choong Sun Kim[156], Donghee Kim[58], Eun-Joo Kim[12], Guinyun Kim[58], Hong Joo Kim[58], Hyunok Kim[58], Shinhong Kim[144], Francois Kircher[49], Danuta Kisielewska[1], Claus Kleinwort[16], Tatsiana Klimkovich[88], Hanna Kluge[17], Peter Martin Kluit[81], Makoto Kobayashi[53], Michael Kobel[100], Hideyo Kodama[53], Peter Kodys[11], U. Koetz[16], Els Koffeman[81], Takashi Kohriki[53], Sachio Komamiya[142], Yoshinari Kondou[53], Volker Korbel[16], Katsushige Kotera[95], Sabine Kraml[68], Manfred Krammer[86], Kaloyan Krastev[68], Bernward Krause[16], Thorsten Krautscheid[108], Dirk Krücker[16], Kirsten Kschioneck[16], Yu-Ping Kuang[106], Jan Kuhlmann[16], Hirotoshi Kuroiwa[91], Tomonori Kusano[103], Peter Kvasnicka[11], Carlos Lacasta Llácer[39], Eric Lagorio[68], Imad Laktineh[48], Wolfgang Lange[17], Patrice Lebrun[48], Jik Lee[20], Frank Lehner[16], Tadeusz Lesiak[102], Aharon Levy[101], Bo Li[106], Hengne Li[60], Ting Li[106], Yulan Li[106], Zuotang Liang[94], Guilherme Lima[83], Frank Linde[81], Lucie Linssen[10], Diana Linzmaier[16], Benno List[128], Jenny List[16], Bo Liu[106], Xavier Llopart Cudie[10], Wolfgang Lohmann[17], Amparo Lopez Virto[40], Manuel Lozano[41], Shaojun Lu[21, 71], Angela Isabela Lucaci-Timoce[16], Nick Lumb[48], Bjorn Lundberg[70], Benjamin Lutz[16, 128], Pierre Lutz[49, 60], Thorsten Lux[107], Pawel Luzniak[134], Alexey Lyapin[109], Wengan Ma[139], Lukasz Maczewski[134, 146], Wolfgang F. Mader[100], Manas Maity[152], Gobinda Majumder[99], Nayana Majumdar[92], Akihiro Maki[53], Yasuhiro Makida[53], Judita Mamuzic[151], Dhellot Marc[67], Ivan Marchesini[16, 128], Michal Marcisovsky[44], Carlos Mariñas[39], John Marshall[121], Cornelius Martens[16], Jean-Pierre Martin[113], Victoria J. Martin[125], Gisele Martin-Chassard[60], Celso Martinez Rivero[40], Hans-Ulrich Martyn[16, 88], Hervé Mathez[48], Antoine Mathieu[63], Takeshi Matsuda[16, 53], Hiroyuki Matsunaga[142,] Takashi Matsushita[55], Georgios Mavromanolakis[22, 121], Kirk T. McDonald[87], Paolo Mereu[38], Marcel Merk[81, 153], Mikhail M. Merkin[64], Niels Meyer[16], Norbert Meyners[16], Satoshi Mihara[53], David J. Miller[109], Owen Miller[118], Winfried A. Mitaroff[86], Akiya Miyamoto[53], Hitoshi Miyata[80], Ulf Mjornmark[70], Joachim Mnich[16], Klaus Moenig[17], Andreas Moll[21, 71], Gudrid A. Moortgart-Pick[14, 18], Paulo Mora De Feitas[63], Frederic Morel[47, 114], Stefano Moretti[90, 140], Vasily Morgunov[16, 45], Takashi Mori[76], Toshinori Mori[142], Laurent Morin[68], Sergey Morozov[16, 128], Fabian Moser[86], Hans-Günther Moser[71], David Moya[40], Mihajlo Mudrinic[151], Supratik Mukhopadhyay[92], Takeshi Murakami[53], Luciano Musa[10], Gabriel Musat[63], Tadahi Nagamine[103], Isamu Nakamura[53], Eiichi Nakano[85], Kenichi Nakashima[91], Kazuo Nakayoshi[53], Hideyuki Nakazawa[78], Jiwoo Nam[20], Shinwoo Nam[20], Stanislav Nemecek[44], Carsten Niebuhr[16], Marcus Niechciol[150], Piotr Nieuzurawski[146], Shohei Nishida[53], Miho Nishiyama[95], Osamu Nitoh[104], Ed Norbeck[131], Mitsuaki Nozaki[53], Val O'Shea[127], Martin Ohlerich[17], Nobuchika Okada[53], Alexander Olchevski[52], Bob Olivier[71], Krzysztof Oliwa[102], Tsunehiko Omori[53], Yasar Onel[131], Hiroaki Ono[82], Yoshimasa Ono[103], Yoshiyuki Onuki[103], Wataru Ootani[142], Risto Orava[130], Marius Ciprian

Orlandea[28], Anders Oskarsson[70], Per Osland[117], Dmitri Ossetski[84], Lennart Osterman[70], Cristobal Padilla[107], Mila Pandurovic[151], Hwanbae Park[58], Il Hung Park[20], Chris Parkes[127], Ghislain Patrick[67], J. Ritchie Patterson[15], Bogdan Pawlik[102], Giulio Pellegrini[41], Antonio Pellegrino[81], Daniel Peterson[15], Alexander Petrov[16], Thanh Hung Pham[67], Marcello Piccolo[59], Roman Poeschl[60], Ivo Polak[44], Elena Popova[73], Martin Postranecky[109], Volker Prahl[16], Xavier Prudent[100], Helenka Przysiezniak[62, 113], Jesus Puerta-Pelayo[13], Wenbin Qian[106], Arnulf Quadt[24], Fatah-Ellah Rarbi[68], Alexei Raspereza[16], Lodovico Ratti[36], Ludovic Raux[60], Gerhard Raven[81, 153], Valerio Re[36], Meinhard Regler[86], Marcel Reinhard[63], Uwe Renz[2], Philippe Repain[67], Jose Repond[4], Francois Richard[60], Sabine Riemann[17], Tord Riemann[17], Jordi Riera-Babures[148], Imma Riu[107], Aidan Robson[127], Philipp Roloff`[16, 128], Aura Rosca[28, 155], Christoph Rosemann[16], Janusz Rosiek[146], Robert Rossmanith[116], Stefan Roth[88], Christophe Royon[49], Manqi Ruan[63], Alberto Ruiz-Jimeno[40], Vladimir Rusinov[45], Pavel Ruzicka[44], Dmitri Ryzhikov[84], Juan J. Saborido[43], Iftach Sadeh[101], André Sailer[17], Masatoshi Saito[53], Takayuki Sakumo[95], Toshiya Sanami[53], Tomoyuki Sanuki[103], Sandip Sarkar[92], Rei Sasaki[103], Yutaro Sato[103], Valeri Saveliev[84], Aurore Savoy-Navarro[67], Lee Sawyer[65], Peter Schade[16], Oliver Schäfer[149], Joern Schaffran[16], Andreas Schälicke[17], Jan Scheirich[11], Dieter Schlatter[10], Ringo Sebastian Schmidt[7, 17], Sebastian Schmitt[16], Uwe Schneekloth[16], Heinz Juergen Schreiber[17], K. Peter Schüler[16], Hans-Christian Schultz-Coulon[129], Markus Schumacher[2], Bruce A. Schumm[120], Sergej Schuwalow[17], Rainer Schwierz[100], Felix Sefkow[16], Rachid Sefri[67], Nathalie Seguin-Moreau[60], Katja Seidel[21, 71], Jadranka Sekaric[132], Hiroshi Sendai[53], Ronald Dean Settles[71], Ming Shao[139], L. I. Shechtman[8], Shoichi Shimazaki[53], Nikolai Shumeiko[5], Petr Sicho[44], Frank Simon[21, 71], Klaus Sinram[16], Ivan Smiljanic[151], Nebojsa Smiljkovic[19], Jan Smolík[44], Blanka Sobloher[16, 128], Christian Soldner[71], Kezhu Song[139], Andre Sopczak[61], Peter Speckmayer[10], Evert Stenlund[70], Dominik Stockinger[100], Holger Stoeck[141], Arno Straessner[100], Raimund Ströhmer[69], Richard Stromhagen[16], Yuji Sudo[144], Taikan Suehara[142], Fumihiko Suekane[103], Yusuke Suetsugu[53], Yasuhiro Sugimoto[53], Akira Sugiyama[91], Kazutaka Sumisawa[53], Shiro Suzuki[91], Krzysztof Swientek[1], Hajrah Tabassam[125], Tohru Takahashi[27], Hiroshi Takeda[55], Tohru Takeshita[95], Yosuke Takubo[103], Tomohiko Tanabe[142], Ken-Ichi Tanaka[53], Manubo Tanaka[53], Shuji Tanaka[53], Stefan Tapprogge[51], Evgueny I. Tarkovsky[45], Kazuya Tauchi[53], Toshiaki Tauchi[53], Valery I. Telnov[8], Eliza Teodorescu[28], Mark Thomson[121], Junping Tian[31, 106], Jan Timmermans[16, 81], Maxim Titov[49], Katsuo Tokushuku[53], Shunsuke Tozuka[95], Toru Tsuboyama[53], Koji Ueno[79], Miguel Ullán[41], Satoru Uozumi[55], Junji Urakawa[53], Andriy Ushakov[17], Yutaka Ushiroda[53], Manfred Valentan[86], Isabelle Valin[47, 114], Harry Van Der Graaf[81], Brian Van Doren[132], Rick J. Van Kooten[34], Muriel Vander Donckt[48], Jean-Charles Vanel[63], Pablo Vazquez Regueiro[43], Marco Verzocchi[22], Christophe Vescovi[68], Henri L. Videau[63], Ivan Vila[40], Xavier Vilasis-Cardona[148], Adrian Vogel[108], Robert Volkenborn[16], Marcel Vos[39], Yorgos Voutsinas[47], Vaclav Vrba[44], Marcel Vreeswijk[81], Roberval Walsh[125], Wolfgang Waltenberger[86], Meng Wang[94], Min-Zu Wang[79], Qun Wang[139], Xiaoling Wang[139], Yi Wang[106], David R. Ward[121], Matthew Warren[109], Minori Watanabe[80], Takashi Watanabe[56], Nigel K. Watson[118], Nanda Wattimena[16], Oliver Wendt[16, 128], Norbert Wermes[108], Lars Weuste[71], Katarzyna Wichmann[16], Peter Wienemann[108], Wojciech Wierba[102], Graham W. Wilson[132], John A. Wilson[118], Matthew Wing[109], Marc Winter[47], Markus Wobisch[65], Malgorzata Worek[147], Stefania Xella[123], Zizong Xu[139], Akira Yamaguchi[103], Hiroshi Yamaguchi[91], Hitoshi Yamamoto[103], Hiroshi Yamaoka[53], Satoru Yamashita[142], M. Yamauchi[53], Yuji Yamazaki[55], Mahfoud Yamouni[68], Wenbiao Yan[139], Koji Yanagida[95], Haijun Yang[136], Jin Min Yang[46], Jongmann Yang[20], Zhenwei Yang[106], Yoshiji Yasu[53], Ryo Yonamine[97], Kohei Yoshida[103], Takuo Yoshida[23], Tamaki Yoshioka[53], Chunxu Yu[77], Intae Yu[98], Qian Yue[106], Josef Zacek[11], Jaroslav Zalesak[44], Aleksandr Filip Zarnecki[146], Leszek Zawiejski[102], Christian Zeitnitz[147], Dirk Zerwas[60], Wolfram Zeuner[10, 16], Renyou Zhang[139], Xueyao Zhang[94], Yanxi Zhang[106], Zhiqing Zhang[60], Ziping Zhang[139], Jiawei Zhao[139], Zhengguo Zhao[139], Baojun Zheng[106], Liang Zhong[106], Yongzhao Zhou[139], Chengguang Zhu[94], Xianglei Zhu[106], Fabian Zomer[60], Vishnu Zutshi[83]

[1] AGH Univ. of Science and Technology, Cracow, Poland
[2] Albert-Ludwigs Univ. Freiburg, Freiburg, Germany
[3] Andrzej Soltan Inst. for Nuclear Studies, Warsaw Poland
[4] Argonne National Laboratory, Argonne, USA
[5] Belarusian State Univ., Minsk, Belarus
[6] Boston Univ., Boston, USA
[7] Brandenburg Univ. of Technology, Cottbus, Germany
[8] Budker Inst. for Nuclear Physics, Novosibirsk, Russia
[9] Carleton Univ., Ottawa, Canada
[10] CERN, Geneva, Switzerland
[11] Charles Univ., Prague, Czech Republic
[12] Chonbuk National Univ., Jeonju, Korea

[13] CIEMAT, Madrid, Spain
[14] Cockcroft Inst., Warrington, UK
[15] Cornell Univ., Ithaca, USA
[16] DESY, Hamburg, Germany
[17] DESY, Zeuthen, Germany
[18] Durham Univ., Durham, UK
[19] ETH Zürich, Zürich, Germany
[20] Ewha Womans Univ., Seoul, Korea
[21] Excellence Cluster Universe, Garching, Germany
[22] Fermilab, Batavia, USA
[23] Fukui Univ., Fukui, Japan
[24] Georg-August-Univ. Göttingen, Göttingen, Germany
[25] Gottfried Wilhelm Leibniz Univ. Hannover, Hannover, Germany
[26] Hanyang Univ., Seoul, Korea
[27] Hiroshima Univ., Higashi-Hiroshima, Japan
[28] Horia Hulubei National Inst. of Physics and Nuclear Engineering, Bucharrest-Maguerele, Romania
[29] Humboldt Univ. zu Berlin, Berlin, Germany
[30] Hungarian Academy of Science, Budapest, Hungary
[31] IHEP, Beijing, China
[32] Imperial College London, London, UK
[33] Indian Inst. of Technology, Guwahati, Guwahati, India
[34] Indiana Univ., Bloomington, USA
[35] INFN, Milano, Italy
[36] INFN, Pavia, Italy
[37] INFN, Roma, Italy
[38] INFN, Torino, Italy
[39] Inst. de Física Corpuscular, Valencia, Spain
[40] Inst. de Física de Cantabria, Santander, Spain
[41] Inst. de Microelectrónica de Barcelona, Barcelona, Spain
[42] Inst. for Mathematics, Astrophysics and Particle Physics, Nijmegen, The Netherlands
[43] Inst. Galego de Física de Altas Enerxias, Santiago de Compostela, Spain
[44] Inst. of Physics, Prague, Czech Republic
[45] Inst. of Theoretical and Experimental Physics, Moscow, Russia
[46] Inst. of Theoretical Physics, Beijing, China
[47] Inst. Pluridisciplinaire Hubert Curien, Strasbourg, France
[48] IPNL, Univ. de Lyon, CNRS/IN2P3, Lyon, France
[49] IRFU, CEA Saclay, Gif-sur-Yvette, France
[50] Japan Aerospace Exploration Agency, Sagamihara, Japan
[51] Johannes Gutenberg Univ. Mainz, Mainz, Germany
[52] Joint Inst. for Nuclear Research, Dubna, Russia
[53] KEK, Tsukuba, Japan
[54] Kinki Univ., Higashi-Osaka, Japan
[55] Kobe Univ., Kobe, Japan
[56] Kogakuin Univ., Tokyo, Japan
[57] Konan Univ., Kobe, Japan
[58] Kyungpook National Univ., Daegu, Korea
[59] Laboratori Nazionali di Frascati, Frascati, Italy
[60] LAL, Univ. Paris-Sud, CNRS/IN2P3, Orsay, France
[61] Lancaster Univ., Lancaster, UK
[62] LAPP, Univ. de Savoie, CNRS/IN2P3, Orsay, France
[63] LLR, École polytechnique, CNRS/IN2P3, Palaiseau, France
[64] Lomonosov Moscow State Univ., Moscow, Russia
[65] Louisiana Tech Univ., Ruston, USA
[66] LPC Clermont, Univ. Blaise Pascal, CNRS/IN2P3, Aubière, France
[67] LPNHE, Univ. Pierre et Marie Curie, Univ. Denis Diderot, CNRS/IN2P3, Paris, France
[68] LPSC, Univ. Joseph Fourier, CNRS/IN2P3, Inst. Polytechnique de Grenoble, Grenoble, France
[69] Ludwig-Maximilians-Univ. München, Munich, Germany
[70] Lunds Univ., Lund, Sweden
[71] Max-Planck-Inst. für Physik, Munich, Germany
[72] McGill Univ., Montreal, Canada
[73] Moscow Engineering Physics Inst., Moscow, Russia
[74] MSU-Iligan Inst. of Technology, Iligan City, Philippines
[75] Nagasaki Inst. of Applied Science, Nagasaki, Japan
[76] Nagoya Univ., Nagoya, Japan
[77] Nankai Univ., Tianjin, China
[78] National Central Univ., Chung-li, Taiwan
[79] National Taiwan Univ., Taipei, Taiwan
[80] Niigata Univ., Niigata, Japan
[81] Nikhef, Amsterdam, The Netherlands
[82] Nippon Dental Univ. School of Life Dentistry, Niigata, Japan
[83] Northern Illinois Univ., DeKalb, USA
[84] Obninsk State Technical Univ. for Nuclear Engineering, Obninsk, Russia
[85] Osaka City Univ., Osaka, Japan
[86] Österreichische Akademie der Wissenschaften, Vienna, Austria
[87] Princeton Univ., Princeton, USA
[88] Rheinisch-Westfälische Technische Hochschule, Aachen, Germany
[89] Royal Holloway, Univ. of London, Surrey, UK
[90] Rutherford Appleton Laboratory, Didcot, UK
[91] Saga Univ., Saga, Japan
[92] Saha Inst. of Nuclear Physics, Kolkata, India
[93] Salalah College of Technology, Salalah, Sultanate of Oman
[94] Shandong Univ., Jinan, China
[95] Shinshu Univ., Matsumoto, Japan
[96] Slovak Academy of Sciences, Kosice, Slovakia
[97] Sokendai, Hayama, Japan
[98] Sungkyunkwan Univ., Suwon, Korea
[99] Tata Inst. of Fundamental Research, Mumbai, India
[100] Technische Univ. Dresden, Dresden, Germany
[101] Tel Aviv Univ., Tel Aviv, Israel
[102] The Henryk Niewodniczanski Inst. of Nuclear Physics, Cracow, Poland
[103] Tohoku Univ., Sendai, Japan
[104] Tokyo Univ. of Agricultural Technology, Koganei, Japan
[105] TRIUMF, Vancouver, Canada
[106] Tsinghua Univ., Beijing, China
[107] Univ. Autònoma de Barcelona, Barcelona, Spain
[108] Univ. Bonn, Bonn, Germany
[109] Univ. College London, London, UK
[110] Univ. de Barcelona, Barcelona, Spain
[111] Univ. de Granada, Granada, Spain
[112] Univ. de Haute Alsace Mulhouse-Colmar, Mulhouse, France
[113] Univ. de Montréal, Montreal, Canada
[114] Univ. de Strasbourg, Strasbourg, France
[115] Univ. dell-Insubria in Como, Como, Italy
[116] Univ. Karlsruhe, Karlsruhe, Germany
[117] Univ. of Bergen, Bergen, Norway
[118] Univ. of Birmingham, Birmingham, UK
[119] Univ. of Bristol, Bristol, UK
[120] Univ. of California, Santa Cruz, USA
[121] Univ. of Cambridge, Cambridge, UK
[122] Univ. of Chicago, Chicago, USA
[123] Univ. of Copenhagen, Copenhagen, Denmark
[124] Univ. of Delhi, Delhi, India
[125] Univ. of Edinburgh, Edinburgh, UK
[126] Univ. of Ghent, Ghent, Belgium
[127] Univ. of Glasgow, Glasgow, UK
[128] Univ. of Hamburg, Hamburg, Germany
[129] Univ. of Heidelberg, Heidelberg, Germany
[130] Univ. of Helsinki, Helsinki, Finland
[131] Univ. of Iowa, Iowa City, USA
[132] Univ. of Kansas, Lawrence, USA
[133] Univ. of Liverpool, Liverpool, UK
[134] Univ. of Lodz, Lodz, Poland
[135] Univ. of Manchester, Manchester, UK
[136] Univ. of Michigan, Ann Arbor, USA
[137] Univ. of Oxford, Oxford, UK
[138] Univ. of Regina, Regina, Canada
[139] Univ. of Science and Technology of China, Hefei, China
[140] Univ. of Southampton, Southampton, UK
[141] Univ. of Sydney, Sydney, Australia
[142] Univ. of Tokyo, ICEPP, Tokyo, Japan
[143] Univ. of Tokyo, Inst. for Cosmic Ray Research, Kashiwa, Japan
[144] Univ. of Tsukuba, Tsukuba, Japan
[145] Univ. of Victoria, Victoria, Canada
[146] Univ. of Warsaw, Warsaw, Poland
[147] Univ. of Wuppertal, Wuppertal, Germany
[148] Univ. Ramon Llull, Barcelona, Spain
[149] Univ. Rostock, Rostock, Germany
[150] Univ. Siegen, Siegen, Germany
[151] VINCA Inst. of Nuclear Sciences, Belgrade, Serbia
[152] Visva-Bharati Univ., Santiniketan, India
[153] Vrije Univ., Amsterdam, The Netherlands
[154] Wayne State Univ., Detroit, USA
[155] West Univ. of Timisoara, Timisoara, Romania
[156] Yonsei Univ., Seoul, Korea

LETTERS OF INTENT SIGNATORIES

The following are signatories to the Letters of Intent of the SiD groups. Names are listed as given in the official signatories list. Institute names are abbreviated to save space.

SiD (Silicon Detector)

T. Abe[68], B. Adeva[64], C. Adloff[26], H. Aihara[68], L. Andricek[30], J. P. Balbuena[18], C. Baltay[73], H. R. Band[70], Y. Banda[62], T. L. Barklow[40], A. Belymam[40], E. L. Berger[1], B. Bilki[52], J. Blaha[26], J.-J. Blaising[26], E. E. Boos[33], D. Bortoletto[38], B. P. Brau[53], J. E. Brau[61], M. Breidenbach[40], P. N. Burrows[62], J. M. Butler[3], S. Cap[26], R. Cassell[40], S. Chakrabarti[41], D. Chakraborty[35], M. Charles[52], J. Chauveau[29], M. Chefdeville[26], S. Chen[34], M. Chertok[44], D. C. Christian[10], G. B. Christian[19], S. Cihangir[10], C. Ciobanu[29], R. Coath[39], C. Colledani[21], J. S. Conway[44], W. E. Cooper[10], R. F. Cowan[31], W. Craddock[40], L. Cremaldi[57], J. Crooks[39], N. D'Ascenzo[36], C. Damerell[39], P. D. Dauncey[15], K. De[66], R. De Masi[21], A. de Roeck[7], C. Deaconu[40], M. Demarteau[10], E. Devetak[62], S. Dhawam[73], A. Dieguez[42], A. Dorokhov[21], A. Dragone[40], C. Drancourt[26], J. Duarte[17], T. Dutta[13], A. Dyshkant[35], K. Elsener[7], A. Espargiliare[26], V. Fadeyev[45], A. Farbin[66], A. Faus-Golfe[16], M. Fernandez[17], F. Feyzi[70], P. Fisher[31], H. E. Fisk[10], C. Fleta[18], B. Foster[62], R. Frey[61], J. Fuster[16], A. Gaddi[7], R. Gaglione[26], V. Galkin[36], A. Gallas Torreira[64], D. Gao[65], L. A. Garren[10], Ll. Garrido[42], N. Geffroy[26], H. Gerwig[7], M. Gibson[39], J. Gill[47], J. Goldstein[4], J. Gonzalez[17], N. A. Graf[40], C. Grefe[7], J. Gronberg[27], M. Grunewald[11], V. Guarino[1], J. Gunion[44], G. Haller[40], D. Hedin[35], R. Herbst[40], J. L. Hewett[40], M. D. Hildreth[60], B. Holbrook[44], C. Hu-Guo[21], C. Iglesias Escudero[64], M. Iwasaki[68], J. Jacquemier[26], R. Jaramillo[17], J. A. Jaros[40], W. Jie[65], A. S. Johnson[40], Y. Junfeng[65], J. Kaminski[43], F. Kapusta[29], P. E. Karchin[72], Y. Karyotakis[26], C. J. Kenney[32], G. N. Kim[25], P. C. Kim[40], T. J. Kim[52], W. Klempt[7], K. Krempetz[10], R. Kriske[56], R. K. Kutschke[10], Y.-J. Kwon[74], C. Lacasta[16], M. Laloum[29], R. L. Lander[44], T. Lastovicka[62], G. Lastovicka-Medin[58], C. Li[65], Y.-M. Li[62], L. Linssen[7], R. Lipton[10], S. Liu[65], Y. Liu[65], A. Lopez-Virto[17], X. C. Lou[67], M. Lozano[18], C. Lu[37], H. J. Lubatti[69], P. Lutz[23], D. B. MacFarlane[40], U. Mallik[52], S. Manly[63], C. Mariñas[16], T. Markiewicz[40], C. Martinez-Rivero[17], T. Maruyama[40], J. McCormick[40], K. T. McDonald[37], M. Merkin[33], C. Milstene[72], K. Moffeit[40], G. Moortgat-Pick[22], H.-G. Moser[30], D. Moya[17], U. Nauenberg[47], H. A. Neal[40], T. K. Nelson[40], A. Nichols[39], A. Nomerotski[62], E. Norbeck[52], G. Oleinik[47], Y. Onel[52], D. V. Onoprienko[24], R. Orava[50], M. Oreglia[46], M. Oriunno[40], D. Ossetski[36], A. Pankov[12], A. Para[10], H. Park[25], S. Park[66], R. Partridge[40], M. E. Peskin[40], J. Prast[26], R. Prepost[70], V. Radeka[5], R. Rahmat[57], K. Ranjan[48], J. Repond[1], J. Riera-Babures[71], K. Riles[55], T. G. Rizzo[40], P. Rowson[40], A. Ruiz-Jimeno[17], J. J. Saborido Silva[64], V. Saveliev[36], A. Savoy-Navarro[29], L. Sawyer[28], D. Schlatter[7], B. A. Schumm[45], S. Seidel[59], R. Shivpuri[48], N. Sinev[61], A. J. S. Smith[37], J. Smith[66], P. Speckmayer[7], A. Srivastava[2], M. Stanitzki[39], D. M. Strom[61], J. Strube[39], D. Su[40], Y. Sun[65], G. N. Taylor[54], J. Thom[8], E. Torrence[61], S. M. Tripathi[44], R. Tschirhart[10], R. Turchetta[39], M. Tyndel[39], M. Ullán[18], R. Van Kooten[51], G. S. Varner[49], P. Vazquez Regueiro[64], J. Velthius[4], I. Vila[17], X. Vilasis-Cardona[71], M. Vos[16], G. Vouters[26], V. Vrba[20], S. R. Wagner[47], S. Walston[27], Q. Wang[65], M. Wayne[60], M. Weber[39], H. Weerts[1], H. Wenzel[10], A. P. White[66], S. Willocq[53], M. Winter[21], M. Woods[40], S. Worm[39], D. Wright[27], L. Xia[1], R. K. Yamamoto[31], H.-J. Yang[55], J. Yang[9], R. Yarema[10], J. Yi[65], W. Yonggang[65], J. Yu[66], J. Zhang[1], Q. Zhang[1, 14], Z. Zhang[39], Z. Zhao[65], R.-Y. Zhu[6], V. Zutshi[35]

[1] Argonne National Laboratory, Argonne, USA
[2] Birla Inst. for Technology and Science, Pilani, India
[3] Boston Univ., Boston, USA
[4] Bristol Univ., Bristol, UK
[5] Brookhaven National Laboratory, Upton, USA
[6] California Inst. of Technology, Pasadena, USA
[7] CERN, Geneva, Switzerland
[8] Cornell Univ., Ithaca, USA
[9] Ewha Womans Univ., Seoul, Korea
[10] Fermilab, Batavia, USA
[11] Ghent Univ., Ghent, Belgium
[12] Gomel State Technical Univ., Gomel, Belarus
[13] GSI, Darmstadt, Germany
[14] IHEP, Beijing, China
[15] Imperial College London, London, UK
[16] Inst. de Física Corpuscular, Valencia, Spain
[17] Inst. de Física de Cantabria, Cantabria, Spain
[18] Inst. of Microelectronics of Barcelona, Barcelona, Spain
[19] Inst. of Nuclear Research, Debrecen, Hungary
[20] Inst. of Physics, Prague, Czech Republic
[21] IPHC, Univ. Louis Pasteur, CNRS/IN2P3, Strasbourg, France
[22] IPPP, Durham, UK
[23] IRFU, CEA Saclay, Gif-sur-Yvette, France
[24] Kansas State Univ., Manhattan, USA
[25] Kyungpook National Univ., Daegu, Korea
[26] LAPP, Univ. de Savoie, CNRS/IN2P3, Annecy-le-Vieux, France
[27] Lawrence Livermore National Laboratory, Livermore, USA
[28] Louisiana Tech Univ., Ruston, USA
[29] LPNHE, Univ. Pierre et Marie Curie, Univ. Denis Diderot, CNRS/IN2P3, Paris, France
[30] Max-Planck-Inst. for Physics, Munich, Germany
[31] MIT, Cambridge, USA
[32] Molecular Biology Consortium, Chicago, USA
[33] Moscow State Univ., Moscow, Russia
[34] Nanjing Univ., Nanjing, China
[35] Northern Illinois Univ., DeKalb, USA
[36] Obninsk State Technical Univ. for Nuclear Power Engineering, Obninsk, Russia
[37] Princeton Univ., Princeton, USA
[38] Purdue Univ., West Lafayette, USA
[39] Rutherford Appleton Laboratory, Didcot, UK
[40] SLAC, Palo Alto, USA
[41] SUNY, Stony Brook, USA
[42] Univ. of Barcelona, Barcelona, Spain
[43] Univ. of Bonn, Bonn, Germany
[44] Univ. of California, Davis, USA
[45] Univ. of California, Santa Cruz, USA
[46] Univ. of Chicago, Chicago, USA
[47] Univ. of Colorado, Boulder, USA
[48] Univ. of Delhi, Delhi, India
[49] Univ. of Hawaii, Honolulu, USA
[50] Univ. of Helsinki, Helsinki, Finland
[51] Univ. of Indiana, Bloomington, USA
[52] Univ. of Iowa, Iowa City, USA
[53] Univ. of Massachusetts, Amherst, USA
[54] Univ. of Melbourne, Melbourne, Australia
[55] Univ. of Michigan, Ann Arbor, USA
[56] Univ. of Minnesota, Minneapolis, USA
[57] Univ. of Mississippi, Oxford, USA
[58] Univ. of Montenegro, Podgorica, Montenegro
[59] Univ. of New Mexico, Albuquerque, USA
[60] Univ. of Notre Dame, Notre Dame, USA
[61] Univ. of Oregon, Eugene, USA
[62] Univ. of Oxford, Oxford, UK
[63] Univ. of Rochester, Rochester, USA
[64] Univ. of Santiago de Compostela, Santiago de Compostela, Spain
[65] Univ. of Science and Technology in China, Hefei, China
[66] Univ. of Texas at Arlington, Arlington, USA
[67] Univ. of Texas at Dallas, Dallas, USA
[68] Univ. of Tokyo, Tokyo, USA
[69] Univ. of Washington, Seattle, USA
[70] Univ. of Wisconsin, Madison, USA
[71] Univ. Ramon Llull, Barcelona, Spain
[72] Wayne State Univ., Detroit, USA
[73] Yale Univ., New Haven, USA
[74] Yonsei Univ., Seoul, Korea

design: form one® visual communications | www.form-one.de

ISSUED BY . . . . ilc international linear collider

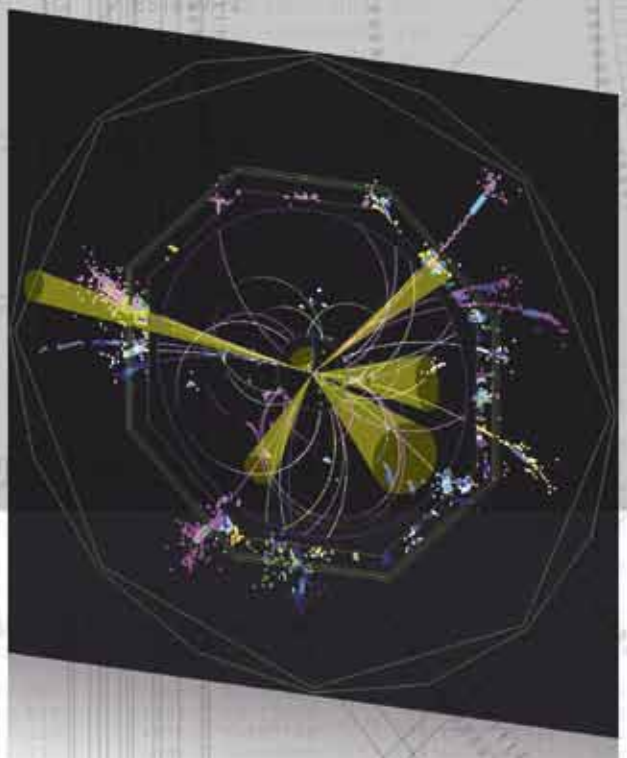

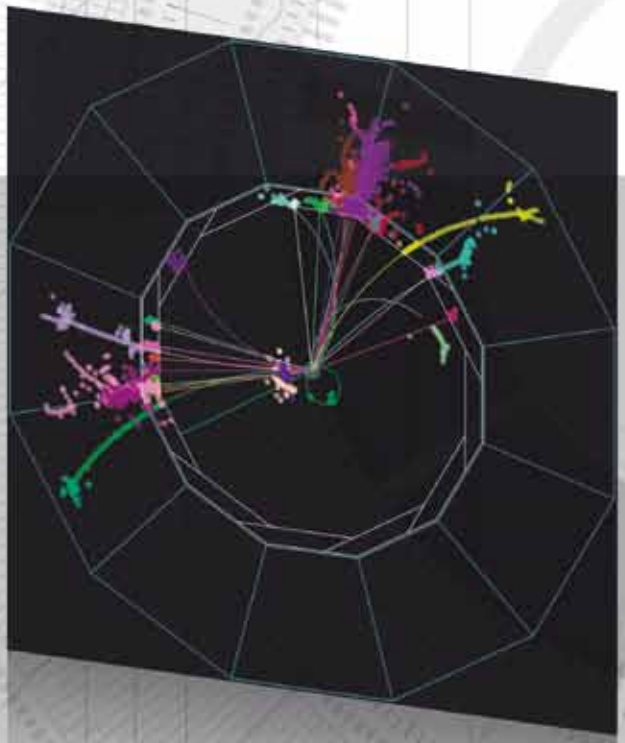

ISBN 978-3-935702-61-4

CERN: CERN-LCD-Note-2011-038
DESY: DESY 2011-190
Fermilab: FERMILAB-FN-0936-PPD
ILC: ILC-REPORT-2011-033
KEK: KEK Report 2011-5
LAL: LAL 11-246
SLAC: SLAC-R-973